Technical Report

Molecular deformation of wood and cellulose studied by near infrared and Raman spectroscopy

Author: Fei Guo

Date: 14th March 2019

Report: SWP-T071

TABLE OF CONTENTS

Disclaimer

supported by
forestgrowers
commodity levy

EXECUTIVE SUMMARY

Eucalyptus can be alternative plantation species to radiata pine for New Zealand. One major problem preventing eucalyptus wood from high-value uses is its high growth-stress level, which causes problems in solid wood processing. Current methods to measure growth-strain are destructive and time-consuming. Growth-stress in wood, like mechanical stress, can cause deformation on the molecular level, which can be detected using spectroscopy. The overreaching objective of this thesis was to investigate the possibility of a non-destructive and rapid spectroscopy-based method to measure strain in wood. The molecular deformation caused by stress or strain was studied in detail using near infrared (NIR) and Raman spectroscopy.

Chapter 1 provides background and a literature review. In Chapter 2, the suitability of Eucalyptus globoidea for veneer and LVL production was investigated in relation to growth-strain levels. Veneer recovery, veneer splitting and wood properties were evaluated and correlated with growth-strain. Veneers with no, or limited, defects can be obtained from E. globoidea. Veneer recovery (54.5%) correlated with growth-strain and was highly variable between logs, ranging from 23.6% to 74.5%. There was a moderate positive association between splitting length and growth-strain (r = 0.73), but no significant association with wood stiffness. Growth-strain reduced veneer recovery by splitting, and was largely independent of stiffness, suggesting the possibility of finding trees with both low growth-strain and high stiffness, desirable for structural wood products. The considerable variation in growth-strain and stiffness indicated a possibility for genetic improvement. The unfavourable effects of growth-strain highlighted the demand for a rapid and non-destructive method to evaluate growth-strain levels in wood.

Chapter 3 describes experiments aimed at better understanding the effects of molecular deformation of wood and cellulose on NIR spectra. Dry wood and paper samples were stretched to different strain levels using a purpose-built tensile test device fitted into an NIR spectrometer while collecting transmission spectra. Consistent spectral changes caused by mechanical strain, assigned to OH stretching bands, were observed for all sample types. Bands at 6286 ± 5 cm^{-1} and 6470 ± 10 cm^{-1} were tentatively assigned to the OH groups connected with the 2OH⋯6O and 3OH⋯5O intramolecular hydrogen bonds of crystalline cellulose Iβ, respectively. Both bands shifted to higher wavenumbers, indicating the elongation of the hydrogen bonds. A linear relationship was found between band shifts and mechanical strain. Band shift rates for the 3OH bond were more than twice that of the 2OH bond, consistent with bending of the glycosidic bond. Bending tests showed that the band at around 6286 cm^{-1} shifted in opposite direction when under tension or compression.

Chapter 4 summarises the roles of water-accessible and -inaccessible cellulose in the load transfer of wood using deuterium exchange combined with NIR spectroscopy. The spectral changes on NIR spectra caused by mechanical strain could be highlighted by averaging the loading and unloading cycles to compensate for effects of desorption and isotope re-exchange due to environmental fluctuations. After deuteration, the bands affected by mechanical strain at around 6420, 6240 and 4670 cm^{-1}, which had been assigned to hydroxyl groups in cellulose, remained at these positions, suggesting that the inaccessible cellulose fraction was the main load-bearing component in wood. A small band at around 4700 cm^{-1} responding to mechanical strain was only visible in the deuterated spectra, indicating that accessible hydroxyls also contributed to the load transfer. Furthermore, the measurements confirmed previous reports of moisture adsorption of wood under tensile stress.

Chapter 5 investigated the possibility of measuring growth-strain non-destructively using NIR spectroscopy. This requires the measurement of water-saturated samples by reflection NIR. Results showed that abundant free water in rewetted and never-dried green samples overlapped with the band of interest and weakened the structural information of crystalline cellulose in the NIR spectra; reflection NIR spectra were shown to be of lower quality than

transmission spectra. Despite the weak signal for rewetted and green samples, the 6286 cm−1 band shifted linearly to higher frequencies with the increase in tensile strain, in both transmission and reflection NIR spectra, because of the elongation of hydrogen bonds in cellulose. Further, NIR band-shift rates were lower for never-dried green samples than for those previously dried, suggesting differences in macroscopic and molecular strain. Lastly, growth-strains of 163 green wood samples were measured destructively using strain gauges and correlated to previously collected NIR spectra. No correlation was found, however, between growth-strain of green stems as measured by strain gauges and the NIR spectra in reflection mode. Challenges included excessive signal overlap at high moisture content, lower signal-to-noise ratio of diffuse reflection compared with transmission NIR spectroscopy, and variations in growth-strain.

In Chapter 6, Raman spectroscopy was examined for its potential to measure growth-strain non-destructively, as the spectra are unaffected by water. A partial least squares model built from the Raman spectra could predict tensile strain with a root mean square error of 427.5 µε, in a dataset with growth-strain ranging from −135 µε to 4780 µε. Apart from the widely reported band shift at 1095 cm−1 upon mechanical strain, spectral changes at 1420, 1120, 895, 456 cm−1 were identified. These bands might be attributed to the molecular deformation of cellulose. The band shift rates during tensile tests were −3.06 and −2.15 cm−1/% for rewetted and green wood, respectively. As for the NIR measurements, the difference in the Raman band shift rates indicated that less macroscopic strain was transferred into molecular strain for green wood than previously dried wood. This indicated irreversible molecular changes in the wood cell walls upon air-drying below fibre saturation point. Further, Raman spectra were collected from the wood surface of 18 green eucalypt stems before measuring growth-strain. A moderate correlation was found between growth-strain measured with strain gauges and the 1095 cm−1 band position. Raman spectroscopy could be used to non-destructively estimate growth-strain with moderate accuracy, but was negatively affected by the inhomogeneity of wood, instrumental instability, and fluorescence effects.
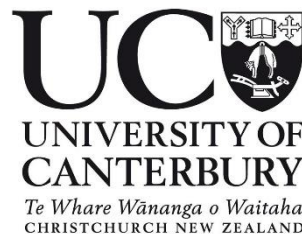
THESIS – NEXT PAGE

Molecular deformation of wood and cellulose studied by near infrared and Raman spectroscopy

A thesis

submitted in partial fulfilment

of the requirements for the Degree of

Doctor of Philosophy in Forestry

by

Fei Guo

UNIVERSITY OF CANTERBURY
Te Whare Wānanga o Waitaha
CHRISTCHURCH NEW ZEALAND

New Zealand School of Forestry
College of Engineering
University of Canterbury
2019

Senior supervisor:

Dr. Clemens Altaner

New Zealand School of Forestry, University of Canterbury

Co-Supervisor:

Dr. Deborah Crittenden

School of Physical and Chemical Sciences, University of Canterbury

TABLE OF CONTENTS

LIST OF FIGURES

LIST OF TABLES

ACKNOWLEDGEMENT

ABSTRACT

Eucalyptus can be alternative plantation species to radiata pine for New Zealand. One major problem preventing eucalyptus wood from high-value uses is its high growth-stress level, which causes problems in solid wood processing. Current methods to measure growth-strain are destructive and time-consuming. Growth-stress in wood, like mechanical stress, can cause deformation on the molecular level, which can be detected using spectroscopy. The overreaching objective of this thesis was to investigate the possibility of a non-destructive and rapid spectroscopy-based method to measure strain in wood. The molecular deformation caused by stress or strain was studied in detail using near infrared (NIR) and Raman spectroscopy.

Chapter 1 provides background and a literature review. In Chapter 2, the suitability of *Eucalyptus globoidea* for veneer and LVL production was investigated in relation to growth-strain levels. Veneer recovery, veneer splitting and wood properties were evaluated and correlated with growth-strain. Veneers with no, or limited, defects can be obtained from *E. globoidea*. Veneer recovery (54.5%) correlated with growth-strain and was highly variable between logs, ranging from 23.6% to 74.5%. There was a moderate positive association between splitting length and growth-strain (r = 0.73), but no significant association with wood stiffness. Growth-strain reduced veneer recovery by splitting, and was largely independent of stiffness, suggesting the possibility of finding trees with both low growth-strain and high stiffness, desirable for structural wood products. The considerable variation in growth-strain and stiffness indicated a possibility for genetic improvement. The unfavourable effects of growth-strain highlighted the demand for a rapid and non-destructive method to evaluate growth-strain levels in wood.

Chapter 3 describes experiments aimed at better understanding the effects of molecular deformation of wood and cellulose on NIR spectra. Dry wood and paper samples were stretched to different strain levels using a purpose-built tensile test device fitted into an NIR spectrometer while collecting transmission spectra. Consistent spectral changes caused by mechanical strain, assigned to OH stretching bands, were observed for all sample types. Bands at 6286 ± 5 cm^{-1} and 6470 ± 10 cm^{-1} were tentatively assigned to the OH groups connected with the 2OH$\cdots$6O and 3OH$\cdots$5O intramolecular hydrogen bonds of crystalline cellulose Iβ, respectively. Both bands shifted to higher wavenumbers, indicating the elongation of the hydrogen bonds. A linear relationship was found between band shifts and mechanical strain. Band shift rates for the 3OH bond were more than twice that of the 2OH bond, consistent with bending of the glycosidic bond. Bending tests showed that the band at around 6286 cm^{-1} shifted in opposite direction when under tension or compression.

Chapter 4 summarises the roles of water-accessible and -inaccessible cellulose in the load transfer of wood using deuterium exchange combined with NIR spectroscopy. The spectral changes on NIR spectra caused by mechanical strain could be highlighted by averaging the loading and unloading cycles to compensate for effects of desorption and isotope re-exchange due to environmental fluctuations. After deuteration, the bands affected by mechanical strain at around 6420, 6240 and 4670 cm^{-1}, which had been assigned to hydroxyl groups in cellulose, remained at these positions, suggesting that the inaccessible cellulose fraction was the main load-bearing component in wood. A small band at around 4700 cm^{-1} responding to mechanical strain was only visible in the deuterated spectra, indicating that accessible hydroxyls also contributed to the load transfer. Furthermore, the measurements confirmed previous reports of moisture adsorption of wood under tensile stress.

Chapter 5 investigated the possibility of measuring growth-strain non-destructively using NIR spectroscopy. This requires the measurement of water-saturated samples by reflection NIR.

Results showed that abundant free water in rewetted and never-dried green samples overlapped with the band of interest and weakened the structural information of crystalline cellulose in the NIR spectra; reflection NIR spectra were shown to be of lower quality than transmission spectra. Despite the weak signal for rewetted and green samples, the 6286 cm^{-1} band shifted linearly to higher frequencies with the increase in tensile strain, in both transmission and reflection NIR spectra, because of the elongation of hydrogen bonds in cellulose. Further, NIR band-shift rates were lower for never-dried green samples than for those previously dried, suggesting differences in macroscopic and molecular strain. Lastly, growth-strains of 163 green wood samples were measured destructively using strain gauges and correlated to previously collected NIR spectra. No correlation was found, however, between growth-strain of green stems as measured by strain gauges and the NIR spectra in reflection mode. Challenges included excessive signal overlap at high moisture content, lower signal-to-noise ratio of diffuse reflection compared with transmission NIR spectroscopy, and variations in growth-strain.

In Chapter 6, Raman spectroscopy was examined for its potential to measure growth-strain non-destructively, as the spectra are unaffected by water. A partial least squares model built from the Raman spectra could predict tensile strain with a root mean square error of 427.5 µε, in a dataset with growth-strain ranging from −135 µε to 4780 µε. Apart from the widely reported band shift at 1095 cm^{-1} upon mechanical strain, spectral changes at 1420, 1120, 895, 456 cm^{-1} were identified. These bands might be attributed to the molecular deformation of cellulose. The band shift rates during tensile tests were −3.06 and −2.15 cm^{-1}/% for rewetted and green wood, respectively. As for the NIR measurements, the difference in the Raman band shift rates indicated that less macroscopic strain was transferred into molecular strain for green wood than previously dried wood. This indicated irreversible molecular changes in the wood cell walls upon air-drying below fibre saturation point. Further, Raman spectra were collected from the wood surface of 18 green eucalypt stems before measuring growth-strain. A moderate correlation was found between growth-strain measured with strain gauges and the 1095 cm^{-1} band position. Raman spectroscopy could be used to non-destructively estimate growth-strain with moderate accuracy, but was negatively affected by the inhomogeneity of wood, instrumental instability, and fluorescence effects.

Deputy Vice-Chancellor's Office
Postgraduate Research Office

Co-Authorship Form

This form is to accompany the submission of any thesis that contains research reported in co-authored work that has been published, accepted for publication, or submitted for publication. A copy of this form should be included for each co-authored work that is included in the thesis. Completed forms should be included at the front (after the thesis abstract) of each copy of the thesis submitted for examination and library deposit.

Please indicate the chapter/section/pages of this thesis that are extracted from co-authored work and provide details of the publication or submission from the extract comes:

Chapter 2 was published as: Guo, F., & Altaner, C. M. (2018). Properties of rotary peeled veneer and laminated veneer lumber (LVL) from New Zealand grown Eucalyptus globoidea. New Zealand Journal of Forestry Science, 48(1), 3.

Chapter 3 was published as: Guo, F., & Altaner, C. M. (2018). Molecular deformation of wood and cellulose studied by near infrared spectroscopy. Carbohydrate Polymers, 197, 1-8.

Chapter 4 was published as: Guo, F., & Altaner, C. M. (2019). Effects of mechanical stretching, desorption and isotope exchange on deuterated eucalypt wood studied by near infrared spectroscopy. Spectrochimica Acta Part A: Molecular and Biomolecular Spectroscopy, 211, 254-259.

Thesis chapter 5 has submitted to Cellulose as: Guo, F., Cramer, M., & Altaner, C. M. (2019) The possibility of non-destructive measurement of growth-stress in trees: A near infrared spectroscopic approach.

Please detail the nature and extent (%) of contribution by the candidate:

Fei Guo led to the experimental design, carried out the field work and the lab experiments, analysed the data and prepared the manuscripts. Clemens Altaner (supervisor) provided guidance on the experimental design, data interpretation and manuscript revision. Marlene Cramer conducted the measuremtns on green E. nitens stems. Fei Guo is the first author on all manuscripts and his contribution for these co-authored chapters was more than 85%.

Certification by Co-authors:
If there is more than one co-author then a single co-author can sign on behalf of all
The undersigned certifies that:
▪ The above statement correctly reflects the nature and extent of the PhD candidate's contribution to this co-authored work
▪ In cases where the candidate was the lead author of the co-authored work he or she wrote the text

Name: *Dr. Clemens Altaner*   Signature: *C. A*   Date: 25/2 /2019

1   INTRODUCTION

1.1   Background

To meet the increasing international demand for wood, some fast-growing species like pines, eucalyptus and poplar, have been favoured for tree plantations. Fast-growing planted trees have wider growth rings and potentially a much higher juvenile wood content than wood from natural forests, and therefore have inferior wood properties (Bao et al., 2001). However, eucalyptus can have relatively high basic density and air-dry stiffness while growing fast (de Carvalho et al., 2004), which can be 0.68 g/cm^3 and 17 GPa for *Eucalyptus globoidea, 0.88* g/cm^3 and 21 GPa for *E. bosistoana* and 0.53 g/cm^3 and 13 GPa for *E. nitens* (Bootle, 2005). In contrast, the dominant plantation species of New Zealand, *Pinus radiata*, only has a basic density of approximately 0.38 g/cm^3 (Chauhan & Walker, 2006) and an air-dry stiffness of 9.1 GPa (Bootle, 2005). Additionally, several eucalyptus species like *E. globoidea*, *E. muelleriana* and *E. bosistoana* can produce naturally durable wood (Millen, 2009; Page & Singh, 2014).

Eucalyptus plantations were estimated in 2009 to cover more than 20 million ha, mainly distributed across Australia, India, Brazil, China and Africa (Iglesias & Wilstermann, 2009). However, plantation eucalyptus is mainly used for low-value applications like pulp, firewood and charcoal. There is an increasing interest in using this resource for higher value solid wood products. Recently, the New Zealand Dryland Forest Initiative (NZDFI) has established a project to breed *Eucalyptus bosistoana* as a high-value timber resource (Millen, 2009; Millen et al., 2018). Instead of merely focusing on high growth rate and improved form, favourable wood properties are key objectives in their breeding programme to produce high-value timber and increase growers' profitability.

A major problem preventing eucalyptus from solid wood uses is its high growth-stress. The release of growth-stress will cause problems like heart checking, end-splitting, internal checking and board distortion during wood processing. Currently, growth-stress is mainly evaluated by measuring the strain released by drilling or cutting, such as the Nicholson method (Nicholson, 1971) and the CIRAD method (Gerard et al., 1995), which are both destructive and cumbersome. Stress causes changes in the wood structure on the molecular level. It has been shown that molecular strain in wood can be studied by X-ray diffraction (Peura et al., 2007) Raman (Eichhorn et al., 2001) and infrared (IR) (Salmén & Bergström, 2009) spectroscopy. Both reflection mode near infrared (NIR) and Raman spectroscopy can be used for in situ measurements due to their easy sampling and portability. It is conceivable, therefore, that rapid and non-destructive methods based on spectroscopy can be developed to predict the growth-strain levels in standing trees or logs, promoting solid wood uses of eucalyptus by segregation based on growth-stress.

In this work, the aim was to investigate the effects of mechanical strain and growth-strain on the NIR or Raman spectra of wood, and thus attempt to measure the molecular strain of wood using NIR and Raman spectroscopy. Additionally, as wood in trees is fully water saturated, the effects of moisture on the spectra need to be investigated. Deuteration and polarisation are useful techniques to understand the band assignments of NIR spectra. This research can potentially provide new insights into the structure of wood and cellulose on a molecular level.

1.2   Wood and stress

1.2.1   The woody cell wall

Natural materials fulfil various functions, for which they are optimised. Wood provides water transportation and mechanical support for trees. Consequently, plant cell walls developed a delicate hierarchical architecture as shown in Figure 1-1 (Harrington, 2002), expressed in

1

cell shape, cell-wall layers, orientation of microfibrils and their chemical composition (Burgert, 2006).

Wood is a natural composite of oriented cellulose microfibrils embedded in a matrix of lignin and hemicellulose. Cellulose has a partly crystalline structure and provides tensile strength and stiffness to the cell wall (Altaner et al., 2014b). Cellulose is believed to be the main component to bear tensile stress, while no response from lignin and hemicellulose was detected for wood samples under tensile stress (Salmén & Bergström, 2009). The role of the matrix under tensile stress and its interaction with microfibrils remains elusive.

Wood cell walls are layered structures (Figure 1-2), consisting of a middle lamella, primary and secondary walls. The middle lamella consists mostly of lignin and pectin, but only 25% of the total lignin occurs in this layer because it is thin compared with the other cell wall layers. The primary cell wall needs to be stretchable to accommodate growth, but still rigid to withstand internal pressure (Burgert, 2006).
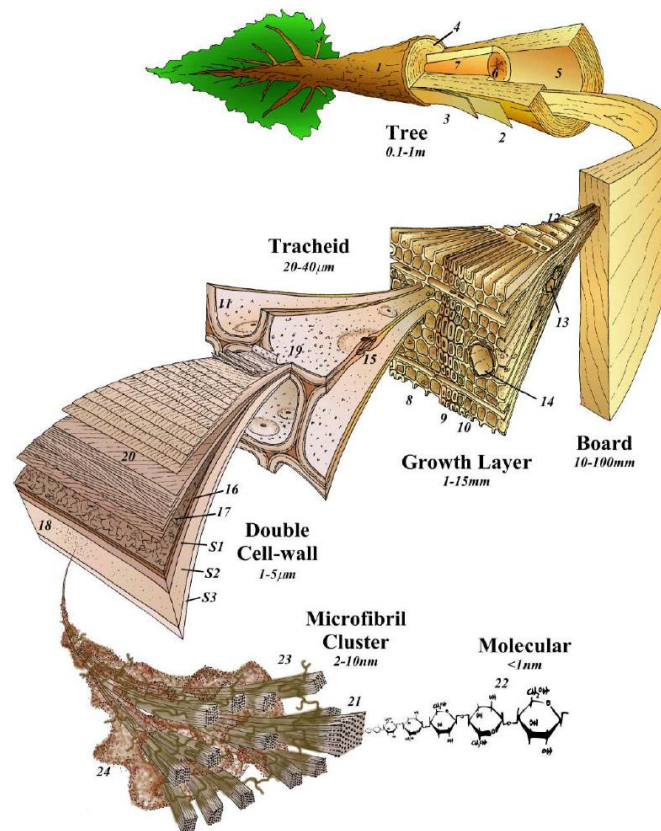
Figure 1-1 Hierarchical structure of wood on various levels (Harrington, 2002)
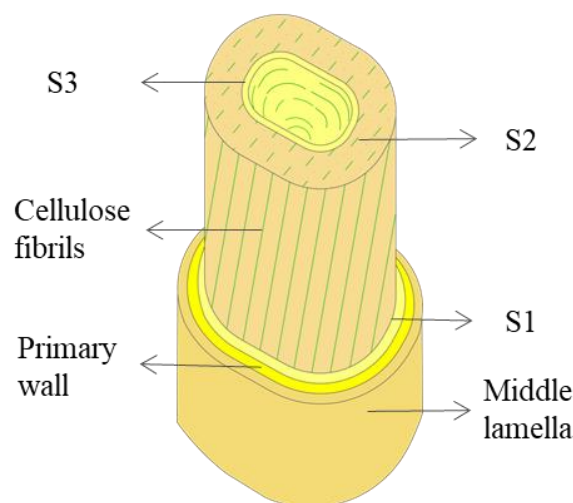
Figure 1-2 Schematic drawing of wood cell wall structure

Secondary call walls typically have three layers, the S1, S2 and S3, among which S2 is the thickest layer and dominates wood properties. Cellulose microfibrils in the S2 are oriented in a certain angle (MFA) with respect to the long axis of the cell (Figure 1-2). The MFA has significant effect on the mechanical and physical properties of wood (Donaldson, 2008; Downes et al., 2002). The MFA depends on the source of plant fibers (De Rosa et al., 2010). The MFA of wood varies significantly between and within trees. The MFA of gymnosperms is generally higher than that of angiosperms, and it decreases from pith to bark for both (Lachenbruch et al., 2011). The MFA of *Pinus radiata* (more than 25 years old) has mean values between 18° and 22° (Downes et al., 2002). In comparison, the MFA of balsa wood can be as low as 1.4° (Borrega et al., 2015). Additionally the MFA was reported to be larger at the base of the tree for a given growth ring. MFA can also be strongly influenced by environmental factors. For instance, MFA for compression wood is higher than in normal wood, while that for tension wood is smaller (Donaldson, 2008).

1.2.2 Growth-stress

1.2.2.1 Generation of growth-stress

Growth-stress refers to the mechanical stresses developing in trees as they grow. Growth-stresses are a combination of two stresses: support stress and maturation stress. Support stress is a response to the weight of the tree, while maturation stress occurs spontaneously during wood formation (Clair et al., 2006). In the following, the term growth-stress is used largely in the sense of maturation stress.

Two theories have been proposed to explain the mechanism for the generation of growth-stress (Archer, 1987; Okuyama et al., 1994). The "lignin swelling" theory claims that the cell wall of newly formed cells thickens during the lignification process of the developing cell wall. As cellulose fibrils are aligned, the swelling of the matrix is restricted to the direction perpendicular to cellulose fibrils, and the rigid fibrils force the cell wall to contract along the cellulose fibrils. Typically, cellulose fibrils are aligned close to the cell's axis direction, resulting in longitudinal contraction; however, when cellulose fibrils wind with a large angle around the cell lumen, longitudinal expansion is observed. The theory fails, however, to explain the large tensile strain in tension wood, a special wood tissue in angiosperms, which has low lignin content.

An alternative theory is the "cellulose contraction" theory. It was hypothesized that cellulose microfibrils tend to contract after they have been deposited onto a forming cell wall (Kubler, 1987). This would induce longitudinal tensile stress in wood with axially aligned cellulose fibrils. But the theory is inappropriate to explain the longitudinal compressive stress in

3

compression wood, a special wood tissue in gymnosperms, which features a high lignin content with cellulose fibrils running at a large angle around the cell lumen (Toba et al., 2013; Yang & Waugh, 2001). The microfibril angle (MFA), the angle at which cellulose fibrils wind around the cell axis, is the most important factor affecting the magnitude and direction of growth-stresses. It was proposed that lignin swelling is effective when the MFA is larger than 30°, while cellulose contraction can explain cases with MFA smaller than 25° (Toba et al., 2013; Yamamoto, 1998).

Okuyama et al. (1994) combined those two theories and suggested that tensile stress from microfibril contraction and compressive stress from deposition of lignin exist at the same time. This "unified hypothesis" was supported by the theoretical prediction and observation of mechanical stresses, both in the cellulose microfibrils and the matrix (Toba et al., 2013). However, the theoretical calculations need further confirmation due to the use of estimated values for Young's modulus of cellulose crystals and Poisson's ratios.

1.2.2.2 **Distribution of growth-stress and its influence on wood uses**

Growth-stress is accumulated during tree growth and will be released when the trees are felled and sawn into boards. To demonstrate the effects of growth-stress, a procedure called "plank-stripping" was developed (Jacobs, 1945). Diametral planks were removed from trees and were then sawn into strips. The changes in lengths as well as curvature were recorded. Results indicated that outer strips tended to contract and strips near the pith tended to expand. Stress states can be inferred from the released strains.

Growth-stress can be resolved into three principal wood directions: longitudinal, tangential and radial. Although transverse stresses cause shakes and checks, most research focused on the longitudinal growth-stress. Following the plank-stripping study, many models of the distribution of stress and strain in trees have been developed. Cutting will cause stress redistribution and stress concentration effects. Detailed mathematical methods and modelling for these issues have been discussed by Archer (1987).

A longitudinal stress model was developed by Kubler (1987). According to this model, longitudinal strain can be expressed as a function of peripheral strain and distance across the radius as follows:

$$\varepsilon_1 = \varepsilon_{1p}[1 + 2\ln(r/R)] \tag{1.1}$$

where ε_1 is the longitudinal strain, ε_{1p} is the peripheral strain, r is the distance to the pith and R is the radius. The model implies that wood near the pith is under compression while wood close to the cambium is under tension.

Growth-stress can cause detrimental effects on wood utilization. When timber is cut, the growth-stress will redistribute to reach a new equilibrium state. End-splits can occur following the crosscut, because the longitudinal stress is released and transformed into transverse stresses. For a full-diameter board, the centre near the pith tends to expand while the outer part tends to shrink. As a result of the low strength of the pith, the board will split from the centre and bend outward, as shown in Figure 1-3. Growth-stresses are also related to other wood defects such as internal checking during drying, board distortion during sawing and brittle-heart. (Archer, 1987; McKinley et al., 2002).

Figure 1-3 Splitting of a diametral eucalyptus board

Some methods have been developed to reduce the undesirable effects of growth-stresses on timber production. For instance, hammering S-shaped hooks into the log ends can reduce end-splitting. Long-term water-spray storage can reduce the residual growth-stress (Yang & Waugh, 2001); however, these methods do not target the root causes. The generation of growth-stress is a biological process and are thus genetically controlled and affected by silviculture (Archer, 1987; Yang & Waugh, 2001). Breeding programmes based on the accurate and rapid evaluation of growth-stress are therefore likely to reduce this problem (Davies et al., 2017).

1.2.2.3 **Measurement of growth-stress**

It is impossible to measure growth-stresses directly. Growth-stresses are usually calculated by the measured strain and modulus of elasticity of the wood. The approaches to measure strains are destructive and involve cutting or drilling to release the growth-stress.
Those methods have been reviewed by Yang and Waugh (2001). In the Nicholson method, two studs are attached to the surface of a debarked tree stem parallel to wood grain. Then a wood segment containing those studs is removed from the tree. The change in distance between the two studs after removal is used to calculate the measured strain. The French method (CIRAD) involves two pins punched into the wood at a known distance (Figure 1-4). Then the change in distance between those two pins is measured after drilling a hole in the middle to release the strain. The strain gauge method originated from Japan: a strain gauge is glued to the wood and growth-stresses are released by sawing or boring around the strain gauge. Notably, strain data measured by the different approaches cannot be directly compared (Yang & Waugh, 2001). Researchers from the University of Canterbury developed a splitting-test method, which involves sawing a log into two halves. The gaps opening at both ends were highly correlated to the axial growth-stress (Chauhan & Entwistle, 2010). This method is suitable for measuring growth-stress in small-diameter trees.
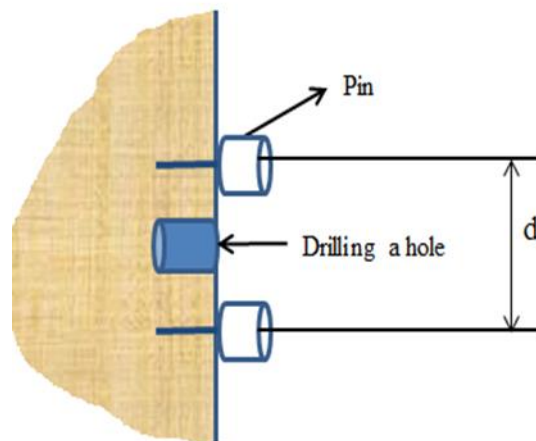
Figure 1-4 Schematic representation of CIRAD method

All those approaches are time-consuming and cumbersome. Rapid and non-destructive evaluation methods for growth-stress are desirable. There have been some attempts using stress waves to predict growth-strain based on the relationship between modulus of elasticity (MOE) and growth-stresses, but the relationship is inconsistent (Yang & Waugh, 2001). SiliviScan measurements were made to establish relationships between growth-stresses and various wood properties (Yang et al., 2006). However, because growth-stress varies within and between trees, a single wood property can only be moderately suitable for the prediction of strain. With a better understanding of the molecular response of wood to stress, spectroscopic methods including NIR and Raman could provide a quick and non-destructive approach.

1.2.3 Structure of cellulose

1.2.3.1 Cellulose microfibrils and crystalline structure

Cellulose is the most abundant organic biopolymer resource on earth. Native cellulose is a long-chain polymer with glucose units connected by β-1,4-glycosidic linkages. The degree of polymerization of cellulose can range from 500 to 15,000 (Brett, 2000). Several cellulose chains constitute a microfibril of a few nanometres in thickness. Cellulose microfibrils combine into aggregates of 10–20 nm in conifer wood (Fernandes et al., 2011). Microfibril diameters depend on the source, and can be 1.5–3.0 nm in primary cell walls, 2.2–3.6 nm for wood and as large as 15–25 nm for algae (Fernandes et al., 2011; Pérez & Samain, 2010).

Cellulose synthase complexes in the plasma membrane of cells are responsible for the polymerization of glucan chains, extruding cellulose chains (Wertz et al., 2010). It is believed that the microtubules inside the cytoplasm control the movement of the terminal complexes, and therefore the orientation (MFA) of microfibrils in the cell wall (Brett, 2000). Two spatial arrangements of terminal complexes have been observed that are thought to affect the shape and size of microfibrils (Wertz et al., 2010). In bacteria and some algae, subunits of terminal complexes are arranged linearly in single or multiple rows, while terminal complexes in the shape of hexagonal rosettes were observed in vascular plants. The synthetic subunits of the terminal complexes can synthesize cellulose chains. Nascent chains close to each other assemble to form a microfibril.

Since the terminal complexes in higher plant have six units, it is hypothesized that the numbers of chains in cellulose microfibrils should be divisible by six. A 36-chain microfibril

model has been frequently discussed (Wertz et al., 2010); however, a 24-chain microfibril model is favoured in spruce wood according to some experimental data (Fernandes et al., 2011; Thomas et al., 2013). Newman et al. (2013) suggested that an 18-chain model showed good consistency with both X-ray scattering and solid nuclear magnetic resonance (NMR) results.

Cellulose has crystalline and non-crystalline (also referred to as amorphous or disordered) regions. Crystalline cellulose regions are those with cellulose chains closely and regularly connected by hydrogen bonds, while cellulose chains in the disordered domain are accessible to water and chemical reactions. The two forms of cellulose were previously thought to alternate along the microfibril axis, but recent NMR and infrared evidence supported the parallel arrangement of those two forms, with crystalline cellulose cores covered by non-crystalline cellulose on the surface (Jarvis, 2018; Salmén & Bergström, 2009). The degree of crystallinity refers to the degree of structural order in cellulose (i.e. the ratio between crystalline and disordered cellulose), which varies between plant species. The crystallinity index of wood measured by X-ray scattering was reported to be ~50% for both pine and spruce wood (Andersson et al., 2004).

Cellulose can form different crystal polymorphs, including cellulose I, II, III and IV, which differ in their crystalline cell parameters. All native celluloses are cellulose I. Using NMR techniques, researchers found that native cellulose (cellulose I) is a composite of two distinct allomorphs: Iα and Iβ (Atalla & Vanderhart, 1984; VanderHart & Atalla, 1984). The proportion of the two crystalline forms depends on the cellulose origin. Cellulose Iα dominates in some bacteria and algae, while cellulose Iβ exists more in higher plants like wood, cotton, flax etc. Almost pure cellulose Iβ can be found in the outer membrane of marine animals like tunicates (*Halocynthia roretzi*) (Nishiyama et al., 2002; Pérez & Samain, 2010).

Cellulose Iα and Iβ differ in their crystal structures and hydrogen bonding systems. Phase Iα has a one-chain triclinic unit with a P1 space group whereas phase Iβ features a two-chain monoclinic unit with a $P2_1$ space group (Wertz et al., 2010). Schematic drawings of the two cellulose unit cells in the 001 crystal plane are shown in Figure 1-5 (Dumitriu, 2004; Pérez & Samain, 2010). Both Iα and Iβ allomorphs are arranged in the "parallel up" configuration with the reducing ends on one side and all the hydroxymethyl groups in tg conformation. The main difference between the Iα and Iβ structures is the relative displacement of adjacent cellulose sheets in the chain axis direction (Nishiyama et al., 2003).
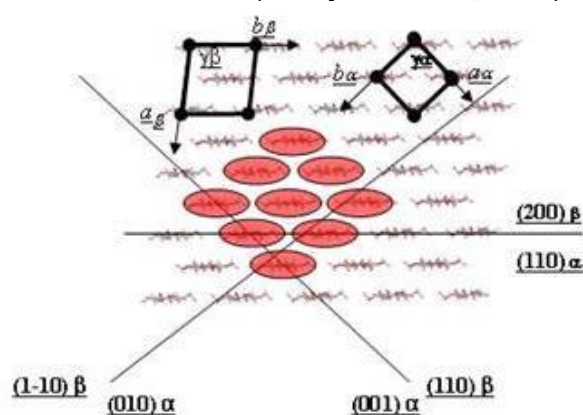
Figure 1-5 Crystal planes of cellulose Iα and Iβ. Reprinted from Pérez and Samain (2010). Copyright (2010), with permission from Elsevier.

1.2.3.2 Hydrogen bonds in cellulose

Cellulose has a substantial number of intramolecular and intermolecular hydrogen bonds. In plant cells, parallel cellulose chains are laterally bonded into sheets by intermolecular hydrogen bonds. Intramolecular hydrogen bonds in the chain axis direction provide linear stability. Those sheets are stacked on top of each other and held together by weak CH⋯O bonds and van der Waals forces (French et al., 2014). The large number of hydrogen bonds and van der Waals interactions make cellulose a stable structure (Jarvis, 2003; Stokke et al., 2013).

Nishiyama et al. (2002) studied the hydrogen bonding system of cellulose Iβ using X-ray and neutron fibre diffraction. The results showed that the O3H⋯O5 intramolecular hydrogen bond has well-defined positions, while other hydrogen bonds involving O6 and O2 are relatively disordered. This result suggests an inherent disorganization of the intermolecular hydrogen bonding system.

Based on the locations of hydrogen atoms shown by neutron crystallography, researchers proposed two hydrogen bonding networks for the centre chains of cellulose Iβ. Most chains (70–80%) are arranged in hydrogen bonding scheme A, and surface regions with defects are features of scheme B (Nishiyama et al., 2008).
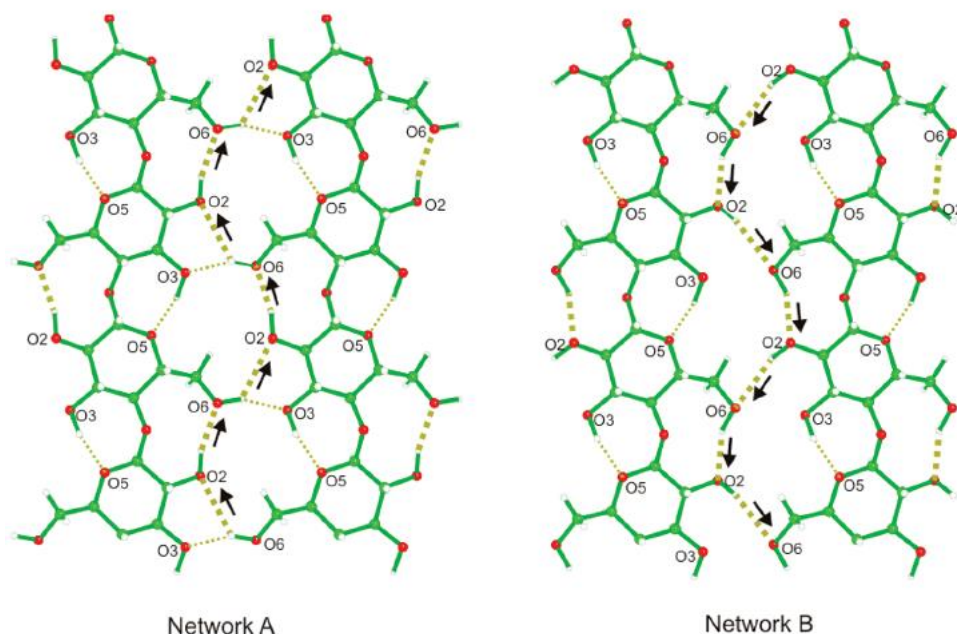
Figure 1-6 Two hydrogen bonding schemes in native cellulose. Reprinted with permission from Nishiyama et al. (2008). Copyright (2008) American Chemical Society.

Hydrogen bonds contribute greatly to the mechanical performance of cellulose. By studying the changes in molecular structure of cellulose under tension, researchers suggested that hydrogen and covalent bonds cooperate to form molecular leverage, and thus provide stiffness to cellulose chains (Altaner et al., 2014b).

According to Hofstetter et al. (2006), different hydrogen bonds have different accessibilities. They studied the interaction of hydrogen bonds between wood pulps with water using Fourier transform infrared spectroscopy (FT-IR) combined with deuteration. Results showed that few O3-H⋯O5 bonds were exchanged by deuterium, while O2-H⋯O6 bonds were much more accessible to deuteration. But the assignments of the IR bands of hydrogen bonds in this study are different from more recent assignments (Christopher M. Lee et al., 2015).

Table 1-1 Assignment of OH groups in native cellulose (Christopher M. Lee et al., 2015)

IR (cm^{-1})	main OH groups	hydrogen bond	6CH2OH conformation
3240	2O-H	Iα (intrachain), 2O−H···6O	tg
3270	2O-H	Iβ (intrachain), 2O−H···6O	tg
3300-3310	2,3,6O-H	(coupled) 2O−H···6O−H···3O−H···5O	tg
~3340	2,3,6O-H	(coupled) 2O−H···6O−H···3O−H···5O	tg
~3350	2,3,6O-H	(coupled) 2O−H···6O−H···3O−H···5O	tg
3370-3380	3O-H	(intrachain) 3O−H···5O	-
3400-3410	6O-H	(interchain) 6O−H···3O	tg
~3450	2,3,6O-H	weakly hydrogen-bonded OH groups in the less-crystalline or surface regions	tg>gt>gg

The assignment of hydrogen bonds in IR spectra is challenging for several reasons. First, the O-H stretching region is quite broad (3,000–3,800 cm^{-1} in mid-range) because of the overlap of several hydrogen bonds and stretching modes. According to Christopher M. Lee et al. (2015), previous attempts to assign OH vibration peaks are inaccurate due to the use of outdated cellulose models with incorrect bond lengths and angles. In addition, vibrational coupling of the OH groups leads to an inaccurate assignment based on the simple correlation of peak position to the O-H···O distance. They compared the calculation results from density functional theory (DFT) and molecular dynamics (MD) simulations with experimental data of IR and sum frequency generation (SFG) measurements, and obtained a full assignment of OH stretching peaks (Table 1-1) for cellulose (Christopher M. Lee et al., 2015).

1.2.4 Molecular deformation of wood and cellulose in response to stress

Cellulose crystals have extraordinary mechanical properties, and their high stiffness provides a framework for wood. There is still no consensus on the modulus of crystalline cellulose (Eichhorn et al., 2010). Recent reports, with a few exceptions, were in the range of 100–160 GPa. Considering the low density, crystalline cellulose has a strong specific modulus compared with steel and glass. However, this value is not found in native plant fibres because microfibrils contain "defects", that is, disordered cellulose fractions. Much research has been done to isolate crystalline cellulose nanofibres and use this strong material as reinforcement in composites (Eichhorn et al., 2010).

1.2.4.1 Deformation due to applied mechanical stress

Tensile mechanical stress is the most widely applied method to study the deformation of wood and cellulose fibres. It not only provides information on the mechanical properties of these biomaterials but also sheds light on the interaction between wood components. The changes of cellulose lattice parameters can be monitored by X-ray diffraction (XRD) during deformation. According to a study on Norway spruce (Peura et al., 2007), cellulose crystals elongated along the molecule axis (c-direction) and shortened between cellulose sheets (a-direction) upon axial stress. The relative elongation of the unit cell was much lower than the macroscopic strain of the sample, which indicated that the deformation of non-crystalline components contribute to the overall elongation (Peura et al., 2007). Contraction in the b-

dimension (within a cellulose chain sheet) and an increase in the monoclinic angle were also reported under axial tension (Altaner et al., 2014b).

Molecular responses to stress can be detected by various spectroscopic techniques, including infrared, Raman and NIR spectroscopy. As shown by a dynamic FTIR study on the deformation behaviour of cellulose, stress was mainly distributed in the glucose ring, the C-O-C glucosidic linkage and the intramolecular the O3-H···O5 bond, while the O2-H···O6 played a minor role (Hinterstoisser et al., 2003). Another FTIR study on wood sections showed that the shift of the 1160 cm^{-1} peak corresponding to C-O-C vibrations was linearly correlated to the applied strain (Salmén & Bergström, 2009).

Raman spectroscopy was applied to study the deformation mechanisms of different cellulose fibres, wood and paper (Eichhorn et al., 2010). Results showed that the 1095 cm^{-1} band assigned to cellulose-ring stretching shifted to lower wavenumbers during tensile stretching. This band shift has been confirmed by other researchers (Peetla et al., 2006). Moreover, stress-induced Raman band shifts of various cellulosic materials were different with strain, and invariant with stress, which indicates that the shift is controlled by stress. Gierlinger *et al.* (2006) proposed that the change in the height ratio of the 1127 and 1097 cm^{-1} bands can be interpreted as the change of torsion angle of the glycosidic C-O-C bond. The changes in the OH stretching region around 3375 cm^{-1} were interpreted as a sign of weakening of hydrogen bonding, but need further investigation.

Based on some multivariate statistical methods like partial least squares (PLS) models, NIR has been used as a non-destructive tool to predict changes in molecular structures, chemical composition and other wood properties (Tsuchikawa, 2007). Wood responses to tensile stress on the molecular level were monitored by NIR spectroscopy and a model was built on the basis of NIR spectra to predict the stress level (Sandak et al., 2013). NIR spectroscopy combined with a PLS model was also applied to predict the load applied to small wood beams in four-point bending (André et al., 2006). Knowledge about the functional groups and band assignment is not necessary for building multivariate models.

1.2.4.2 Deformation induced by growth-stress

Dimensional changes of cellulose microfibrils in tension wood can be detected by X-ray diffraction. It was found that the cellulose lattice spacing in the c-axis direction decreased after the release of maturation stress (Clair et al., 2006). This value was larger for the gelatinous layer of tension wood than that of normal wood (Clair et al., 2011).

Another research group measured the lattice spacings of crystalline cellulose in wood samples using wide-angle X-ray diffraction before and after boiling (Toba et al., 2013). Results showed an increase in d_{200} (a-direction) and a decrease in d_{004} (c-direction) lattice spacing after boiling, which indicates that a part of the growth-stresses remained in the wood even after relaxation by removal from the tree stem.

A recent study tried to predict longitudinal growth-strain using a partial least squares regression model based on NIR spectra collected on the surface of green Sugi (*Cryptomeria japonica* D. Don) logs (Watanabe et al., 2013). The results indicated that NIR is a possible approach but needs further refinement with more samples. This research did not analyse band shifts and band assignments and most likely relied on pre-announced differences in the chemical compositions of normal and compression wood (Timell, 1986).

1.2.5 Molecular deformation due to moisture or temperature

Apart from mechanical stress, temperature can affect the cellulose structure at the molecular level. A study by Altaner et al. (2014a) investigated the changes of IR-spectra of cellulose Iβ at low temperatures in the range between −180 °C and +20 °C. The results are consistent with weak C–H···O hydrogen bonds between cellulose sheets. Furthermore, it was

suggested that the blue shifts of O-H stretching with increasing temperature were not caused by the thermal expansion of crystal structure.

The thermal expansion behaviour of cellulose Iβ at temperatures from 20 °C to 300 °C has been studied using X-ray diffraction (Wada et al., 2010). The anisotropic thermal expansion behaviour of cellulose Iβ was interpreted as a result of the intermolecular hydrogen-bonding system (Wada, 2002; Wada et al., 2010). Another IR study monitored the structural changes of cellulose Iβ over the range from 30 °C to 360 °C and attributed the phase transition at 220 °C to the dissociation of intramolecular hydrogen bonds (Watanabe et al., 2006a).

It is widely accepted that moisture affects the amorphous matrix substance in the cell wall, but has little effect on cellulose crystals; however, X-ray measurements of wood samples revealed that cellulose crystals shrank longitudinally and expanded transversely during drying (Abe & Yamamoto, 2006). Hill et al. (2010) also observed changes in the molecular packing of cellulose during drying of wood. The deformations of cellulose crystals as a result of tensile and dehydration stress were measured through X-ray diffraction (Zabler et al., 2010). Those two effects caused different deformations in nature and magnitude. Dehydration shortened cellulose crystals in the longitudinal direction (by 0.2%), but expanded it in the transverse direction (by 0.6%), whereas with tensile strain, a longitudinal elongation was observed without transverse contraction.

Researchers hold different views on the mechanisms of cellulose deformations caused by moisture content change. Abe and Yamamoto (2006) suggested that cellulose crystals in green wood are compressed by the swollen matrix. During drying, the decline of compression stress resulted in the transverse expansion of the cellulose crystals. However, considering the strong lateral stiffness of cellulose crystals, Zabler et al. (2010) argued that it was unlikely for the matrix to generate enough compressive stress. They assumed that the capillary condensation of water in nanoporous structures leads to strong compressive stresses, sufficient to shorten the lateral a-axis by 0.6%.

Recently, by studying the dimensional changes of cellulose microfibrils in wood during repeated wet–dry treatments using X-ray diffraction, researchers concluded that microfibrils expanded laterally during drying because the matrix shrank laterally (Toba et al., 2012). They suggested that an interfacial separation between cellulose microfibrils and matrix will occur after repeated wetting and drying.

To predict the drying stress levels of wood, a PLS model was built based on NIR spectra in relation to released strain (Watanabe et al., 2013). However, it is difficult to separate the effect of strain on NIR spectra from that of moisture content changes, contributing to the relatively poor estimation ability ($R^2 = 0.72$) of the PLS model.

1.3 Spectroscopy applied to wood and cellulose analysis

1.3.1 Vibrational spectroscopy

Molecules can absorb and emit electromagnetic radiation of certain frequencies, resulting in transitions between energy levels in the molecules. Absorption of visible light causes a transition in the energy state of electrons, while infrared and near infrared can cause changes in vibrational or rotational states. Based on classical mechanics the vibrational frequency can be determined for a diatomic molecule from the following equation (Larkin, 2011):

$$v = \frac{1}{2\pi}\sqrt{\frac{k}{\mu}} \qquad\qquad (1.2)$$

where v is the vibrational frequency; k is the force constant and μ is the reduced mass defined as $(m_1 m_2)/(m_1+m_2)$ with m_1 and m_2 being the masses of the two atoms. Therefore, the vibrational frequency of a chemical bond depends on the masses of its atoms as well as its bond strength, which is in turn affected by bond length.

Infrared spectra contain rich information about the chemical composition and molecular structure of wood cell walls. The electromagnetic spectrum can be divided into three regions

(Osborne et al., 1993). Normally, the NIR region ranges from 14300 cm^{-1} to 4000 cm^{-1} (700−2500 nm), the mid-infrared (MIR) region from 4000 cm^{-1} to 200 cm^{-1}, and the far-infrared (FIR) region from 200 cm^{-1} to 10 cm^{-1}.

1.3.1.1 Near infrared (NIR) compared with mid-infrared (MIR) spectroscopy

Fundamental stretching and deformation vibrations are located in the MIR region. NIR spectra contain the overtones and combinations of fundamental vibrations of bands. NIR spectra are dominated by bonds involving hydrogen-like O-H and C-H bonds, due to the low reduced mass of H-related bonds (Osborne et al., 1993). Therefore, NIR is sensitive to hydrogen bonding and interactions with water.

Since overtones are weaker than fundamental vibrations, less energy is absorbed in the NIR region. This allows the analysis of a few millimetres thick wood samples in transmission mode (Schwanninger et al., 2011). For MIR, only very thin samples (20–30 µm) can be used in transmission mode due to the high absorption (Tsuchikawa & Siesler, 2003a). Powdered samples are an alternative, but factors like particle size, surface roughness and porosity affect the spectra (Faix & Böttcher, 1992). Sample size has been reported to affect mechanical performance (Buchelt & Pfriem, 2011). Thicker wood samples keep their cellular structure intact, being stronger and stiffer (Yu et al., 2009). Damage caused by cutting has a significant effect on the mechanical performance of microtomed wood samples, used in previous studies (Altaner et al., 2014b; Salmén & Bergström, 2009). Interactions between thick wood samples and water or mechanical stress are observable only by NIR, but such experiments have not been reported.

MIR and NIR spectroscopy can be performed in transmission and reflection mode. Instead of measuring light transmitted through a sample, the reflection mode measures absorption properties of a sample from the reflected light. Diffuse reflection mode is very useful for powders and solid samples with rough surfaces (Khoshhesab, 2012). Spectroscopy of wood in diffuse reflection mode does not need much sample preparation. In contrast, MIR has a higher requirement for sample preparation, such as cutting thin tissue sections with a microtome or pressing KBr (potassium bromide) pellets with powder. The simplicity of sample preparation is a significant advantage of NIR.

The transmission mode provides a strong signal and consequently good spectra. Diffusely reflected radiation is scattered in all directions, most of which cannot be collected by the detector. For MIR, since more energy is absorbed and less is scattered than with NIR, the diffuse reflection is weak, and the diffuse reflection mode is therefore less common for MIR (Khoshhesab, 2012). Due to the easy sample preparation and more efficient diffuse reflection, it is possible for NIR spectrometers to be manufactured as portable devices. NIR analysis can be non-destructive, fast and simple to perform, and allows deeper sampling rather than just the surface. These advantages enable NIR to be used for online monitoring and production control (Meglen & Kelley, 2003) and have the potential to measure growth-stress in standing trees. However, NIR spectra are less resolved and dominated only by CH and OH bonds.

1.3.1.2 Interpretation of NIR spectra

NIR spectra contain rich information, but it is difficult to assign the underlying molecular causes. Many factors make it challenging to establish a good relationship between NIR spectra and the molecular structure. Wood is a natural composite of cellulose, hemicellulose and lignin, bearing similar functional groups, and causing their signals to overlap. Their

native structure is invariably altered during isolation from wood, making it impossible to obtain references.

As mentioned above, the NIR region corresponds to the overtones and combinations of fundamental vibrations. Overtones are weaker than fundamental vibrations. The relative absorption intensity of the first overtone is approximately 1% of the fundamental vibrations (Schwanninger et al., 2011). The low absorption and broad shape result in highly overlapped NIR bands.

Although quantum theory and anharmonic oscillators can be applied to calculate the location of overtones, the chemical environment and coupling between neighbouring bonds make it difficult to predict signal frequencies. For instance, the fundamental stretching of CH bonds occurs in the region of 2972–2843 cm^{-1} for alkanes, 3010–3095 cm^{-1} for alkenes and 3310–3320 cm^{-1} for alkynes (Osborne et al., 1993). As two or more bonds are connected to a common atom or the frequencies of two vibrations are similar, their frequencies will change due to the coupling effect. In addition to coupling, combination bands that represent the sum of two or more different vibrations make it a rather entangled situation.

NIR contains rich but repetitive information. CH bonds are present in all organic compounds and CH vibrations occur throughout the entire NIR spectrum. According to Schwanninger et al. (2011), the first overtone of CH stretching in methyl groups can have four bands. Deformation vibrations and different combinations make assignments even more complex. Hydroxyl groups are often involved in hydrogen bonding, which affects the strength of the OH bonds and results in a band shift compared to free OH groups. Cellulose has abundant intermolecular and intramolecular hydrogen bonds (Figure 1-6). Temperature and mechanical stress can induce changes in bond length and bond strength (Altaner et al., 2014a; Altaner et al., 2014b). These changes of OH bonds are reflected in MIR and NIR spectra. Lastly, wood is a hydrophilic material and the adsorbed water affects the NIR spectrum significantly. Changes of moisture content in wood are associated with the formation and breaking of hydrogen bonds. In summary, NIR spectra are informative, but it is challenging to understand the origin of spectral bands.

1.3.1.3 **Far-infrared spectroscopy (FIR)**

FIR, also termed "terahertz spectroscopy", fills the gap between the MIR region and microwaves (Mantsch & Naumann, 2010). There is no consensus on the delimitation of the terahertz region, and it can be 10–100 cm^{-1} (0.3-3 THz), or a wider region of 3.3–333.3 cm^{-1} (0.1–10 THz). Time domain terahertz spectroscopy measures the transmitted and reflected terahertz pulse as a function of time, which then can be Fourier-transformed into a spectrum. Compared with traditional frequency domain spectroscopy, time domain terahertz spectroscopy can detect both the amplitude and the phase of terahertz radiation (Mantsch & Naumann, 2010).

FIR spectroscopy has several advantages over the other spectroscopic techniques. Many non-conducting materials are very transparent to terahertz waves, including paper, wood, clothing, plastics. This means materials can be detected through packaging and clothing, whereas water and metal are opaque to it. Terahertz radiation is non-ionizing and safe for biological tissues. Most importantly, many materials have a distinctive fingerprint in FIR spectra; FIR can therefore be used as a spectroscopic imaging method not only to identify materials such as explosives in the security area but also cellulosic fibres like ramie and bamboo for quality control (Mantsch & Naumann, 2010; Yan et al., 2013).

Apart from imaging, terahertz spectroscopy can be informative about molecular structure. For small molecules like water, rotational frequencies can be observed in this region. For organics and biopolymers, the region contains information about collective vibrational motions and intermolecular interactions, and is especially sensitive to hydrogen bonds (Lee, 2009).

FIR spectra of powdered saccharides samples including glucose and cellobiose were measured in the region of 500 to 50 cm^{-1} several decades ago, but the observed peaks were not assigned (Hineno & Yoshinaga, 1972). A variety of modified cellulose samples pressed into tablets were studied in the region of 700–10 cm^{-1} and it was indicated that absorption bands can be assigned to the vibrations of polymeric chains in the crystalline area (Mukhamadeeva et al., 1990).

To date, the application of FIR in the wood science area is very limited. Solid wood showed birefringence and attenuation properties in the far-infrared region, and wood samples as thick as 1 cm can transmit FIR radiation (Reid & Fedosejevs, 2006). Terahertz imaging was examined as a non-destructive method for density mapping, and the absorption correlated well with wood density (Koch et al., 1998). Considering the sensitivity of FIR to water and hydrogen bonds, it might be a useful tool to study the molecular deformation of cellulose and the hydrogen bonding system.

1.3.1.4 **Raman spectroscopy**

When electromagnetic radiation is directed onto a sample, it will be scattered elastically and inelastically. Elastic scattering is referred to as Rayleigh scattering; inelastic scattering from the interaction of laser light with matter is called Raman scattering. Raman scattering contains information about molecular vibration, but Raman scattering is much weaker than Rayleigh scattering.

Raman spectroscopy and MIR are in the same wavelength region, and both are based on the transitions between vibrational energy levels of chemical bonds. Raman spectroscopy can use visible or NIR light sources. Only a small portion of the energy is absorbed by the sample, causing changes in vibrational energy levels. A vibration is infrared active if there is a change in the electric dipole moment of a band. In order for a molecule to be Raman active, there must be a change in its polarizability. As a result, those two techniques are complementary. Some vibrations that are weak or inactive in MIR spectra can be strong or active in Raman spectra and vice versa. Water has a weak signal in Raman spectra, and so the absence of disturbance from moisture changes can be an advantage for Raman spectroscopy over infrared spectroscopy in hydrophilic materials like wood and cellulose.

Raman spectroscopy has evolved greatly in the past 30 years and is becoming increasingly popular because of its easy sampling and high resolution. Nowadays, portable Raman spectrometers with a resolution of 8–12 cm^{-1} are available. Portability opens up a wide range of applications including plastics identification, forensic science and medical diagnostics (Carron & Cox, 2010). Raman spectroscopy has potential as a non-destructive method of measuring wood properties on standing trees or logs.

Raman spectroscopy has been a feasible method to determine the chemical composition of *Eucalyptus sp.* (Ona et al., 1997). A recent study of various cellulose materials using Raman spectroscopy indicated that internal chains of never-dried wood cellulose were accessible to deuterium exchange. This work also suggested cellulose existed in both tg and gt conformations (Agarwal et al., 2016). Apart from spectroscopy, Raman microscopy is becoming increasing popular due to its high resolution. It has been used to characterize the chemical distribution within wood cell walls with a spatial resolution less than 0.5 µm (Gierlinger & Schwanninger, 2006; Richter et al., 2011).

Raman spectroscopy has been proven to be a powerful tool to study the response of wood or cellulose to stress at a molecular level. The band shift of the stretching motion of the cellulose ring around 1095 cm^{-1} has been investigated by different research groups (Eichhorn et al., 2001; Gierlinger et al., 2006; Peetla et al., 2006). This, combined with the easy sampling, good resolution and portability, shows that Raman spectrometers could be a potential tool to predict the stress level in standing trees.

1.3.2 Polarization combined with spectroscopy

Polarizers are useful tools in spectroscopy for the measurement of samples with molecular orientation. Polarizers are usually made of a fine grid placed on a suitable transparent substrate that causes passing electromagnetic light radiation to align. When the grid spacing is much smaller than the wavelength of the light, light can only pass in the direction parallel to the grid.

The main use of polarizers is to study the molecular orientation of samples. As the polarized light interacts with molecular dipoles, their interaction increases when its orientation coincides with the orientation of molecular groups of interest. The comparison of polarized spectra obtained from different directions (dichroic behaviour) allows conclusions about the orientation of the molecular groups in the sample. This has been used to aid the assignment of IR bands and the alignment of polymers in a material.

In wood cellulose, microfibrils are aligned, winding around the cell wall axis at an angle (MFA), as shown in Figure 1-2, and therefore, peak intensities in polarized spectra depend on the angle between the polarization direction and the fibre axis and are closely related to MFA (Schmidt et al., 2006).

Polarized MIR spectroscopy has been widely used to study the molecular structure of native cellulose. Researchers applied this technique to distinguish OH bonds by their orientation; for example, no significant difference was found in the temperature-induced band shifts between parallel-polarised OH bonds and perpendicular-polarised OH groups (Altaner et al., 2014a), and the hydroxyls in the hydrated fractions of cellulosic fibres were shown to be almost randomly orientated (Driemeier et al., 2015). The calculated angles between the OH stretch dipole moments and the chain axis were suggested to be close to random and ranged from 38° to 57° (Christopher M. Lee et al., 2015). The authors pointed out that it is therefore inappropriate to compare those values to individual OH groups in cellulose Iβ.

1.3.3 Hydrogen-deuterium exchange

Hydroxyl groups of cellulose can exchange hydrogen and deuterium atoms. This can provide valuable information about the hydrogen bonding system and molecular structure. Only the amorphous area and surface of the crystalline region of native cellulose are accessible for deuterium exchange when exposed to heavy water in the vapour or the liquid state. Under these conditions, inaccessible (intracrystalline) hydroxyl groups can be deuterated at high temperature or with the help of a swelling agent like NaOD (Nishiyama et al., 1999). Deuteration therefore makes it possible to differentiate between accessible and inaccessible hydroxyls, as this can be studied by gravimetric or spectroscopic methods (Hofstetter et al., 2006). According to vibration theory (Equation 1.2), the mass increase of deuterium compared to hydrogen will cause a theoretical shift in frequency by a factor of 1.34 (Hofstetter et al., 2006; Šturcová et al., 2004). The wavenumber of OD bands will be the corresponding wavenumber of OH bands divided by 1.34, although experiments showed a more complicated situation (Driemeier et al., 2015).

Deuteration does not change the structure of cellulose (Nishiyama et al., 2002). Hydrothermal deuteration of *Halocynthia* and *Cladophora* cellulose showed that absorption bands in the OH stretching region shifted to lower wavenumbers without any loss of resolution and retained all peak features (Nishiyama et al., 1999); however, as vapour-phase deuteration only happens in accessible hydroxyls, and signals from disordered surface chains are different from crystalline cellulose, OD band patterns differ from OH bands for partially deuterated cellulose (Thomas et al., 2013).

By studying the deuteration process of hardwood and softwood with different deuteration agents, researchers proposed that the spaces between aggregates of elementary fibrils vary between species (Tsuchikawa & Siesler, 2003a, 2003b). Dynamic (samples under sinusoidal strain) FT-IR of deuterium-exchanged cellulose showed limited exchange for load-bearing O3-H···O5 bonds and suggested that deuterated regions do not carry load (Hofstetter et al.,

2006). Deuterium exchange was also used to assist in the assignments of the OH and OD bending vibrations of cellulose in the region 1900–700 cm^{-1} (Driemeier et al., 2015). Another application of vapour-phase deuteration is to reduce the interference of hydroxyls from the amorphous region when studying ordered crystalline cellulose (Christopher M. Lee et al., 2015; Šturcová et al., 2004).In contrast, deuteration of only the crystalline region by partial internal deuteration can be achieved (Altaner et al., 2014b). First, samples were immersed in an alkali D_2O solution to exchange all OH groups, including those in the internal crystalline region. Then, samples were washed with H_2O to reconvert only the accessible OH groups. This method allowed the collection of MIR spectra of OD stretching bands from crystalline cellulose (Altaner et al., 2014b).

1.4 Thesis outline

Chapter 1 provides an overall introduction and a literature review regarding growth-stress in trees, the structure of wood cell wall and cellulose and the molecular deformation of wood and cellulose. It gives a brief summary of the generation, distribution and measurement of growth-stress and its effects on wood utilization. It also covers an overview of the spectroscopic techniques to investigate the deformation mechanism of wood on the molecular level, including NIR, MIR, Raman spectroscopy, deuteration and polarization.

Chapter 2 aims to measure growth-strain in trees and study the effects of growth-stress on wood utilization. Eucalypts can be an alternative fast-growing plantation species to radiata pine for New Zealand. Considering their high stiffness, eucalypts have great potential to produce high-value wood products. There is growing domestic as well as international interest from the wood processing sector in these species. The chapter will describe investigations into the suitability of *Eucalyptus globoidea* for veneer and LVL production with an emphasis on the effects of growth-strain levels. Veneer recovery, splitting and wood stiffness was analysed and correlated with growth-strain levels.

Chapter 3 focuses on the molecular deformation of air-dry wood and cellulose studied by NIR spectroscopy, which contains rich information about molecular structures. Although NIR spectroscopy combined with multivariate statistical analysis has wide applications in various research areas, few studies have used it to unravel the structure of wood and cellulose at a molecular level. Transmission NIR spectra of wood and paper under different tensile strain levels will be analysed in detail. The deformation mechanism of cellulose will be discussed, based on the NIR data. Additionally, non-destructive NIR measurements were conducted using reflection NIR spectroscopy with a fibre optics probe. It was used to monitor the tensile and compressive stress during the bending tests of wood.

Chapter 4 investigates the effects of mechanical stretching, desorption and isotope exchange on eucalypt wood using NIR spectroscopy coupled with deuteration and polarization techniques. Wood is a hygroscopic material and the NIR signal is sensitive to moisture desorption. Attempts were made to distinguish the spectral changes caused by mechanical stress from those by desorption and isotope exchange. Deuteration can separate accessible and inaccessible cellulose in wood, so NIR spectroscopy was used to monitor the deuteration process of wood. Protonated and deuterated wood were both stretched while NIR spectra were collected. This work could potentially provide new structural information about wood under mechanical stress and help to better understand the load transfer process on a molecular level.

Chapter 5 examines the possibility of non-destructive measurement of growth-stress in trees using NIR spectroscopy. No rapid and non-destructive method for measuring growth-strain is currently available but it is necessary to identify logs with low growth-strain for solid wood processing. High moisture content might interfere with the structural information about wood in the NIR spectra. The combined effects of mechanical strain and drying on the NIR spectra of water-saturated and green wood samples were investigated. Non-destructive measurements using a fibre optic probe was conducted on green wood, in an attempt to predict mechanical strain and growth-strain.

Chapter 6 deals with the use of Raman spectroscopy to study the molecular deformation of wood and to predict mechanical strain and growth-strain in water-saturated and green wood. An advantage of Raman over NIR spectroscopy is that Raman spectra are less influenced by high moisture content. Partial least squares (PLS) modelling was applied to predict strain in wood based on Raman spectra. The spectral changes caused by mechanical strain were analysed. Raman spectra were collected on the surface of green wood before measurements of growth-strain. The suitability and reliability of predicting growth-strain using Raman spectroscopy will be discussed.

Chapter 7 presents a summary of the major findings from each chapter. The limitations and problems needing further study will be discussed. Chapters 2, 3 and 4 have been published in peer-reviewed journals.

2   PROPERTIES OF ROTARY PEELED VENEER AND LVL FROM *EUCALYPTUS GLOBOIDEA*

2.1 Background

Eucalyptus species are hardwoods and make up 26% of the global forest plantation estate (FSC, 2012). Plantation eucalypt species can grow fast, reaching up to 30 cm at the base in 8 years (de Carvalho et al., 2004), and are currently mostly grown for chip wood to supply the pulp & paper industry. However, eucalypt timber is generally of higher stiffness than that of most softwood species, the main plantation resource for solid-wood processing. High stiffness is beneficial for products used in structural applications, such as in laminated veneer lumber (LVL) (Bal & Bektaş, 2012). Plantation-grown eucalypts have been investigated previously for use in LVL. In general, good veneer qualities (Acevedo et al., 2012b), satisfactory mechanical properties (de Carvalho et al. 2004; Palma and Ballarin 2011) and no major gluing problems were reported for eucalypt resources with air-dry densities less than 650 kg/m^3 (Hague 2013, Ozarska 1999).

A major obstacle to using eucalypts for veneers and LVL is the high level of growth-stresses present in the logs. These growth-stresses are generated by the newly formed wood cells. The exact molecular mechanism by which the cell walls generate such large stresses is unknown (Alméras & Clair, 2016; Okuyama et al., 1994; Toba et al., 2013; Yang et al., 2005). However, the newly formed cells tend to contract longitudinally and expand transversely during cell wall maturation. As a consequence, the centre of the stem is under axial compression while the outside is under axial tension (Kubler, 1987). These growth-stresses are released when cutting into the stem i.e. during felling, sawing or veneer peeling. The release of growth-stresses can lead to severe end-splitting following a crosscut, board distortion during sawing and breakage of veneers in the peeling process (Archer, 1987; Jacobs, 1945; Yang & Waugh, 2001). These defects are more prominent in smaller diameter logs, i.e. a plantation resource. Splitting of veneers caused by growth-stress lowers veneer quality and reduces yield. For example, only 20% usable veneers were recovered from *E. grandis* W.Hill due to severe end-splitting (Margadant, 1981). To date, no technological solution to reduce the effects of growth-stresses has been implemented successfully.

Unlike the global plantation estate, eucalypts and other hardwood species account for only 2% of the New Zealand plantation area, which is dominated by *Pinus radiata* D.Don (radiata pine) (90%) (MPI, 2016). Interest in establishing commercial eucalypt plantations dates back to the late 19th century with the introduction and testing of many eucalypt species around that time (Barr, 1996; McWhannell, 1960; Miller et al., 1992; Miller et al., 2000; Shelbourne et al., 2002; Simmonds, 1927). Their work identified various *Eucalyptus* species that suit New Zealand conditions. However, today *E. nitens* (H.Deane & Maiden) Maiden is the only *Eucalyptus* species that is currently grown commercially on a large scale. There are more than 10,000 ha *E. nitens* in Southland and Otago (in the southern South Island), but the species suffers from fungal and insect attack in the warmer North Island (McKenzie et al. 2003; Miller et al. 1992). Some small commercial plantings of *E. fastigata* H.Deane & Maiden and a small amount of *E. regnans* F.Muell can also be found (Miller et al. 2000). The development of these three species is supported by breeding programmes: *E. nitens* (Telfer et al., 2015); *E. fastigata* (Kennedy et al., 2011); and *E. regnans* (Suontama et al., 2015).

Eucalyptus nitens is currently grown for chip wood export for the pulp industry. Generally, it is possible to manufacture quality LVL from 15-year old *E. nitens*, which was reported to have an average MOE of 14.3 GPa and achieving F17 grade according to AS/NZS 2269 (Gaunt et al., 2003). This compares favourably to the majority of radiata pine LVL products manufactured in New Zealand, the MOE of which range between 8 and 13 GPa, and which relies on using the better part of the radiata pine resource. Apart from growth-stress, *E. nitens* has been reported to suffer from collapse and internal checking during drying (Lausberg et al., 1995; McKenzie et al., 2003; McKinley et al., 2002).

None of the currently commercially grown eucalypts produce naturally ground-durable and coloured timber even though the value of such a resource was identified many years ago by early eucalypt enthusiasts (McWhannell, 1960; Simmonds, 1927). Interest in growing these eucalypt species to produce high-value speciality timbers continued in the forestry sector but smaller growers favoured different species so no critical mass has been achieved to date. Furthermore, a successful plantation industry needs to be supported by a breeding programme (Miller et al., 2000). Tree-breeding programmes require a wide genetic basis and are costly, highlighting the need to focus resources on a few species.

Three major research initiatives involving durable eucalypts in New Zealand have been initiated in the last two decades. The Forest Research Institute (Scion) and the New Zealand Forestry Association undertook a series of trials on eucalypts with stringy bark. However, these were either were discontinued due to a lack of funding or have a narrow genetic base (van Ballekom & Millen, 2017). The New Zealand Dryland Forests Initiative (NZDFI) has been working since 2008 to establish a eucalypt forest industry producing naturally durable timber based on a large scale-breeding programme of three species *E. bosistoana* F.Muell., *E. quadrangulata* H.Deane & Maiden and *E. globoidea* (Millen, 2009). This breeding programme took a range of wood-quality traits into account (including low growth-stress). While primarily chosen for the natural durability of their heartwood, these species also produce wood of high stiffness - up to 20 GPa (Bootle, 2005). Demand for engineered timber products with exceptional stiffness has been generated by the emergence of high-rise timber buildings (van de Kuilen et al., 2011). These species also have naturally durable heartwood so it may be possible to produce preservative-free durable LVL (McKenzie, 1993; Page & Singh, 2014). Some information on the wood properties of *E. bosistoana*, *E. quadrangulata* and *E. globoidea* is available from old-growth resources in Australia (Bootle, 2005), but only young plantation-grown *E. globoidea* has been studied previously in New Zealand. *Eucalyptus globoidea* has been reported to be well suited for plantation forestry with good tree health, growth and adaptability combined with favourable timber properties of good stiffness and natural durability (Barr, 1996; Haslett, 1990; Millner, 2006). Additionally, it is easy to dry and has relatively low growth-stress levels (Jones et al., 2010; Poynton, 1979). No information on peeling parameters, veneer drying or bonding has been reported for this species, however.

Eucalyptus globoidea was selected for the present study to evaluate its suitability for veneer and LVL production considering the fact that sufficiently large trees could be sourced from a farm-forestry operation. To the best of our knowledge, no sufficiently large *E. bosistoana* or *E. quadrangulata* trees are available in New Zealand for processing research. Growth-strain of logs was measured and then peeled into veneers. Green veneer recovery and peeling quality were evaluated and relationships between these attributes and both growth-strain and dynamic modulus of elasticity (MOE) were investigated. Physical properties including density, shrinkage and moisture content of dried veneer were also monitored. *E. globoidea* veneers were used to manufacture pure eucalypts LVL and mixed LVL with radiata pine veneers to investigate the bonding performances.

2.2 Materials and methods

Nine *E. globoidea* trees with straight form were randomly chosen and felled from a 30-year-old stand in the lower North Island (latitude 40° 11' 12" S, longitude 175° 20' 35" E, elevation 60 m) in May 2016. The stems were manually debarked immediately after felling. From these stems, 26 suitable logs for peeling of 2.7 m length were recovered. The small end (SED) and large end diameters (LED) were measured for each log in order to calculate log volume.

1) Growth-strain measurement

For each log, the amount of growth-strain was determined with the CIRAD method (Gerard et al., 1995). It was calculated from the measured change in distance between the pins according to Equation (2.1). The growth-strain is variable on the surface of a stem (Gerard et al., 1995). Therefore, growth-strain was measured on four positions at ~1.35 m spaced by ~90º around the circumference of each 2.7 m log. The four assessments for each log were averaged. Measuring points were chosen in straight-grained areas in close proximity to the above described positions in order to avoid knots.

$$\alpha = -\varphi\, \delta$$
(2.1)

where α is the strain in microstrain; δ is the measured displacement in µm and φ is a constant dependent on tree species. The published value for eucalypt of $\varphi = 11.6$ was used (Fournier et al., 1994).

2) Rotary peeling and veneer evaluation

The trees were transported to Nelson Pine Industries Ltd (NPI), Richmond, NZ for processing. All logs were heated at 85 °C for 24 h in a water bath before peeling 8 days after felling. 23 of the 26 logs were peeled to a core diameter of 82 mm using a spindled lathe (Raute, Finland) with three-stage chucks. The remaining three logs fell off the lathe with a larger peeler core (266 to 324 mm in diameter) due to severe splitting. All logs produced veneers with a thickness of 3.74 mm. During the peeling process, the recovery and volumes of different types of waste (core, round-up, spur, clipper defects) were recorded for each log. After clipping, 296 veneer sheets were obtained. Recovery was defined as the ratio of the obtained veneer volume to log volume. Veneer volume was calculated based on the number of sheets and the thickness and dimensions of sheets. For comparison, NPI provided the average recovery data of more than 46,000 radiata pine logs (2.7 m long) collected previously from the production line. The radiata pine logs used in this study were sourced from plantations and woodlots in Nelson and Marlborough. Veneer splitting was the major defect with few knots or other defects found so the aggregate defect rule according to AS/NZ 2269.0 was not applied. The green veneer sheets were visually graded to four classes (face, core, composer, waste) according to their splitting severity by the technical manager in NPI. Only face and core grades were considered to be usable veneer.

From the dryer line with the Metriguard 2655 DFX instrument (USA), ultrasonic propagation velocity and width data were made available for each veneer sheet. The individual veneer sheets could be tracked back to the individual logs. With the clipping width known, the width data were used to calculate the tangential shrinkage. The number of splits in each veneer

was counted from the Novascan grader (Grenzebach, Germany) images. ImageJ software (National Institute of Health, USA) was used to analyse the splitting lengths.

After drying, a strip approximately 200-300 mm wide was taken from a sheet near the start and the end of each veneer mat. The dimension and weight of this strip were measured to obtain dried density. These test pieces were then dried further in an oven at 103 °C until constant weight to obtain the moisture content.

The dynamic modulus of elasticity (MOE) was calculated from ultrasound acoustic propagation velocity and wood density data according to Equation (2.2).

$$E = V^2 \rho \tag{2.2}$$

Where V is the ultrasonic velocity, E is the dynamic MOE and ρ is the density. Static MOE for the population of sheets was estimated by multiplying the dynamic MOE with a factor of 0.868. The factor was empirically determined by laminating test panels of *Eucalyptus globodiea* veneers with known dynamic MOE and conducting static 4-point bending tests in the edgewise direction.

3) Bonding quality of eucalyptus veneer

Ten laboratory-scale 10-ply LVL panels were manufactured. Six panels were made of eucalypt veneer only, choosing veneer sheets of defined MOE grades based on their dynamic MOE values. One panel each was made from 12, 14, or 17.5 GPa sheets and three panels were made from 16 GPa sheets). Each LVL panel contained veneer from one or two logs only. Another four panels were made of five radiata pine and five eucalypt veneer plies. The first (14 GPa), third (17 GPa), sixth (14 GPa), eighth (12 GPa) and tenth layers (12 GPa) were eucalypt veneers and the rest were radiata pine. Two panels were made from each of G2 and G4 radiata-pine grades. A range of eucalypt grades were used in these panels. A typical phenolic formaldehyde adhesive manufactured by Aica NZ Limited was used at a rate of 180 g/m^2. Panels were hot-pressed at 160 °C with a pressure of 1.2 MPa.

The quality of the glueline was assessed according to AS/NZS 2098.2 (2012), which measures the percentage of area covered by wood after two veneers have been split apart. According to AS/NZS 2269.0 (2012) , bonding between the plies in LVL shall be a Type A bond. Achieving this standard requires the phenolic adhesive to comply with AS/NZS 2754.1 (2016) and also a bond quality of any single glueline not less than 2 and an average of all gluelines not less than 5 when tested according to AS/NZS 2098.2 (2012). Both a steam and a vacuum pressure method were used to assess glueline quality (AS/NZS 2098.2, 2012).

2.3 Results and Discussion

2.3.1 Rotary peeling and veneer recovery

For the 26 logs of 2.7 m tested, the small end diameter averaged 34.4 cm with a standard deviation of 4.3 cm while the large end diameter averaged 38.9 cm with a standard deviation of 6.3 cm. The average diameter of the *E. globoidea* logs (36.3 cm) was comparable to the radiata pine logs (34.9 cm) used in the plant for LVL production. In a preliminary test, an additional *E. globoidea* log was peeled cold. This was unsuccessful and, therefore, preheating to soften the wood was deemed necessary.

The average veneer recovery for the 26 *E. globoidea* logs (54.5%) was lower than for radiata pine logs (69.8%) but the best *E. globoidea* log had a recovery of 74.5% (Table 2-1 and Table 2-2). This result was mainly due to a 6% higher loss in the peeler core caused by severe splits in the supplied *E. globoidea* logs and an 11.7% greater clipper loss caused by end-splitting of the veneers compared with the radiata pine logs. However, the amount of round-up waste was lower for the eucalypt logs than the radiata pine logs, which indicated a better log form for *E. globoidea*. Veneer recovery from individual logs was highly variable ranging from 23.6% to 74.5% (Table 2-2). A previous peeling study with *E. nitens* reported an overall recovery of 59% (McKenzie et al., 2003). However, part-sheets were included in that study while only full sheets were calculated in the present study.

Table 2-1 Green veneer recovery and amount of waste of *E. globoidea* compared to *P. radiata* data

	Green Veneer Recovery (%)	Amount of Waste (%)			
		Round Up	Spur	Core	Clipper Defects
E. Globodiea	54.50	4.63	2.49	11.99	19.93
P. Radiata	69.78	11.23	2.73	5.97	8.28

A spindled lathe was used to peel the logs in the current study but spindleless lathes are extensively used in China. They are suitable for rotary peeling smaller diameter logs from young and fast-grown hardwood plantations (McGavin, 2016). Spindleless lathes achieve higher yields because they can peel logs to smaller peeler core diameters compared to spindled lathes currently used for radiata pine. Moreover, spindleless lathes can control splits by pressing the splits together during peeling. Therefore, using this type of lathe may generate higher recovery and quality of veneer sheets.

2.3.2 Growth-strain and veneer splitting

High quality veneers can be obtained from *E. globoidea* although splitting significantly degraded the visual appearance of many veneers (55% of the veneers had splitting lengths longer than 2 m). Veneers with no and severe splitting are shown in Figure 2-1.
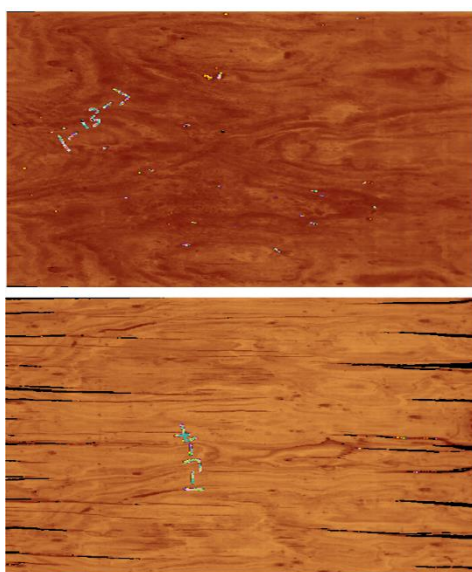
Figure 2-1 Face grade veneer with no splitting (top) and composer grade veneer with severe splitting (bottom)

The average recovery of useable veneer (face and core grades) from *E. globoidea* was 33.4%. Severe splitting caused by growth-stress contributed to the low recovery. The average growth-strain was 839.4 µε measured by the CIRAD method. The log with the lowest growth-strain had approximately half the growth-strain compared with that with the highest. Usable veneer recovery was negatively associated with growth-strain (Figure 2-2). The average useable veneer recovery for the logs in the bottom quartile (growth-strain > 965.7 µε) was 5.8%, while that for the top quartile (growth-strain < 701.8 µε) was 57.2%.
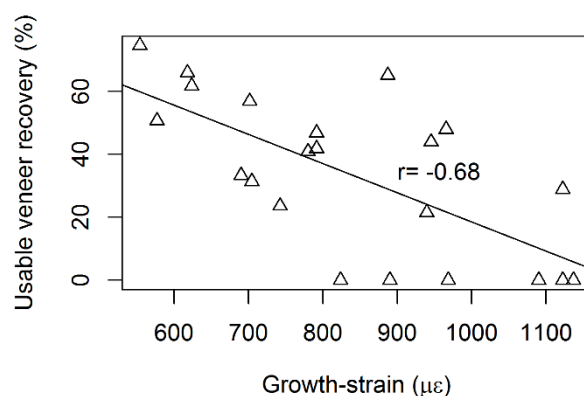
Figure 2-2 Dependence of usable veneer conversions on growth-strain of the individual *E. globoidea* logs

The mean splitting length per veneer for individual logs ranged from 0.15 m to 8.66 m. For a veneer 2.65 m in length and 1.26 m in width, the average total splitting length was 3.01 m. This suggested splitting was limiting veneer quality.

Table 2-2 Summary of veneer recovery and splitting

	Recovery (%)	Useable veneer (%)	Strain (με)	Splitting length per veneer (m)	Split counts
Mean	54.5	33.4	839.4	3.01	8.63
SD	14.2	23.7	181.7	2.57	5.11
Minimum	23.6	0.0	553.9	0.15	1.14
Maximum	74.5	74.5	1136.8	8.66	16.86

SD, Min and Max represent standard deviation, the minimum and maximum values respectively.

The splitting length was measured after the veneers were dried. Drying was likely to exaggerate the splitting lengths but was assumed to affect all veneers equally in this study. In addition, rough handling and peeling settings can also contribute to the splitting of veneers. It was assumed that all veneers were equally affected in these ways and the differences among them were mainly caused by growth-stress.

A positive correlation (r = 0.73) was observed between splitting lengths in veneers and growth-strain of corresponding logs (Figure 2-3). In this study, average splitting length was low when growth-strain was less than ~800 με (CIRAD). Longitudinal growth-strain was reported to be positively related to end-splitting of *E. nitens* and *E. globulus* logs (Valencia et al., 2011; Yang & Pongracic, 2004). The number of splits in a veneer sheet is another measure to evaluate veneer spitting. A strong linear relationship (r = 0.91) was obtained between splitting length and split numbers (Figure 2-3). Considering that the measurement of the number of splits is less time consuming than quantifying splitting length, it might be a better option for future studies.
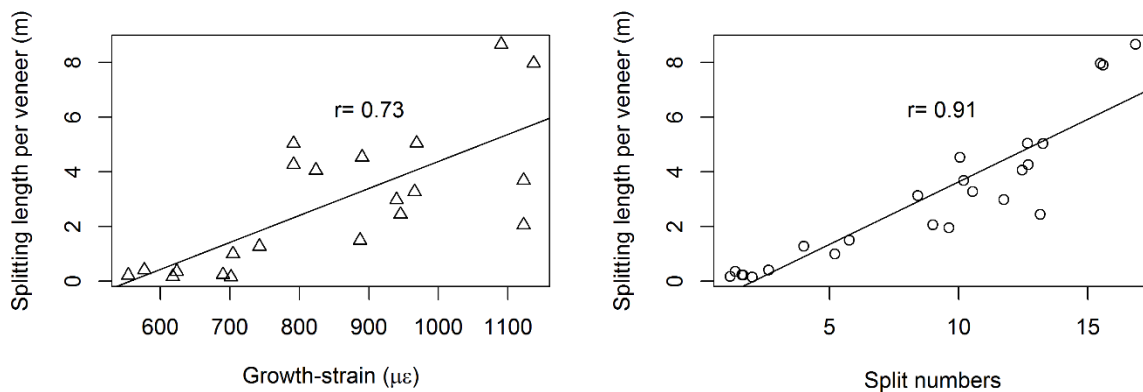
Figure 2-3 Association between splitting length and growth-strain (left) as well as number of splits (right)

This result indicated that higher veneer recovery and quality would be possible if growth-stresses were reduced. Methods to control the growth-stress and minimise splitting are difficult to perform, have not been successful in industrial applications and incur ongoing costs (Archer, 1987; Malan, 1995; Yang & Waugh, 2001). Growth-stresses are heritable and selecting trees with low growth-stress in a breeding programme can potentially solve this problem for a future resource such as *E. globoidea* (Davies et al., 2017; Malan, 1995). For

existing eucalypt plantations grown for the lower-value wood chips, such as *E. nitens*, segregation would be an option. However, current methods of measuring growth-stress are time consuming and cumbersome, making this approach impractical (Yang & Waugh, 2001). Rapid and non-destructive segregation methods need to be developed. For example, Yang et al. (2006) measured growth-strain of 10-year-old *E. globulus* and found correlations with cellulose crystallite width measured using a SilviScan-2 instrument.

The relationship between splitting length and radial position for five logs is shown in Figure 2-4. The splitting length of the veneer sheets tended to increase towards the centre of the stem (position 0). The decreasing circumference with decreasing radius results in shorter tangential distances between the radial end-splits of the logs. Furthermore, the increasing curvature with decreasing radius can facilitate splitting. However, the variation between the stems was much bigger than the radial effect, with the veneer splitting independent of radius for the worst and the best logs.
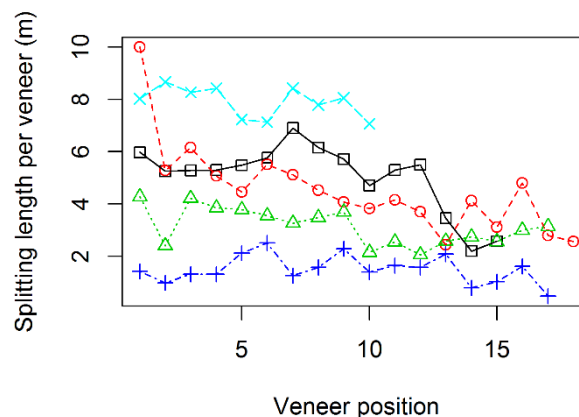
Figure 2-4 Splitting length for veneers obtained from the centre to the outside of five individual logs

It is worth noting that the log preheating and peeling settings in this study were optimised for radiata pine. Acevedo et al. (2012a) reported that better quality veneers were obtained from *E. nitens* by adjusting nose bar pressure and peeling knife angle.

2.3.3 Physical and mechanical properties of veneer

After drying, the average dry density was 668 kg/m^3 and the average moisture content was 7.3% (Table 2-3). No excessively high or low moisture contents were found, which indicated homogeneous drying of the *E. globoidea* veneers.

The average shrinkage of the *E. globoidea* veneers was 9.9 % tangentially and varied between 8.5 and 11.3%. Most veneers were heartwood as the sapwood in *E. globoidea* is very narrow. For comparison, typical tangential shrinkage values for radiata pine veneers are 6.4% for sapwood and 4.4% for heartwood. Higher shrinkage will result in greater volume loss. It should be noted that, within species, heartwood typically displays lower shrinkage than sapwood.

The average dynamic MOE calculated for the *E. globoidea* veneer sheets from Metriguard acoustic velocity and interpolated lab density was 14.67 GPa ranging from 9.59 to 20.26 GPa (Figure 2-5). The equivalent static MOE was estimated to be 12.73 GPa based on the

empirical conversion equation. Common LVL products manufactured from radiata pine range from 8 to 11 GPa. Jones et al. (2010) investigated 25-year-old *E. globoidea* for high-quality solid wood production. Boards from the butt logs were reported to have an average density of 655 kg/m³, dynamic MOE of 13 GPa and static MOE of 12 GPa. According to Haslett (1990), the timber of *E. globoidea* (over 25 years old) in New Zealand has an MOE of 14.6 GPa at a moisture content of 12%.

Table 2-3 Physical and mechanical properties of dried *E. globoidea* veneers

	Dried density (kg/m³)	Moisture content (%)	Shrikage (%)	Velocity (km/s)	Dynamic MoE (GPa)
Mean	688.13	7.31	9.85	4.657	15.14
SD	68.55	1.09	0.77	0.240	2.05
Minimum	557.41	5.51	8.46	4.322	11.04
Maximum	824.00	9.32	11.31	5.097	19.51
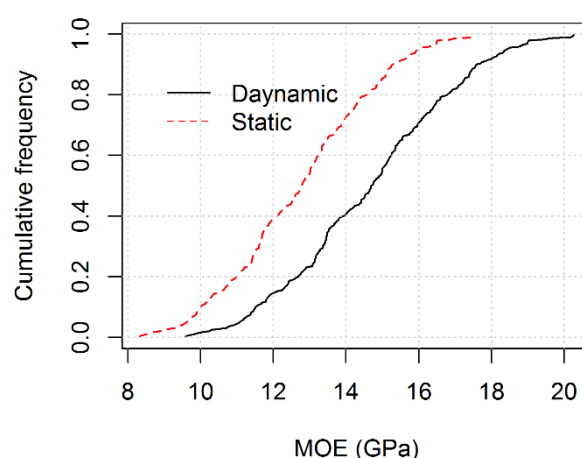
Figure 2-5 Cumulative distribution of dynamic and static MOE of veneer sheets

High stiffness wood tended to have higher growth-strain (Figure 2-6). This is an unfavourable association as stiff wood with low growth-strain is desirable. However, the association between MOE and growth-strain was moderate (r = 0.65) implying the existence of stiff logs which are low in growth-strain. Several logs produced veneers with MOEs above 15 GPa and growth-strain levels below 800 με. More importantly no association (r = 0.27) was found between veneer splitting and stiffness, which demonstrated that peeling quality needs to be improved through reducing growth-stress rather than through MOE. The stiffest logs yielded veneers with an MOE of up to 19.5 GPa, but these did not necessarily have a severe splitting problem. Therefore, it seems possible to obtain a stiff eucalypt resource that yields high-quality veneers.
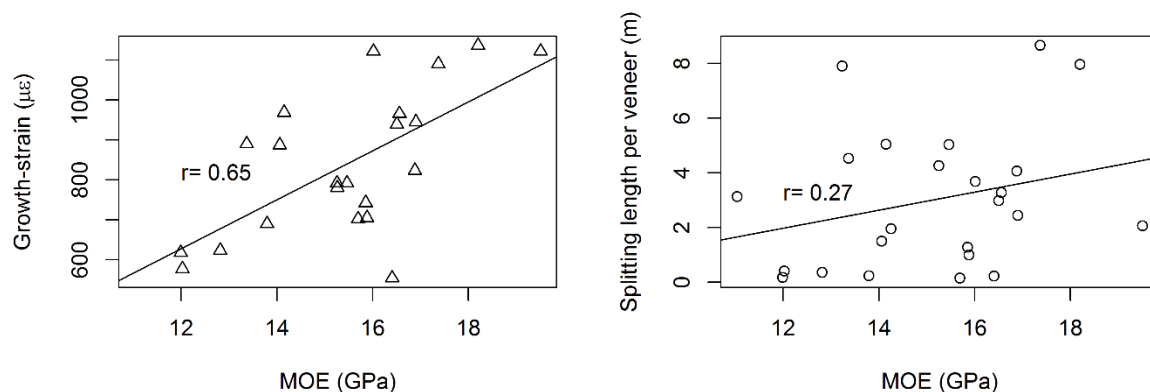
Figure 2-6 Association between MOE and growth-strain (left) as well as veneer splitting (right)

A weak positive association (R^2=0.26) between CIRAD longitudinal displacement and MOE has been found previously in *E. globulus* (Yang et al., 2006). With the increase of longitudinal displacement, microfibril angle tended to decline while density increased. Similar associations between growth-strain and wood properties have been reported for wood from *Populus deltoides* Bartr (Fang et al., 2008). However, no statistically significant associations were found between growth-stain and dynamic MOE or density for *E. nitens* (Chauhan & Walker, 2004).

The average distribution of MOEs for the veneers obtained from the nine trees assessed is shown in Figure 2-7. As for veneer splitting, the variance in MOE among trees was large with the average stiffness ranging from 12.1 GPa to 18.0 GPa. Analysis of variance found significant differences (P<0.001) in MOE values of veneers from different trees.

It has to be noted that the tested *E. globoidea* was genetically unimproved material of unknown provenance. Wood properties like growth-stress and MOE are under genetic control (Davies et al., 2017). Murphy et al. (2005) reported a heritability of 0.3 to 0.5 for growth-strain in *Eucalyptus dunnii* Maiden and indicated tree breeding can be an effective method to reduce growth-stress. Considerable variation among trees was observed, indicating a potential for genetic improvement. The relatively high acoustic velocity of eucalypts in the corewood could allow peeling veneers to a smaller peeler core with spindleless lathes, improving yields and allowing the use of a small diameter younger resource.
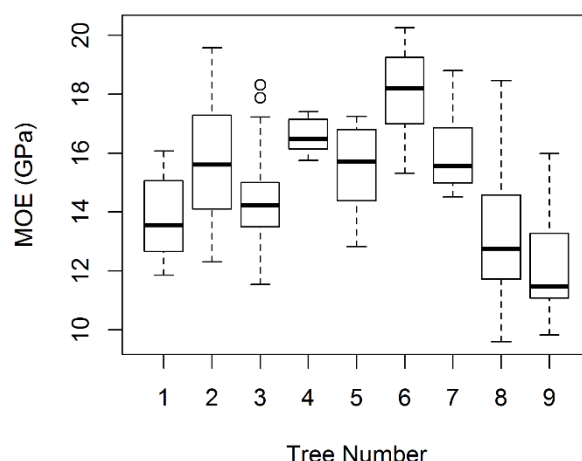
Figure 2-7 Whisker plots of veneer MOE from nine trees. Dotted lines show minimum and maximum values; the thick black line shows the mean; and outliers are marked using open circles.

2.3.4 Bonding quality

The bond test revealed poor bonding of the plies. None of the panels made with *E. globoidea* alone passed the specifications for structural LVL (Table 2-4). Density seemed to exaggerate the bonding difficulty for the 100% *E. globoidea* LVL. *Eucalyptus globoidea* panels with densities higher than 800 kg/m^3 had average bonding qualities lower than 3. Alternating *E. globoidea* and *P. radiata* veneers improved bond quality, and all samples passed the steam test, but only one sample passed the immersion test. The glueline between radiata pine plies was excellent (Table 2-5).

Eucalypts have a higher density and extractive content than radiata pine, and both these factors can make gluing difficult. In Australia, difficulty in bonding veneers from dense eucalypts (air-dry density above 700 kg/cm^3) are known and some special adhesive formulations have been developed for these species (Carrick & Mathieu, 2005; Ozarska, 1999). It is commonly stated that low and medium density (below 650 kg/cm^3) eucalypts glue well but young *E. nitens* was found to have bonding issues however (Farrell et al., 2011). Plywood products made from various *Eucalyptus* species have been reported in China, Malaysia, Uruguay and Brazil indicating that satisfactory bonding can be achieved for many *Eucalyptus* species (de Carvalho et al., 2004; Hague, 2013; Turnbull, 2007; Yu et al., 2006). Therefore, it seems probable that a technical solution for gluing *E. globoidea* can be found.

Table 2-4 Bond tests of six LVL panels made from *E. globoidea* veneers (listed in order of increasing density)

Grade (GPa)	Density (g/cm^3)	Steam			Immersion		
		EE$_{min}$	EE$_{max}$	EE$_{mean}$	EE$_{min}$	EE$_{max}$	EE$_{mean}$
12	640.51	1	9	5	1	5	2
16	696.92	3	8	6	4	9	6
16	702.52	1	9	6	3	8	7
16	806.83	0	5	1	0	3	2
14	809.22	0	3	2	2	3	2
17.5	860.05	1	4	2	0	7	3

EE represents bond quality values between *E. globoidea* veneers (0 no bond – 10 excellent bond). The minimum, maximum and mean values are shown.

Table 2-5 Bond tests of four LVL panels made from a mixture of *E. globoidea* and *P. radiata* veneers

Sample	Radiata pine grade	Steam test				Immersion test			
		ER$_{min}$	ER$_{max}$	RR	Mean	ER$_{min}$	ER$_{max}$	R-R	Mean
1	G4	4	9	9	7	1	9	9	7
2	G4	3	7	10	5	0	9	8	6
3	G2	2	9	9	7	3	9	9	6
4	G2	2	9	9	6	1	8	9	6

G4 and G2 are radiata pine veneer grades; 12, 14 and 17.5 GPa grade eucalypt veneers were used in each sample. ER represents the gluelines between eucalypts and radiata pine veneers and RR stands for the glueline between two radiata pine veneers. Mean is the average value of all 9 gluelines.

2.4 Conclusions

1) Veneer recovery ranged from 23.6% to 74.5% among 26 *E. globoidea* logs. Larger peeler core and higher clipper losses occurred compared to radiata pine.

2) High-quality veneers could be obtained from *E. globoidea*. Low growth-strain logs produced more usable veneers. Splitting degraded veneer quality.

3) Splitting length in veneers was correlated to growth-strain of the corresponding logs. Split number was strongly associated with splitting length and can be used to evaluate veneer

splitting severity. Veneers from inner wood tended to a have longer splitting lengths; however differences among logs were more pronounced.

4) Moisture contents of dried veneers indicated good drying of *E. globoidea*. The average tangential shrinkage was 9.9 % and the volume loss was higher than for radiata pine. Larger shrinkage is a common feature of high-density timbers.

5) The average dynamic MOE was 14.67 GPa ranging from 9.59 to 20.26 GPa. No association was found between splitting length and stiffness. It should be possible to find stiff logs, however, which would yield satisfactory veneers. The considerable variation in stiffness observed here indicated a potential for genetic improvement.

6) The lack of association between stiffness and splitting length suggested that quick acoustic measurements for segregating eucalypt logs suitable peeling are unlikely to be successful.

7) Bond performance of *E. globoidea* LVL was poor and did not meet the New Zealand standard. Alternating *E. globoidea* and *P. radiata* veneers improved bond quality, but bonding of *E. globoidea* veneers still needs to be addressed.

3 MOLECULAR DEFORMATION OF WOOD AND CELLULOSE STUDIED BY NEAR INFRARED SPECTROSCOPY

3.1 Introduction

Wood cell walls have evolved a delicate hierarchical architecture to fulfil their mechanical functions. They contain cellulose aggregates embedded in a matrix of lignin and hemicellulose (Salmén, 2015). Cellulose microfibrils are known to be stiff and strong, and their orientation in the thickest layer (S2) of the secondary cell wall determines the mechanical properties of wood (Barnett & Bonham, 2004). Cellulose molecules elongate as wood are under tensile stress in axial direction (Altaner et al., 2014b; Eichhorn et al., 2005; Gierlinger et al., 2006; Hinterstoisser et al., 2003) confirming its load-bearing role in cell walls. Hemicellulose chains are thought to act as bridges connecting adjacent cellulose microfibrils through hydrogen bonding and this interaction can strengthen cell walls against shear loading (Altaner & Jarvis, 2008; Jin et al., 2015; Keckes et al., 2003; Zhang et al., 2015). Dynamic Fourier-transform infrared spectroscopy (FTIR) has provided evidence that lignin is also taking part in the stress transfer through an indirect coupling to cellulose (Salmén et al., 2016).

Mechanical tests combined with characterization techniques like X-ray diffraction, Raman spectroscopy and infrared spectroscopy have been proven powerful tools to investigate the deformation mechanism of wood and cellulose on a molecular level (Burgert, 2006; Salmén & Burgert, 2009). X-ray diffraction was applied to monitor the changes in the unit cell of crystalline cellulose under mechanical load, showing that the molecular strain was smaller than the macroscopic strain (Peura et al., 2007). For various wood and cellulosic materials, band shifts at around 1095 cm^{-1} were observed upon tensile stress using Raman spectroscopy (Eichhorn et al., 2001; Gierlinger et al., 2006; Peetla et al., 2006). The band shift rate with respect to applied strain was used to estimate the Young's modulus of cellulose (Eichhorn & Young, 2001; Hsieh et al., 2008; Šturcová et al., 2005). Dynamic FTIR studies of cellulose and wood samples showed that the C-O-C glycoside bond, the glucose ring as well as the 3OH···5O intramolecular hydrogen bonds deformed under stress, while the 2OH···6O intramolecular hydrogen bonds were barely affected (Figure 3-1) (Hinterstoisser et al., 2001, 2003; Salmén & Bergström, 2009).
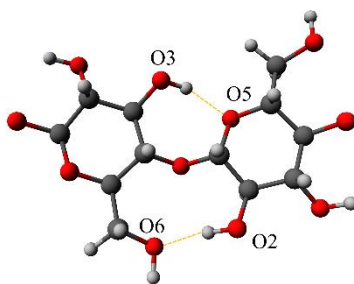
Figure 3-1 Section of a cellulose molecule showing the intramolecular hydrogen bonds represented by yellow dashed lines. The glycosidic C-O-C linkage between glucose units is flanked by 2 intramolecular hydrogen bonds. Oxygen atoms are in red, carbon atoms in black and hydrogen atoms in grey.

Near infrared (NIR) has been largely ignored to investigate molecular mechanics of wood and cellulose. NIR is dominated by overtones and combinations of bonds involving hydrogen, like O-H and C-H, due to their small reduced mass (Osborne et al., 1993). NIR spectra are informative of molecular structures particularly in hydrogen bonding, but it is challenging to understand their underlying molecular origin due to coupling effects and its sensitivity to moisture (Schwanninger et al., 2011). However, NIR has its own advantages including easy sample preparation, fast and simple execution and its non-destructive nature. More importantly for this research, in transmission mode, NIR spectroscopy allows measurements of up to several millimeter thick wood samples compared to microtomed sections needed for mid-infrared spectroscopy (Salmén & Bergström, 2009). Microtomed wood samples have their cells cut, while thick wood samples keep most of their cellular structure intact. When subjected to axial tension, thin samples (150 μm in thickness) were shown to behave differently to solid wood including significant stress relaxation. The difference was explained by a heterogeneous wood microstructure along the cell axis (Navi et al., 1995). Wood microsections also had lower modulus of elasticity (MOE) compared to thick samples because shearing in thick samples is restrained (Yu et al., 2009).

NIR reflectance spectroscopy has the potential to be used for online assessment of wood's chemical and physical properties in industrial settings (Leblon et al., 2013; Tsuchikawa, 2007). With the assistance of chemometrics, NIR has been widely used as a non-destructive and rapid method to assess physical, chemical and mechanical properties of wood (Tsuchikawa & Kobori, 2015). It has also been used to predict mechanical stress in wood. Sandak et al. (2013) monitored the wood responses to tensile stress by NIR spectroscopy and built a multivariate statistical model based on NIR spectra to predict the stress level. NIR spectroscopy combined with partial least squares (PLS) analysis was also applied to predict the load applied to small wood beams in four-point bending (André et al., 2006). Knowledge about the functional groups and band assignment is not necessary for building such multivariate statistical models. These methods give little insights into the molecular deformation. A more detailed analysis of NIR spectral changes under mechanical stress can make NIR a useful tool to investigate the molecular structure of wood and cellulose.

This study hypothesized that NIR can be used to analyse the molecular deformation of wood and cellulosic materials. Tensile tests in combination with transmission NIR spectroscopy were conducted on thick wood and paper samples under different strain levels. In addition, bending tests were carried out on wood samples and NIR spectra were collected in reflection mode for both the tension and the compression surfaces. Spectral changes caused by tensile stress were first visualized in the normalized spectra, the second derivative spectra

and the calculated 'slope' spectra. Then band shift rates were quantified for both, tensile and bending tests.

3.2 Materials and methods

Wood samples with a length of 80 mm in longitudinal direction and width of 16 mm were used for tensile tests. 10 samples of radiata pine (*Pinus radiata*) and 10 samples of eucalypt (*Eucalyptus regnans*) were sawn from air-dried boards. The radiata pine and eucalypt boards, with an air-dry density of 0.47 and 0.54 g/cm^3 respectively, were sourced from Canterbury, New Zealand. The thickness for pine samples was approximately 0.8 mm, while that for eucalypt samples was approximately 0.5 mm to allow for increased signal absorption caused by its higher density. A typical softwood tracheid cell wall is about 30 µm in diameter (Bucur, 2011). Therefore the pine samples had about 25 cells in thickness compared to a few cells in a typical microtomed section. Oriented paper samples were manufactured from a commercially available bleached eucalypt pulp with a basis weight of 80 g/m². Detailed description was provided by Kröling et al. (2013). 10 paper samples were cut along the machine direction for tensile tests, having the same length and width as with the wood strips. Another 8 eucalypts samples with dimensions of 450 (L) × 25 (T) × 25 (R) mm^3 were prepared for the bending tests. Samples were kept air-dried in the laboratory.

3.2.1 Relaxation behavior

Stress relaxation, the phenomenon of decreasing stress in strained samples over time, was reported to be significant for thin wood sections required for IR spectroscopy (Altaner et al., 2014b). The extent of stress relaxation during spectra acquisition will influence the accuracy in determining the band position. A universal mechanical testing machine (Instron 5566, USA) equipped with a 10 kN load cell was used for tensile tests. For the samples described above, relaxation behaviors were characterized using one sample for each type with a loading rate of 1 mm/min. Samples were held at a constant force for 300 seconds in the elastic region. The maximum forces used were 300 N and 30 N for wood and paper samples, respectively.

The relaxation behavior of pine, eucalyptus and paper samples are shown in Supporting Figures 1 and 2 (Appendix A). After 300 seconds, the tensile force reduced from 300.0 N to 294.6 N (98.2%) and 289.6 N (96.5%) for the 0.5 to 0.8 mm thick pine and eucalypt sample in air-dry condition, respectively. More than 98% of the stress was retained after 60 seconds, roughly the time needed to acquire a NIR spectrum. Therefore, the effect of stress relaxation on the NIR spectra was negligible for the air-dry wood samples. Paper samples showed larger stress relaxation with 90.8% and 85.1% of the initial stress remaining after 60 and 300 seconds, respectively. The modulus of elasticity of wood and paper based on 10 samples was calculated from the stress-strain curves using the same universal mechanical testing machine. The paper used in this study had an estimated MOE of 5.8 ± 0.2 GPa, which was lower than that of pine (10.8 ± 1.1 GPa) and eucalypt (13.2 ± 1.6 GPa) samples.

3.2.2 NIR measurements of wood under tension

To study the effect of strain on NIR spectra, a test rig (Figure 3-2) had been built based on a toolmakers vice. Two clamps with a width of ~25 mm were attached to the fixed and sliding component of the toolmakers vice. Samples were fixed longitudinally between the clamps. Care was taken to ensure uniform stress distribution across the sample width and avoid twisting of the samples. The sliding clamp was driven by a screw to stretch the sample. This test rig was fitted into the sample compartment of a NIR spectrometer (Bruker Tensor 37, Germany). Transmission spectra in the region of 9000 to 4000 cm^{-1} were recorded at a resolution of 8 cm^{-1} as averages of 128 scans.

A circular NIR polariser (oriented silver particles embedded in soda lime glass, CODIXX, Germany) with a diameter of 20.8 mm was used to polarize the incident beam parallel to the longitudinal direction of the sample. Parallel polarisation was reported to provide slightly stronger signal compared to perpendicular polarisation in the first overtone of OH stretching region for wood samples because intrachain hydrogen bonded OH groups in cellulose and glucomannan are preferably oriented in the cell axis direction (Fackler & Schwanninger, 2010; Tsuchikawa & Siesler, 2003a, 2003b). In the OH stretching region, both eucalypt and pine samples showed higher intensity in parallel polarised light after baseline correction (Supporting Figure 3 in appendix B).
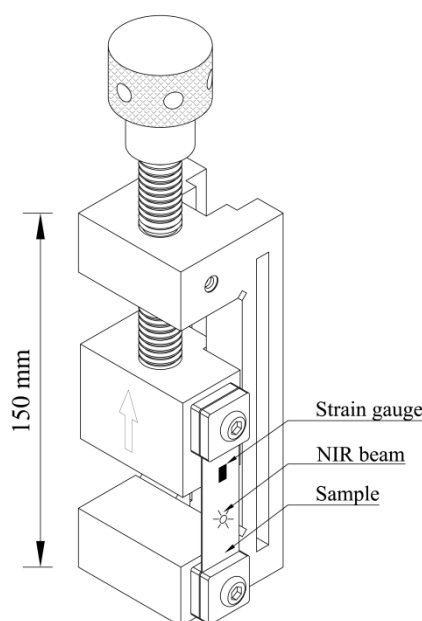
Figure 3-2 Test rig for stretching wood and paper samples with a thickness up to 0.8 mm while acquiring transmission NIR spectra.

Parallel polarised NIR spectra of the 30 samples were collected in transmission at 8 strain levels (0 to 7) by driving the screw of the test device. "Strain 0" represented the relaxed state with no applied tensile force, while "Strain 7" had the greatest tensile force applied. The strain was recorded with strain gauges (FLA-5-11, Tokyo Sokki Kenkyujo, Japan) glued onto the samples with instant adhesive (Loctite 454, Australia) and connected to a strain-meter (TC-31K, Tokyo Sokki Kenkyujo, Japan). Each sample was measured twice and 16 spectra were collected for each sample.

The effect of polarisation on NIR spectra were investigated by stretching three eucalypt and three radiata pine samples at 8 strain levels. NIR spectra collected using parallel and perpendicular polarisation directions were compared with unpolarised spectra.

3.2.3   Bending tests of eucalypt samples with NIR

Bending tests cause tension and compression stresses on the convex and concave surfaces, respectively. 3-point bending tests were conducted using a self-developed test rig with a span of 260 mm. The test rig consisted of a clamp to apply forces and a frame fixed to the lab bench. Eight strain levels were applied on the midpoint. The readings of the TC-31K strain-meter connected to strain gauges glued at midpoint onto the concave and convex surfaces of the sample were recorded. NIR spectra were collected close to the midpoint from the convex and concave surfaces using a fibre optic probe (Model N-500, Bruker, Germany) connected to a Tensor 37 spectrometer at 8 cm^{-1} resolution averaging 128 scans.

3.2.4   Analysis of spectra

Spectra were analysed in R software (R Core Team, 2017). The original spectra in the region of 6100 to 7200 cm^{-1} were normalized using the standard normal variate (SNV) method by the "scale" function. Second derivative spectra were calculated using Savitzky-Golay smoothing filters in the "pls" package with a filter length of 39 (Mevik et al., 2016a).

A 'slope' spectrum was calculated based on normalized spectra, as the rate of intensity change dependent on the strain level at a given wavenumber. The 'slope' spectra reveal information about band shifts and intensity changes in spectra (Altaner et al., 2014a). The 'slope' values presented here were the average of the linear regression coefficients of 10 samples.

Band positions in the second derivative spectra were determined to calculate band shift rates with respect to strain. The signal at around 6286 cm^{-1} was fitted with a Gaussian function, while the signal at around 6470 cm^{-1} was fitted with a skewed Lorentzian function (Supporting Figure 4 in Appendix C). The peak position or the wavenumber of the minimum was obtained from the fitted function.

3.3   Results and discussion

3.3.1   Visualization of spectral changes upon tensile stretching

3.3.1.1   Normalized spectra in the OH stretching region

Signals in the region from 7200 to 6100 cm^{-1} assigned to the first overtones of OH stretching vibrations (Schwanninger et al., 2011) were examined after normalization (Figure 3-3). Free OH groups are found at higher frequencies (6954-6974 cm^{-1}), while OH bonds involved in hydrogen bonds from crystalline cellulose occur at lower wavenumbers (Schwanninger et al., 2011). No obvious differences were found for eucalypt and pine wood samples in this region. The NIR spectra of paper in this region differed from wood, with relatively lower intensity at higher frequencies. This could be explained by their differences in chemical composition. The lignin contents for *E. regnans* and *P. radiata* wood were reported to be 28.6% and 27.5%, while chemical pulp has a lignin content of 4% to 10% depending on the pulping method (Lin & Dence, 1992). First overtones of phenolic hydroxyl groups in lignin appear at

around 6913 cm^{-1} (Fackler & Schwanninger, 2010; Mitsui et al., 2008). NIR spectra of alkali lignin, oven-dry wood, and oven-dry paper in the OH stretching region are shown in Supporting Figure 5 (Appendix D) confirming that it is the lower lignin content of paper that primarily explains the lower relative intensity at around 7000 cm^{-1}. Additionally, a study of microcrystalline cellulose found that, formation of water-water hydrogen bonds during water adsorption can be observed around 7073 cm^{-1} (Watanabe et al., 2006b). Consistent with literature (Glass & Zelinka, 2010; Twede et al., 2014), the paper sample had a lower moisture content (4.9%) in the lab environment compared to wood (8.6%). This also contributed to the lower relative intensity at these frequencies.

Tensile stretching resulted in subtle changes in the normalized NIR spectra. When enlarged, it can be seen that the signal intensity around 6450 cm^{-1} decreased with the increase of strain for all three sample materials (Figure 3-3). This can be attributed to hydrogen bonded OH groups in cellulose as this spectral change was shared between paper and wood samples. Spectral changes in this region implied the deformation of hydrogen bonding system under tensile stress.
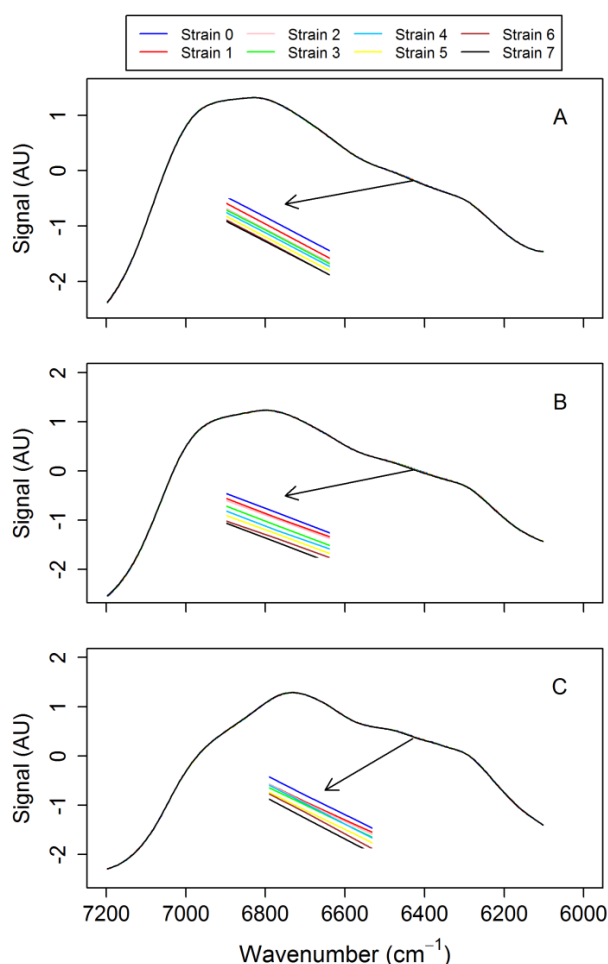
Figure 3-3 Normalized NIR spectra of the first overtone of OH stretching vibrations (7200 to 6100 cm^{-1}) for an air-dry eucalypt (A), pine (B) and paper (C) sample under 8 tensile strain levels. NIR light was parallel polarised with respect to the cell axis of wood and the machine direction of paper. Strain level increased from "Strain 0" (relaxed state) to "Strain 7" (maximum strain level)

3.3.1.2 **Band shifts and band assignments in the second derivative spectra**

Figure 3-4 shows the changes in the second derivative spectra of the first overtone of OH stretching vibrations (7000 to 6100 cm^{-1}) caused by mechanical stress. Second derivative spectra are commonly used to resolve overlapping signals. Positive peaks in the original spectra correspond to negative signals in the second derivative. The band shape below 6200 cm^{-1} in the second derivative spectra differed between the three materials (Figure 3-4). A band at 6188 cm^{-1} had previously been associated with the =CH$_2$ structure of resin or extractives in wood, which are non-structural cell wall components (Baillères et al., 2002). With the increase of tensile strain, two bands below 6600 cm^{-1} shifted to higher wavenumbers for all three sample types. The locations of those bands in the relaxed state were at around 6289 and 6464 cm^{-1} for eucalypt, 6286 and 6470 cm^{-1} for pine and 6284 and 6476 cm^{-1} for paper. Based on their low accessibility to exchange with D$_2$O, these absorption bands at 6450 ± 20 cm^{-1} and 6287 ± 20 cm^{-1} have been assigned to intramolecular hydrogen bonded OH groups particularly in crystalline cellulose (Tsuchikawa & Siesler, 2003a, 2003b).

Detailed assignment of OH groups in infrared spectra is challenging. Firstly, only part of the cellulose is in crystalline form (Andersson et al., 2004; Kljun, 2011) with defined signals. Secondly, the crystalline cellulose in wood cell walls is a mixture of two allomorphs: cellulose Iα and Iβ (Atalla & Vanderhart, 1984; Wang et al., 2015). Cellulose Iα and Iβ differ in the crystal structure and the hydrogen bonding system. Cellulose Iβ, the dominant crystal form in wood has two distinct hydrogen bonding networks: network A and B (Nishiyama et al., 2008). Further, stretching vibrations of hydroxyl groups are likely to be coupled (Lee et al., 2013), so it is difficult to assign one vibrational absorption band to a single localized OH bond.

There is no consensus on the band assignments in the OH stretching region. Neutron scattering studies (Nishiyama et al., 2002; Nishiyama et al., 2003) contradicted previous assignments based on the assumption that intermolecular hydrogen bonds are shorter than intramolecular hydrogen bonds (Altaner et al., 2014b). By comparing theoretical calculations with polarised spectra, a detailed assignment of fundamental stretching frequencies of OH groups was given for the hydrogen bonding network A of native cellulose (Christopher M. Lee et al., 2015). Bands between 3270 and 3240 cm^{-1} were attributed to the intrachain hydrogen-bonded 2OH groups (2OH···6O) and the bands around 3370 cm^{-1} were assigned to the intrachain hydrogen-bonded 3OH groups (3OH···5O) (Hayakawa et al., 2017; Christopher M. Lee et al., 2015). According to the order of the signals, the NIR band at around 6470 cm^{-1} was then attributed to the hydroxyl bond involved with 3OH···5O (intrachain) hydrogen bonds and the band at around 6286 cm^{-1} should be due to the intrachain hydrogen-bonded 2OH groups (2OH···6O). The assignment of 3OH···5O in NIR is consistent with a study of the structural changes in OH groups in microcrystalline cellulose depend on temperature (Watanabe et al., 2006c). The ratios between the locations of the first overtone and the fundamental vibration bands were approximately 1.92 reflecting the effect of anharmonicity on vibrational energy levels. These tentative assignments were used in the following discussion.

Observed band shifts in this study were results of molecular deformation. Under tensile stress, cellulose molecules are stretched and the glucose rings and the C-O-C bridges elongate. Elongation weakened covalent bonds and therefore their IR stretching bands shift

to lower wavenumbers. Raman and IR spectroscopy have observed linear correlation of band shifts with applied strain (Eichhorn et al., 2001; Salmén & Bergström, 2009). Stretching bands of OH groups involved in hydrogen bonds, on the other hand, shift to higher frequencies as the elongation weakens the acceptor (H···O) hydrogen bonds and consequently strengthens the donor OH bonds (Salmén & Bergström, 2009).
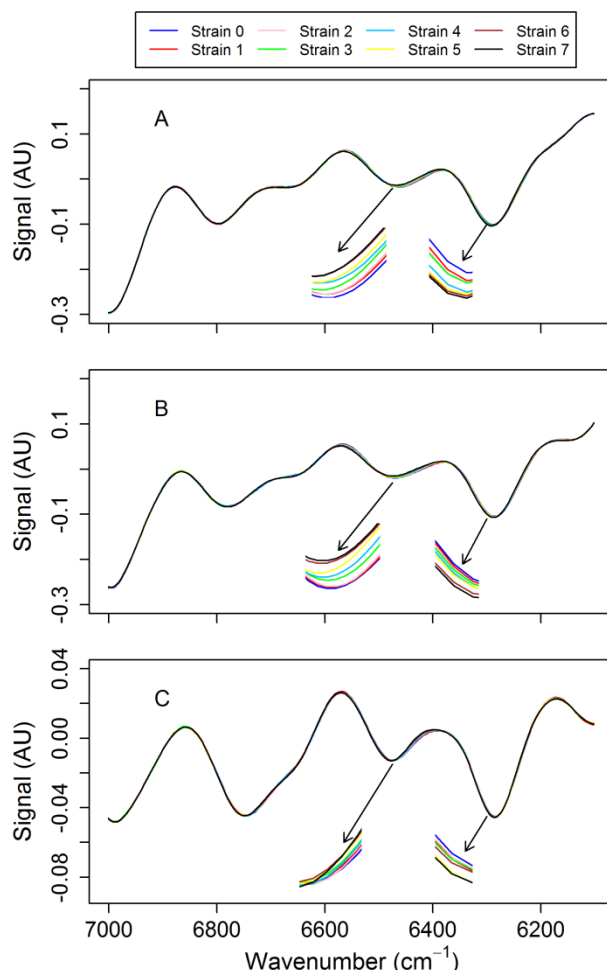
Figure 3-4 Second derivative parallel polarised NIR spectra of eucalypt (A), pine (B) and paper (C) samples of the first overtone of the OH stretching vibrations (7000 to 6100 cm^{-1}) under different tensile strain levels. Strain levels were the same as in Figure 3. Two bands were observed to shift to higher frequencies with increasing tensile strain. In the relaxed state, the peak positions were at 6289 ± 1 and 6464 ± 2 cm^{-1} for eucalypt, 6286 ± 1 and 6470 ± 3 cm^{-1} for pine, as well as 6284 ± 1 and 6476 ± 3 cm^{-1} for paper samples.

3.3.1.3 'Slope' spectra in response to tensile stretching

'Slope' spectra reflect the rate of change in signal intensity with regard to the applied strain (Altaner et al., 2014a), and are similar to the dynamic spectra analysed by Åkerholm and Salmén (Åkerholm & Salmén, 2001). At frequencies where the 'slope' values are close to 0, the signal is not consistently affected by mechanical stretching. On the contrary, peaks with

high absolute 'slope' values reveal frequencies at which intensities are linearly influenced. Theoretically, in the 'slope' spectra, band shifts are characterised by 'split' peaks and a decrease in bandwidth with increasing strain levels by a positive peak flanked by two negative peaks. Despite overlapped signals compromised interpretation, clear signals indicating the effect of strain on NIR spectra were observed (Figure 3-5). The three types of samples shared clear peaks at around 7344, 6785, 6418, 6240 cm^{-1}.

The major changes in NIR spectra caused by mechanical strain were found in the region between 6600 and 6000 cm^{-1}. The peaks at around 6418 and 6240 cm^{-1} corresponded to the shifted bands at around 6470 and 6286 cm^{-1} in the second derivative spectra, respectively. As discussed above, this region was related to the overtones of OH stretching of crystalline cellulose (Fackler & Schwanninger, 2010; Tsuchikawa & Siesler, 2003a; Watanabe et al., 2006c). Spectral changes in the region confirmed that cellulose was the main load bearing component. A band at around 7321 cm^{-1} was assigned to the combination of CH deformation and first overtone of CH stretching vibrations (Ali et al., 2001; Schwanninger et al., 2011). A previous study showed that CH stretching signals shifted to higher wavenumbers with increasing of temperature (Altaner et al., 2014a) indicating existence of CH···O hydrogen bonds (French et al., 2014; Nishiyama et al., 2003). The peak at 7344 cm^{-1} in the slope spectra could be related to CH···O bonds between cellulose sheets. But further investigation is required.

Figure 3-5 shows the effect of polarisation on the 'slope' spectra of wood samples. Tensile strain was reported to cause cellulose microfibrils to tilt towards the strain direction (Keckes et al., 2003). Re-alignment of cellulose fibrils in respect to the direction of polarised light can result in spectral changes, while no changes are expected when using non-polarised light. The angle of cellulose microfibrils in respect to the cell axis in the S2 layer is usually in the range of 3° to 30° for normal wood (Tsoumis, 1991). Assuming an angle of 15° between the strain direction and the orientation of the cellulose fibrils, the maximum strain levels of approximately 0.25% used in this study would induce reorientation of 0.5° according to a published model (Keckes et al., 2003). However, no significant differences were detected in the 'slope' spectra with or without polariser in this study (Figure 3-5). Therefore, molecular deformation due to mechanical stretching rather than reorientation of cellulose fibrils is proposed here as the major reason for the observed changes in the region from 6000 to 6600 cm^{-1}.
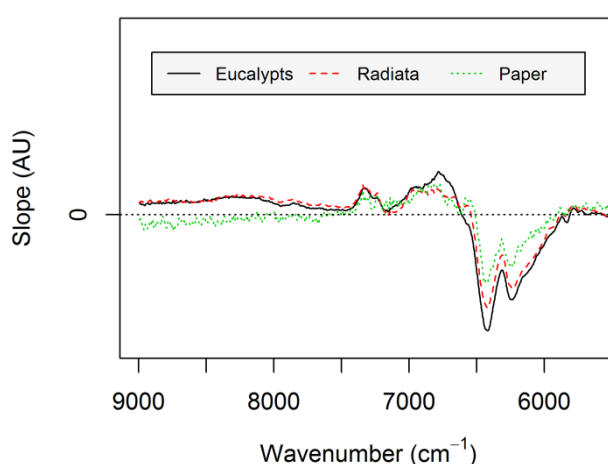
Figure 3-5 Average 'slope' spectra of 10 samples in regard to mechanical tensile strain for eucalypt, radiata and paper in the range of 9000 to 5500 cm^{-1}. Spectra were taken with parallel polarisation. Spectra were taken with parallel polarisation. Strain levels were the same as in
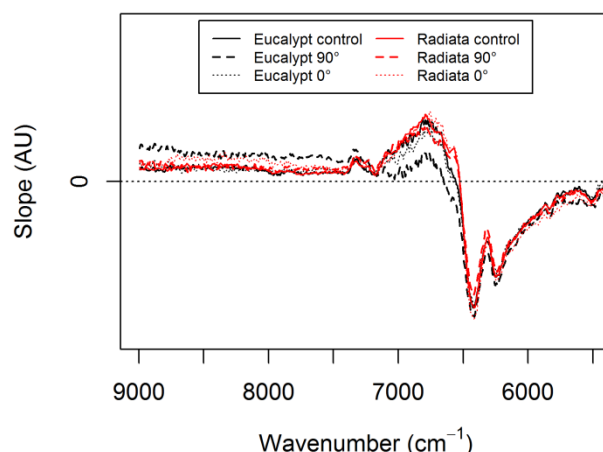
Figure 3-3.

Figure 3-6 Effect of polarisation on the 'slope' spectra of eucalypt and radiata pine samples. Three samples were averaged for each 'slope' spectrum. No polariser was used for the control group. 0° represents polarisation direction parallel to the cell and strain direction; 90° a polarisation direction perpendicular to that. Strain levels were the same as in Figure 3-3.

3.3.2 Quantification of band shifts caused by stretching

3.3.2.1 Variation of band positions

In the relaxed state, the intrachain $2OH\cdots6O$ hydrogen bond resonated at around 6289.36, 6286.01 and 6284.42 cm^{-1} for eucalypt, pine and paper, respectively (Table 3-1). The peak assigned to the $3OH\cdots5O$ was at approximately 6463.81 cm^{-1} for eucalypt, and at 6469.86 and 6474.96 cm^{-1} for pine and paper respectively. The slightly different peak positions in the relaxed state were most likely caused by their different chemical composition resulting in baseline variation form overlapping signals. A previous vibrational study reported that the energy of the hydrogen bonds and hydrogen bonding distances are different between softwood and hardwood (Popescu et al., 2009).

The standard deviation of the peak position from 8 spectra of the same sample was calculated as a measure for the accuracy of the determination of the peak position from the second derivative of the NIR spectra by peak fitting. In transmission mode, the signal associated with the $3OH\cdots5O$ hydrogen bond showed more variation (0.30 - 0.69 cm^{-1}) compared to the signal assigned to $2OH\cdots6O$ (0.11 - 0.16 cm^{-1}) (Table 3-1). This could be due to the lower signal intensity and the skewed band shape of the former. Spectra obtained in diffuse reflection mode had a lower signal to noise ratio compared to the transmission mode, resulting in higher standard deviations (0.36 and 1.33 cm^{-1}).

Analysis of variance (ANOVA) revealed significant differences ($P<0.001$) in the peak positions between the samples of the same material. The standard deviation within samples was smaller than that between the samples of the same material (Table 3-1). For instance, the standard deviation was 0.13 and 0.4 cm^{-1} when calculated within and between samples respectively, for the $2OH\cdots6O$ band for eucalypt. One reason for the difference between the

samples could be residual strain within small wood pieces, which was reported to exist after wood specimens were removed from the living stem and only released after boiling (Toba et al., 2013). Additionally, wood is a heterogeneous material with variable chemical and anatomical features on various scales.

Table 3-1 Peak positions in the relaxed state for the 2OH···6O and 3OH···5O bands and their band shift rates with respect to strain. Values in parentheses are the standard deviations. Peak positions in the relaxed state ("Strain 0") were the average value of 10 or 8 samples for tensile and bending tests, respectively. "Mean SD" representing measurement accuracy, is the average standard deviation of 8 measurement of one sample at "Strain 0". Band shift rates were calculated based on the peak positions at 8 strain levels ("Strain 0" to "Strain 7"). Band shift rates measured in reflection mode were the average of band shifts in the compression and tension surfaces. "r^2" represent the coefficients of determination for the linear models of peak position against mechanical strain.

Sample	Mode	2OH···6O				3OH···5O			
		Peak position (cm^{-1})	Mean SD (cm^{-1})	Band shift rate (cm^{-1}/%)	r^2	Peak position (cm^{-1})	Mean SD (cm^{-1})	Band shift rate (cm^{-1}/%)	r^2
Eucalypt	Reflection	6289.28 (1.08)	0.36	8.93 (2.78)	0.47 (0.17)	6461.02 (4.23)	1.33	23.32 (10.45)	0.43 (0.23)
	Transmission	6289.36 (0.40)	0.13	10.04 (1.02)	0.98 (0.01)	6463.81 (0.69)	0.52	23.30 (3.60)	0.92 (0.06)
Pine	Transmission	6286.01 (0.32)	0.12	9.02 (1.26)	0.96 (0.02)	6469.86 (1.49)	0.58	20.05 (4.48)	0.80 (0.10)
Paper	Transmission	6284.42 (0.46)	0.14	5.38 (1.32)	0.83 (0.10)	6474.96 (1.36)	0.30	14.27 (2.90)	0.81 (0.09)

3.3.2.2 Correlation of band positions with macroscopic tensile strain

For all three sample materials tensile strain shifted the bands associated with the 2OH···6O and 3OH···5O hydrogen bonds to higher wavenumbers (Figure 3-7). The relationship was linear with coefficients of determination (r^2) between 0.80 and 0.98 when measured in transmission mode (Table 3-1). The band shift rates for paper and the wood samples were significantly different (P<0.001). The lower band shift rate for paper indicated that less macroscopic strain was transformed into molecular strain. This could partly be explained by its larger stress relaxation (Supporting Figure 1 and 2 in Appendix A) caused by slippage between pulp fibres.

Furthermore differences between molecular strain and macroscopic strain, which have been reported for wood (Montero et al., 2012), could result from the structure of the cell walls. According to Montero et al (2012), the main reason is misalignment between the cellulose fibrils to the strain direction amplified by bending and shearing of anatomical structures as well as straightening of slightly waved cellulose macrofibrils, forming lenticular spaces between adjacent fibrils (Bonnet et al., 2017; Boyd, 1982; Salmén, 2015).
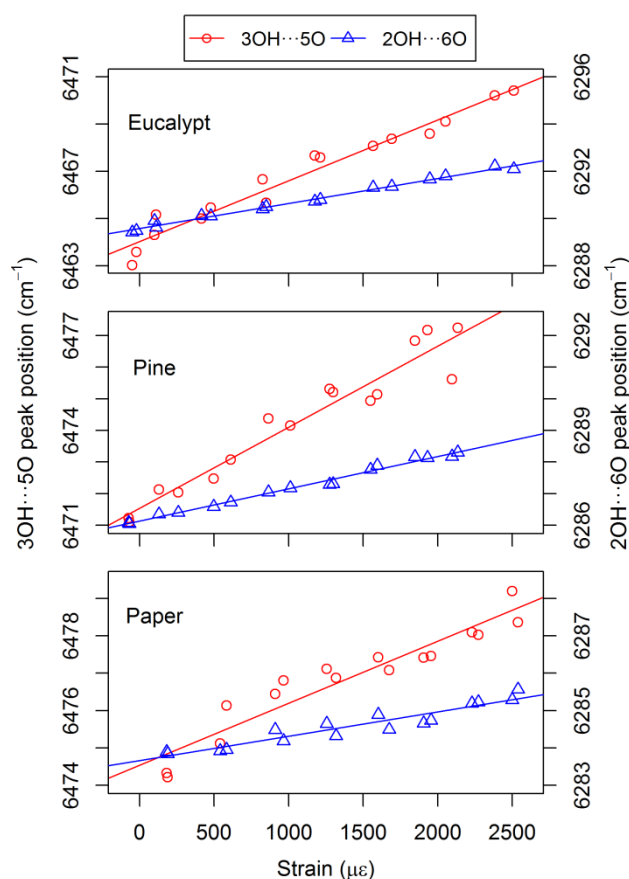
Figure 3-7 Positions of signals assigned to the OH groups associated with intramolecular 2OH⋯6O and 3OH⋯5O hydrogen bonds of cellulose at different strain levels in parallel polarised NIR spectra for a eucalypt, pine and paper sample. A linear model was fitted for each sample.

Band shift rates for the signal at around 6470 cm^{-1} assigned to the 3OH⋯5O hydrogen bonded OH group of cellulose were more than twice that of the signal of the 2OH⋯6O hydrogen bonded OH group at around 6286 cm^{-1} (Table 3-1). This was consistent with reports based on mid-range IR and molecular modelling studies describing bending of the glyosidic bond and consequently differential elongation of the two flanking intramolecular hydrogen bonds upon stretching of cellulose molecules (Altaner et al., 2014b; Djahedi et al., 2016). However, no band shifts of the 2OH⋯6O bonds were detected for the fundamental frequencies. Band shifts in the mid-range are expected to be smaller and therefore 2OH⋯6O might be undetectable for fundamental frequencies.

The band shift rates of the 3OH⋯5O bond (>20 cm^{-1}/%) were considerably larger than the band shift rates of 3 cm^{-1}/% and 1 cm^{-1}/% reported for fundamental 3OH⋯5O and 3OD⋯5O bonds measured on microtomed wood sections, even if corrected for overtone (factor of 1.92) and isotope effects (factor of 1.34) (Altaner et al., 2014b; Salmén & Bergström, 2009). The increased difference between macroscopic and molecular strain in thin wood sections is contributing to this difference (Navi et al., 1995; Yu et al., 2009).

No significant difference (P>0.05) was found between radiata pine and eucalypt wood samples in regard to their band shift rates caused by macroscopic tensile strain. This indicated that band shifts depended on strain rather than stress for two timber species. This supported previous findings by Salmen *et al.* (Salmén & Bergström, 2009), who reported that

42

spruce wood sections had constant band shift rate with regard to macroscopic strain at around 1160 cm^{-1}. This was interpreted as evidence of the parallel arrangement of crystalline and noncrystalline cellulose.

3.3.3   NIR band shifts quantified in bending tests

The effect of compression strain on NIR spectra of wood was investigated in a bending test. NIR spectra of eight eucalypt samples were collected from both, tension and compression surfaces, using a fibre optic probe. Although the spectra were of lower quality than the transmission spectra (Table 3-1), a clear shift for the band at 6286 ± 5 cm^{-1} with applied strain was observed (Figure 3-8). The peak position shifted to lower frequencies under compression indicating a shortening of the 2OH···6O hydrogen bond (Figure 3-8). The average band shift rate with respect to strain was not significantly (P > 0.05) different for the tension and compression surfaces and averaged 8.93 cm^{-1}/%. This was close to the band shift rate of 10.04 cm^{-1}/% calculated from polarised transmission spectra combined with tensile tests (Table 3-1).

This finding was consistent with X-ray diffraction data from poplar specimens during a bending test, which suggested that the crystal strain in cellulose was positive on the tension and negative on the compression side and that the ratio of cellulose and overall strain did not differ significantly in tension and compression (Montero et al., 2012).

André et al. (2006) reported changes in NIR spectra of poplar wood under 4-point bending. They suggested that, the absorbance at around 5200 cm^{-1} decreased with the increase of load, both in tension and compression. This region is associated with water (Schwanninger et al., 2011) and our results did not support their findings (data not shown). Another study investigated compression of microcrystalline cellulose into tablets by NIR spectroscopy (Shinzawa et al., 2011). A band at 6960 cm^{-1} (assigned to amorphous cellulose) shifted to lower wavenumbers while a band at 6310 cm^{-1} (assigned to crystalline cellulose) shifted to higher wavenumbers with increasing pressure. The crystallinity of cellulose decreased during the compression process as measured by X-ray diffraction. As the compression loads were independent of the cellulose orientation and released prior to NIR measurements, the mechanism of band shift in this study was related to changes in crystallinity and possibly density and particle size rather than molecular deformation.
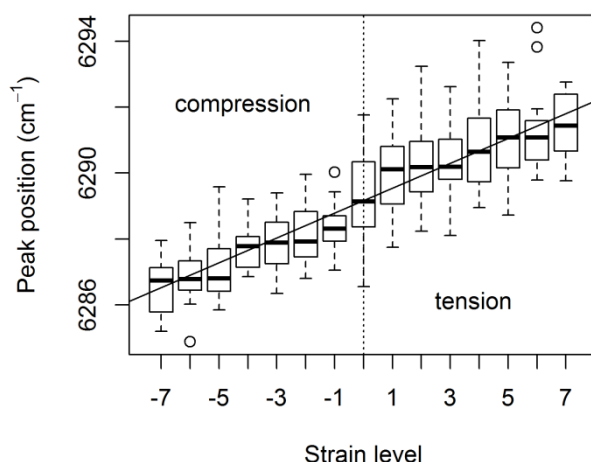
Figure 3-8 Relationship between strain levels and peak positions of the band associated with the

intrachain 2OH⋯6O bond for 8 eucalypt samples in 3 point bending tests. The solid line shows the linear regression of peak positions against strain levels considering all 256 data points. Strain levels ranged from -7 (compression) to 7 (tension), ranging approximately between -2100 µε and 2100 µε.

3.4 Conclusions

With the increase of tensile stress, consistent spectral changes can be observed especially in the first overtone of the OH stretching region. Peak positions of both bands at 6286 ± 5 cm^{-1} and 6470 ± 10 cm^{-1} were linearly correlated with strain levels. Those two bands were assigned to 2OH and 3OH involved in intramolecular hydrogen bonds, respectively. The bands shifted to higher wavenumbers with the increase of tensile strain and shifted in the opposite direction when under compression. The band shifts were interpreted as the strengthening of OH groups caused by the elongation of hydrogen bonds in crystalline cellulose in tension. Wood samples had a greater band shift rate than paper samples. For wood samples, a strain of 0.1% would induce a band shift of approximately 1 cm^{-1} at around 6286 cm^{-1}. The band shift rate at around 6470 cm^{-1} (3OH⋯5O) was more than twice that at around 6286 cm^{-1} (2OH⋯6O) indicating bending of the glycosidic bond during stretching. The results suggest that it might be possible to predict stress levels in cellulose materials non-destructively using NIR spectroscopy.

4 EFFECTS OF MECHANICAL STRETCHING, DESORPTION AND ISOTOPE EXCHANGE ON DEUTERATED EUCALYPT WOOD STUDIED BY NEAR INFRARED SPECTROSCOPY

4.1 Introduction

Wood is a hygroscopic material and it is well known that below fibre saturation point mechanical properties such as stiffness and strength increase with decreasing moisture content (Green et al., 2010). Less known is the fact that conversely tensile stress increases the equilibrium moisture content of cellulose and wood (Simposon, 1971; Treloar, 1953). However, the effect of mechanical strain on the equilibrium moisture content is small and difficult to observe as slight changes in the atmosphere can cause adsorption or desorption of moisture in wood, confounding the two effects. Zabler *et al.* (Zabler et al., 2010) studied the deformation of cellulose induced simultaneously by tensile stress and dehydration on spruce wood using X-ray diffraction and proposed two deformation mechanisms of different nature and magnitude.

Cellulose microfibrils, comprised of a bundle of parallel aligned cellulose molecules, are covered by hemicelluloses in wood cell walls (Altaner et al., 2006; Salmén & Burgert, 2009). These microfibrils aggregate into 10-20 nm thick bundles, which are surrounded by a matrix of lignin and hemicellulose (Jarvis, 2018). NMR showed that each cellulose microfibril contains crystalline and less ordered forms of cellulose (Fernandes et al., 2011; Wickholm et al., 1998), which were suggested to be arranged in parallel rather than alternating along its axis, with limited axial disorder in the crystalline region (Jarvis, 2018; Salmén & Bergström, 2009). Hydroxyl groups in the compact and crystalline regions of cellulose aggregates are inaccessible to water and have lower chemical reactivity compared to those in the less ordered regions. Deuteration refers to the exchange of protons in hydroxyl groups with deuterium atoms (OH to OD) (Hofstetter et al., 2006). By exposing wood or cellulose to heavy water, signals from hydroxyl groups with different accessibilities can be separated by infrared spectroscopy, providing information of the cellulose structure on the molecular level.

Although NIR combined with multivariate statistical analysis has many applications in material science (Li & Altaner, 2018; Popescu & Popescu, 2013; Tsuchikawa & Kobori, 2015), few studies used it to unravel the structure of wood and cellulose on a molecular level. Polarized NIR spectroscopy found that the hydroxyl groups in wood were preferably oriented along the grain, i.e. in direction of the cellulose fibrils (Fackler & Schwanninger, 2010; Tsuchikawa & Siesler, 2003a). NIR can also be used to study the molecular deformation of cellulose and wood under mechanical stress. Spectral changes and NIR band shifts with the increase of tensile strain were shown for air-dry wood samples (Guo & Altaner, 2018). The bands at around 6470 and 6286 cm^{-1} (second derivative spectra), which were tentatively assigned to intramolecular hydrogen bonded hydroxyls, shifted to higher frequencies under tensile stretching as a result of weakening hydrogen bonds. Hofstetter et

al. (2006) investigated the roles of accessible and inaccessible cellulose in load transfer using dynamic mid-infrared spectroscopy combined with deuteration (Hofstetter et al., 2006). This data suggested that only hydroxyls in the non-load bearing parts were exchanged by deuterium (Hofstetter et al., 2006).

Deuterated cellulose and wood samples will be subject to re-protonation when exposed in the ambient environment during sample handling. The deuteration and re-protonation were found to be fast in the beginning, while exchange takes place at the disordered surface regions and levels-off later for the less accessible regions (Pönni et al., 2013; Pönni et al., 2014). Re-protonation was reported inevitable during ATR infrared spectroscopy and use of a freshly cut surface of deuterated wood was suggested to be essential to obtain reproducible results (Tarmian et al., 2017). In this work the effects of desorption and isotope re-exchange were separated from those of mechanical strain by collecting NIR spectra in loading and unloading processes.

NIR is sensitive to moisture and it was investigated whether NIR spectroscopy can be used to characterize the dependence of moisture adsorption on tensile stress. In this work, we first monitored the drying process of deuterated eucalypt samples to assign NIR bands of deuterated wood. To study the spectral changes caused by pure mechanical stress, equilibrated wood samples were stretched under constant humidity. In order to characterize the roles of accessible and inaccessible cellulose in load transfer under tensile stretching, NIR spectral changes caused by strain were studied for both, protonated (control) and deuterated wood samples.

4.2 Materials and Methods

4.2.1 Sample preparation and characterization

Five thin *Eucalyptus regnans* samples with a thickness of 0.5 to 1 mm in preferably radial direction were cut from sapwood of a quarter-sawn board with an air-dry density of 0.54 g/cm^3 sourced from Canterbury, New Zealand. Their width was 16 mm and the length was 85 mm along the longitudinal direction. Samples were conditioned to constant weight in a sealed container over a saturated K_2CO_3 solution, equating to a relative humidity of 42.3%. Transmission NIR spectra were acquired using a Tensor 37 infrared spectrometer (Bruker, Germany) at a resolution of 8 cm^{-1} averaging 128 scans before and after deuteration.

Subsequently, four samples were oven dried at 103 °C before being immersed in a sealed container containing 25 mL deuterium oxide (99.9%, Sigma Aldrich, Australia) at room temperature for 7 days. One of the samples was dried in a container over phosphorus pentoxide (P_2O_5) to 0.8% while spectra were taken at different drying stages to monitor the drying process. The other three samples used to study the effect of polarization and mechanical stretching were dried over P_2O_5 close to FSP (monitored by sample mass) and then equilibrated over saturated K_2CO_3 solution in D_2O.

The orientation of hydroxyl groups in wood was investigated based on the NIR spectra of the three equilibrated samples before and after deuteration. Parallel (0°) and perpendicular (90°) polarization were achieved by manually aligning a NIR polarizer (CODIXX, Germany) with respect to the wood cell axis. A linear baseline was constructed by connecting the intensities at 7197 and 6150 cm^{-1}. The dichroic ratio was defined as the ratio ($A_{0°}/A_{90°}$) of absorbance in the parallel and perpendicular polarized spectra after baseline correction.

4.2.2 Mechanical stretching combined with NIR spectroscopy

Tensile tests were conducted with a self-developed device (Guo & Altaner, 2018), which enabled simultaneous collection of transmission NIR spectra. Six tensile strain levels ("Strain 0" to "Strain 5") were applied representing displacement of 0, 0.04, 0.08, 0.12, 0.16 and 0.20 mm measured using a dial gauge (Starrett 3809MA, USA) with a graduation of 0.01 mm. Humidity was controlled by sealing the sample compartment fitted with the stretching device. For examining the effect of tensile stress on NIR spectra of wood, beakers with saturated K_2CO_3 solution were put into the sealed sample compartment to obtain a constant relative humidity. Protonated samples were equilibrated over K_2CO_3 solution in a sealed container before being placed in the sample compartment overnight to further equilibrate. Three loading-unloading strain cycles were conducted consecutively and 36 NIR spectra were collected for the same sample.

To investigate the combined effect of desorption and stress, three protonated samples pre-conditioned over K_2CO_3 (42.3% RH) were measured in the sample compartment at ~30% RH. The three protonated samples lost moisture due to the drier environment during mechanical stretching and spectra collection. Each sample underwent one loading-unloading cycle.

The tensile tests for deuterated samples were conducted while purging the sample compartment with D_2O vapour (RH: 42.3%) from a humidity generator (Surface Measurement Systems, UK) filled with heavy water in an attempt to limit desorption and re-protonation (OD to OH). A loading-unloading and an unloading-loading strain cycle were carried out separately for each sample. In the unloading-loading strain cycle the strain was successively released from level "Strain 5" to "Strain 0" followed by successive re-loading to "Strain 5". NIR spectra were taken at each strain level. The samples were weighed before and after NIR collection and moisture content was calculated based on oven-dry weight. The experimental design of this study was summarized in Figure 4-1.
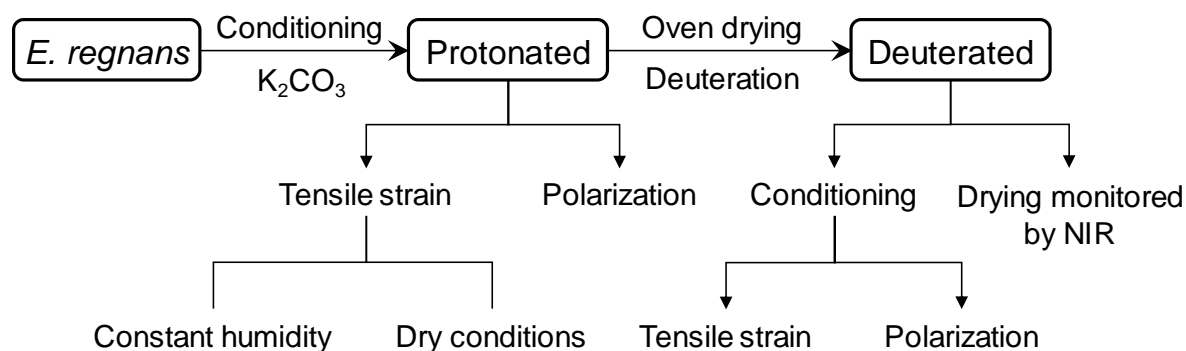
Figure 4-1 Flowchart of the experimental design in this study

4.2.3 Spectra manipulation

NIR spectra were normalized using the "scale" function in R (R Core Team, 2017). 'Slope' spectra were defined as the rate of change of the intensity with increasing tensile strain (Altaner et al., 2014a; Guo & Altaner, 2018) and calculated as the slope coefficient of the linear regression between normalized spectral intensity at each wavenumber and applied strain. Consequently, monotonous changes in moisture content or isotope exchange can be observed as opposite peaks in the 'slope' spectra of the loading and unloading processes. To reduce these effects and highlight the effect of mechanical strain, the 'slope' spectra of the loading process (a) were added to those of the unloading process (b) multiplied by a

scaling factor (k). The scaling factor was optimized to minimize c in Equation 4.1 using the nonlinear solving method in Microsoft EXCEL.

$$c = \sum_{i=1}^{n}(a_i + k \times b_i)^2 \qquad (4.1)$$

Where a_i and b_i are the ith data in the 'slope' spectra of the loading and unloading process, respectively; n is the number of data points in one spectrum and k is the scaling factor.

4.3 Results

4.3.1 NIR band assignments of deuterated wood samples based on its drying process

NIR spectroscopy was used to monitor the drying process of a deuterated wood sample at ambient temperature over P_2O_5 in a sealed container, while the moisture content decreased from 140.9% to 0.8% (Figure 4-2). Saturation in heavy water resulted in a peak at around 4990 cm^{-1}, which was assigned to the combination band of symmetric (v_1) and asymmetric (v_3) stretching of D_2O molecules (Workman & Weyer, 2008). Above fibre saturation point (FSP), the overall absorbance increased with the decrease of moisture content (Figure 4-2A). As free water in wood reduced the refractive difference between cell wall and cell lumen the light transparency was higher when more cells were filled with free water (Foroughi et al., 2016). However, as the moisture content decreased below FSP, the absorbance decreased because less bound water molecules were present, absorbing near infrared radiation (Figure 4-2A).

Normalizing the NIR spectra based on signals assigned to CH stretching vibrations (5800 to 5740 cm^{-1}), which should be less affected by deuteration, removed the above described effect on transparency and highlighted spectral changes (Figure 4-2B). A shoulder peak at around 5190 cm^{-1} and the broad peak in the OH stretching region intensified upon drying. The signal at around 5190 cm^{-1} was assigned to water (H_2O) (Inagaki et al., 2008; Workman & Weyer, 2008), indicating that the wood sample had been slightly re-protonated during sample handling and spectra collection. A study using ATR infrared spectroscopy to measure the accessibility of wood with D_2O highlighted the risk of re-protonation (Tarmian et al., 2017). Below FSP, a peak around 4760 cm^{-1}, assigned to combination bands of OH and CH) became prominent (Schwanninger et al., 2011). The band shape at around 4760 cm^{-1} of deuterated wood differed from protonated wood. Considering the isotope effect with a factor of 1.34 this was probably due to the overlap of the first overtone of the OD stretching band (Jarvis & McCann, 2000). The band at around 5975 cm^{-1} disappeared below 5.6%. This band was tentatively assigned to semiheavy water (HDO) (Workman & Weyer, 2008). Those assignments have been summarised in Table 4-1.
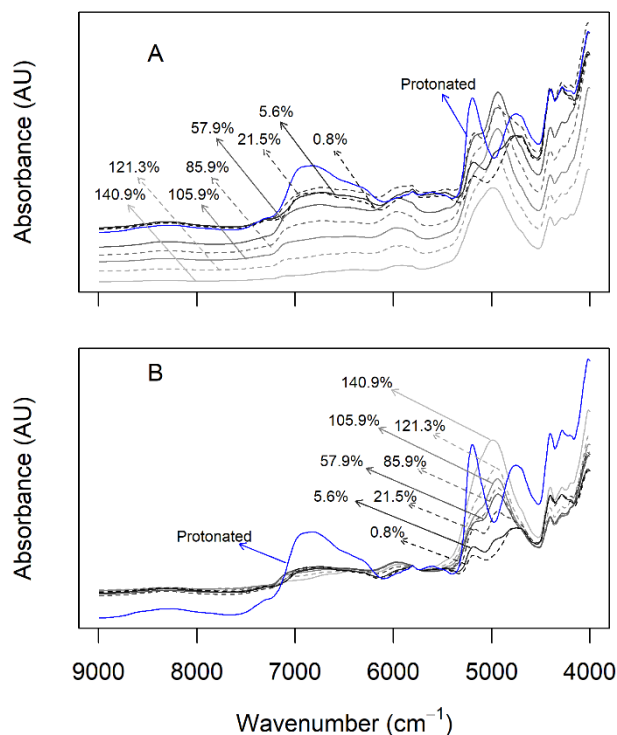
Figure 4-2 Drying process of a deuterated eucalypt sample monitored by NIR spectroscopy.
Original spectra (A) and normalized spectra (B) of the same sample in the region of 5800 to 5740
cm⁻¹. The deuterated sample was dried at ambient temperature over P_2O_5 in a sealed container
from a moisture content of 140.9% to 0.8%. A protonated eucalypt sample conditioned at a
relative humidity of 42.3% corresponding to a moisture content of 8.4% was included as reference
(blue).

Table 4-1 Assignment of NIR signals in deuterated wood samples

Peak position (cm⁻¹)	Assignment	Note
~ 4700	First overtone of OD stretching	Isotope effect 1.34
~ 4739	Combination bands of OH or CH deformation with OH stretching	(Schwanninger et al., 2011)
4940 to 4990	$v_1 + v_3$ of D_2O	(Workman & Weyer, 2008)
~ 5190	$v_2 + v_3$ of H_2O in wood	(Inagaki et al., 2008; Workman & Weyer, 2008)
~ 5975	$v_1 + v_3$ of HDO	(Workman & Weyer, 2008)

6286	First overtone of OH stretching in $2OH\cdots6O$ of cellulose	(Guo & Altaner, 2018)
6470	First overtone of OH stretching in $3OH\cdots5O$ of cellulose	(Guo & Altaner, 2018)
~ 6955	First overtone of OH stretching of free hydroxyl groups and $v_1 + v_3$ of water	(Schwanninger et al., 2011; Workman & Weyer, 2008)
7073	Weak hydrogen bonds between water molecules	(Watanabe et al., 2006b)

Note: v_1 and v_3 represent symmetric and asymmetric stretching vibrations respectively, while v_2 stands for the bending mode.

4.3.2 Orientation of hydroxyl groups in deuterated samples investigated by polarised NIR spectroscopy

Typically, in wood most of the cellulose microfibrils are oriented close to the axial cell direction and as a consequence, the hydroxyl groups in crystalline cellulose are oriented. In cellulose Iβ with hydrogen bond network A (Nishiyama et al., 2002), the hydroxyls at C2 and C3 are almost parallel to the chain direction while the hydroxyl at C6 is oriented almost perpendicular to the chain direction (Hayakawa et al., 2017). Polarised infrared spectroscopy is sensitive to molecular orientation and consistent with these directions of OH groups in cellulose (Nishiyama et al., 1999).

Based on the assumption that intermolecular hydrogen bonds are approximately in the transverse direction and intramolecular hydrogen bonds are in the axial cellulose chain direction, polarised mid-infrared spectroscopy was used to assign hydroxyl groups in cellulose (Altaner et al., 2014b; Hayakawa et al., 2017; Maréchal & Chanzy, 2000). Distinct peak shapes and positions in the OH stretching region (3500 to 3200 cm^{-1}) were reported for parallel and perpendicular polarised spectra of cellulose and wood (Christopher M Lee et al., 2015; Nishiyama et al., 1999). In comparison, the effect of polarisation on near infrared spectra was shown to be less prominent, manifested in a slightly higher intensity in parallel polarised spectra in the range from 7200 to 6100 cm^{-1} assigned to the first overtone of OH stretching (Fackler & Schwanninger, 2010; Tsuchikawa & Siesler, 2003a).

At ~9% moisture content, the dichroic ratio of the first overtone of OH stretching of the protonated eucalyptus wood samples was greater than 1, indicating a preferred parallel orientation of the hydroxyl groups (Figure 4-3). Similar observations were reported for spruce (*Picea sitchensis*) and beech (*Fagus crenata*) wood (Tsuchikawa & Siesler, 2003a, 2003b). The dichroic ratio of the *E. regnans* samples increased after deuteration of the accessible hydroxyls (Figure 4-3). This matched previous reports for a softwood (spruce) (Tsuchikawa & Siesler, 2003a). The increase in the dichroic ratio of the remaining inaccessible hydroxyl groups after removing the accessible hydroxyls by deuteration supports that a cellulose fibril having a crystalline fraction, which is preferably oriented along the wood grain. The accessible, less oriented fraction of hydroxyls in wood not only includes hemicelluloses but also disordered parts of the cellulose fibrils, which have been shown to have a more

randomized orientation (Driemeier et al., 2015). The absence of a preferred parallel orientation of the inaccessible hydroxyls in the hardwood (beech) was tentatively explained by the amount of ray cells, which have cellulose preferably aligned in radial direction (Tsuchikawa & Siesler, 2003b). However, ray cells in beech wood account for 27% of the total wood volume (Fengel & Wegener, 1984). The proportion of the rays by mass will be smaller, which is linked to NIR absorption, as rays are made of thin walled parenchyma cells. The ray volume of eucalyptus has been reported to vary between 10% and 20% (Wilkes, 1988). Here, we found that hardwood also showed an increase in the NIR dichroic ratio after deuteration.
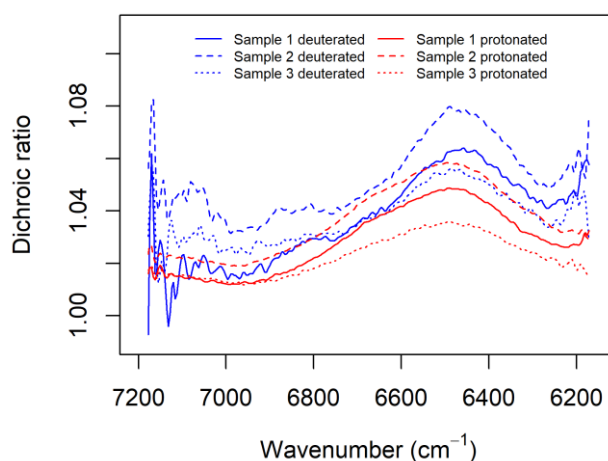
Figure 4-3 Dichroic ratio of protonated and deuterated eucalyptus wood in the first overtone of OH stretching range from 7200 to 6200 cm^{-1}. Moisture content of protonated and deuterated samples were 8.4% and 9.1%, respectively.

4.3.3 NIR spectral changes of wood caused by tensile strain and desorption

Spectral changes caused by mechanical stretching were examined by conducting three loading-unloading strain cycles consecutively on a protonated eucalypt sample equilibrated in an environment of constant humidity (Figure 4-4). The 'slope' spectra of the loading and the unloading processes showed the same features, indicating a stable environment and consequently that the sample was in a moisture equilibrium. The two negative peaks at around 6420 and 6240 cm^{-1} in the 'slope' spectra (Figure 4-4) were interpreted as the weakening of intramolecular hydrogen bonds in crystalline cellulose upon mechanical stretching of cellulose chains (Guo & Altaner, 2018).

A small positive peak at around 5440 cm^{-1} could be assigned to the combination of OH stretching and second overtone of CO stretching (Schwanninger et al., 2011). The bands ranging from 4800 to 4700 cm^{-1} were assigned to combinations of OH stretching and OH deformation or CH deformation vibrations (Schwanninger et al., 2011). The spectral changes at around 5440 cm^{-1} and 4670 cm^{-1} (Figure 4) in response to mechanical strain could also be attributed to the deformation of hydrogen bonded hydroxyl groups. Bands below 4500 cm^{-1} were difficult to assign due to various possibilities of coupling (Schwanninger et al., 2011). The band affected by mechanical strain at around 7340 cm^{-1} (Figure 4-4) could be

related to CH···O bonds (Altaner et al., 2014a; Guo & Altaner, 2018). Another evidence for the existence of CH···O bonds was the small negative peak at around 5830 cm⁻¹ (Figure 4-4), which was assigned to the first overtone of CH stretching (Schwanninger et al., 2011).

The weak positive peak at around 5200 cm⁻¹ indicated adsorption of moisture with increasing tensile strain, indicating that stress affected the hygroscopic property of wood. This was consistent with experimentally confirmed theoretical consideration based on thermodynamics of gels (Simposon, 1971; Treloar, 1953). This effect is larger for isotropic materials. A tensile stress of 40 MPa was reported to increase the moisture content by roughly 1% in viscose cellulose filaments (Treloar, 1953). Conversely, changes in moisture content was reported to induce stresses and deformation in cellulose and wood (Fang & Catchmark, 2014; Toba et al., 2012; Zabler et al., 2010).

The combined effects of water desorption and mechanical stress were tested on three samples without humidity control in the sample compartment (Figure 4-5). During the loading cycle the moisture content of the samples reduced by less than 0.5% (ΔMC). Continuous changes in moisture content during the experiment will resulted in opposite signals in the 'slope' spectra during loading and unloading. Negative values in the loading and positive values in the unloading processes appeared at around 7120 and 5160 cm⁻¹ (Figure 4-5), indicating a decrease in water signal intensity due to desorption. This was consistent with the measured decrease in moisture content. The signals in the 'slope' spectra at around 7120 and 5160 cm⁻¹ were close to those assigned to water (Table 4-1). The signal at around 7073 cm⁻¹ was assigned to hydrogen bonds between water molecules (Table 4-1) (Watanabe et al., 2006b). The band at 7120 cm⁻¹ could be due to the breakage of water-water hydrogen bonds in the desorption process. Signals attributed to tensile strain at around 7340, 6420, 6240 and 4670 cm⁻¹ mirrored those observed at constant moisture content (Figure 4-4).
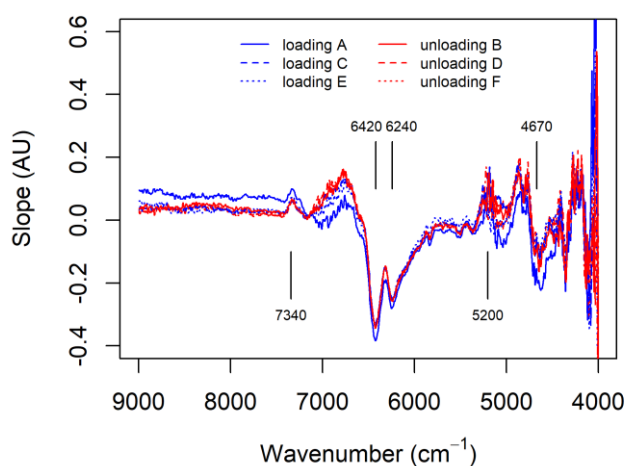
Figure 4-4 'Slope' spectra of one protonated eucalypt sample going through three consecutive "loading - unloading" strain cycles in constant humidity. The wood sample was equilibrated above a saturated K₂CO₃ solution (42.3% RH).
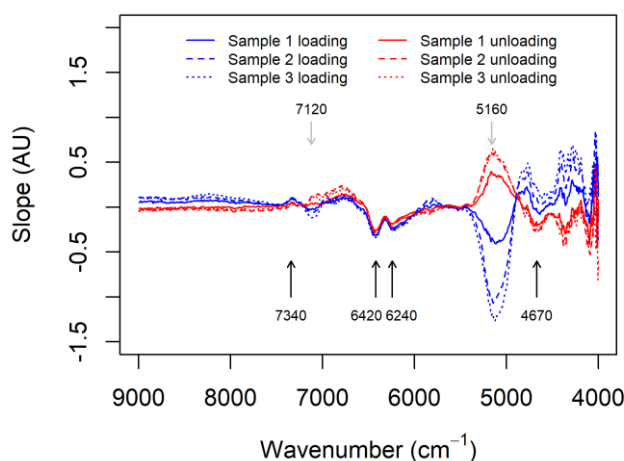
Figure 4-5 'Slope' spectra of three protonated eucalypt samples undergoing a loading-unloading strain cycle during desorption. The initial moisture content was around 8.4% and decreased by less than 0.5% at the end of the loading cycle. The major changes caused by mechanical strain and desorption were marked by black and grey arrows, respectively.

4.3.4 NIR spectra of deuterated wood samples under tensile strain

The spectral changes of three deuterated samples, with a moisture content of 9.1% undergoing a loading-unloading strain cycle as well as an unloading-loading strain cycle, are shown in Figure 4-6. The intense opposite peaks in the loading and unloading processes suggested significant effects of desorption and isotope exchange. However, two negative peaks at around 6420 and 6240 cm^{-1} caused by mechanical strain were visible for all samples independent of the loading cycle.

The MC of the samples, which had been previously equilibrated over D_2O saturated with K_2CO_3 (42.3% RH), decreased less than 0.5% (ΔMC) during the experiments, despite purging the sample compartment with D_2O vapour at RH of 42.3%. The negative bands in the loading process at 5160 and 4900 cm^{-1} represented the loss of H_2O and D_2O, respectively. The intensities of those bands were greater in the loading process than the unloading process in the loading-unloading cycle (Figure 4-6A) and the contrary behaviour was observed for the unloading-loading cycle (Figure 4-6B), suggesting that the desorption rates reduced over time. The broad band at around 6930 cm^{-1} in the 'slope' spectra were assigned to the $v_1 + v_3$ vibrations of water and free and weakly bonded hydroxyl groups of polysaccharides in wood (Table 1). This opposite band was absent in loading cycles of protonated samples (Figure 4-5), suggesting isotope exchange rather than desorption was responsible for this spectral change. Handling deuterated samples in the normal atmosphere can cause re-protonation (OD to OH) (Tarmian et al., 2017). Without purging the sample compartment with D_2O vapour, the intensity at around 6930 cm^{-1} increased over time (Supporting Figure 6 in Appendix E), while it decreased over time when purged with D_2O vapour (Figure 4-6). Consequently, the deuterated samples experienced OD to OH exchange (re-protonation) during sample handling and OH to OD exchange (deuteration) by purging during the stretching tests.
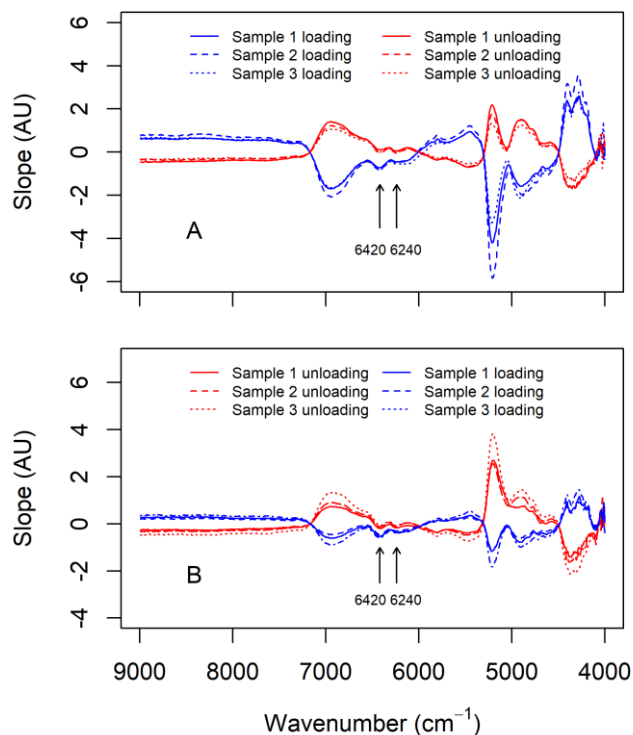
Figure 4-6 'Slope' spectra of three deuterated eucalyptus wood samples conditioned at 42.3% RH experiencing a loading-unloading (A) and an unloading-loading (B) strain cycle. Initial moisture contents were approximately 9.1% and decreased by was less than 0.5% at the end of the loading cycle. The prominent spectral changes at 6420 and 6240 cm^{-1} due to mechanical strain were labelled by black arrows.

By adding the 'slope' spectra of the loading to those of the unloading process (Figure 4-6) the effects of desorption and isotope exchange could be reduced (Equation 4.1). After correction, the effect of mechanical stretching was highlighted (Figure 4-7). However, the opposite bands at 5160 cm^{-1} and 4900 cm^{-1} assigned to water and D_2O were not fully removed, suggesting that desorption and isotope exchange occurred at different rates.

Compared to protonated samples (Figure 4-5), bands responding to tensile strain occurred at the same positions. The prominent bands at 7340, 6420, 6240 and 4670 cm^{-1} as well as the region below 4500 cm^{-1} showed a similar pattern. Small sharp bands at 5830, 5440, 4360 and 4110 cm^{-1} appeared at similar positions as in protonated samples in Figure 4-4, but were clearer. No clear assignments for these smaller bands were found in the literature.

Hydrogen bonded hydroxyls in inaccessible cellulose (6420 and 6240 cm^{-1}) took part into the load transfer process in wood. This was consistent with the results of infrared and Raman spectroscopy studies (Gierlinger et al., 2006; Hofstetter et al., 2006; Salmén & Bergström, 2009). Additionally previous mid-infrared and Raman spectroscopy studies showed that the covalent glycosidic bond (COC) and the CO bonds in the glucose ring were also load-carrying structures (Eichhorn & Young, 2001; Gierlinger et al., 2006; Salmén & Bergström, 2009). As NIR spectra are dominated by bonds involving hydrogens (Osborne et al., 1993), these bonds are not detectable in the near infrared region.

The first overtone of OD stretching involved in hydrogen bonds was expected to be at around 4700 cm^{-1} (Table 4-1), overlapping with the combination of OH stretching with OH or

CH deformation vibrations. However, a small band at around 4700 cm^{-1} showed a response to mechanical strain in deuterated samples (Figure 4-7 inset). This could be an indication that exchangeable hydrogen bonds, probably from the accessible surface chains of cellulose fibrils, elongated and participated in load transfer. However, while dynamic mid-range IR of deuterated spruce pulp showed that most stress in cellulose was transferred by the inaccessible crystalline cellulose chains, accessible hydroxyl groups showed some, also a less defined, response to mechanical strain (Hofstetter et al., 2006). Additionally, dynamic FTIR studies suggested that glucomannan and lignin were also involved in the load transfer of wood (Åkerholm & Salmén, 2001; Salmén et al., 2016).
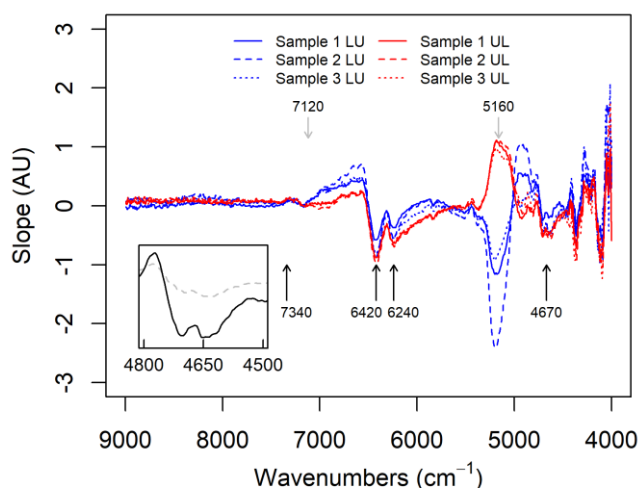
Figure 4-7 'Slope' spectra of three deuterated eucalyptus wood samples, which have been 'corrected' for desorption and isotope exchange effects. "LU" represents the loading-unloading and "UL" the unloading-loading strain cycle. The inset illustrated the "slope spectra" of protonated samples (grey dashed line) and deuterated samples (black solid line) in the region from 4800 to 4500 cm^{-1}, which were average of 6 "slope spectra" from Figure 5 and this figure, respectively.

4.4 Conclusions

Polarised NIR spectroscopy of deuterated *E. regnans* wood confirmed that inaccessible hydroxyl groups were oriented more parallel to the grain compared to the accessible fraction. NIR spectroscopy also confirmed that tensile stress caused wood to adsorb moisture. The effect of mechanical strain on NIR spectra could be highlighted by removing desorption and re-protonation effects through averaging loading and unloading cycles. The prominent bands at 6420, 6240 and 4670 cm^{-1}, assigned to hydroxyl groups, remained after deuteration, suggesting that the inaccessible fraction of cellulose was the major load-carrying structure. A small band responding to mechanical strain at around 4700 cm^{-1} in deuterated wood might indicate a contribution of accessible hydroxyls in load transfer.

5 THE POSSIBILITY OF NON-DESTRUCTIVE MEASUREMENT OF GROWTH-STRESS IN TREES: A NEAR INFRARED SPECTROSCOPIC APPROACH

This chapter has been submitted as:

Guo, F., Cramer, M., & Altaner, C. M. (2019) The possibility of non-destructive measurement of growth-stress in trees: A near infrared spectroscopic approach.
The manuscript presented here may different from any published version due to peer-review and editorial processes.

5.1 Introduction

Wood cell walls consist of crystalline cellulose microfibrils embedded in a matrix of hemicellulose and lignin. The cellulose fibrils are oriented close to the cell axis in the thickest secondary cell wall layer. Under axial tensile stress, cellulose molecules in wood cell walls will be stretched along the molecule chain. This molecular deformation has been detected by Raman spectroscopy (Eichhorn et al., 2001; Gierlinger et al., 2006), mid-range infrared spectroscopy (Altaner et al., 2014b; Hinterstoisser et al., 2003) and X-ray diffraction techniques (Montero et al., 2012; Peura et al., 2007). Near infrared (NIR) spectroscopy has the advantage of quick and easy spectra collection and contains structural information of hydroxyl groups (Osborne et al., 1993). Recently, for air-dry wood samples, bands tentatively assigned to the intramolecular hydrogen bonded $3OH\cdots5O$ (6470 ± 10 cm^{-1}) and $2OH\cdots6O$ (6286 ± 5 cm^{-1}) of cellulose were reported to shift to higher wavenumbers with axial tensile strain (Guo & Altaner, 2018). This could be explained by the stretching of intramolecular hydrogen bonds ($O\cdots H$) of cellulose resulting in the strengthening the covalent donor (O-H) bond. Therefore, it should be possible to predict molecular strain levels in wood using NIR spectroscopy.

Growth-stress in trees is thought to originate from the cell formation and maturation process (Alméras & Clair, 2016; Yamamoto, 1998) and causes problems like heart-checking, end-splitting and board distortion for wood utilization, preventing plantation-grown eucalypts from being used for solid wood products (Yang & Waugh, 2001). Growth-stress induces molecular strain. Changes in the cellulose lattice spacing caused by the release of growth-stress was detected by X-ray diffraction (Clair et al., 2006). Growth-stress is a function of growth-strain and the modulus of elasticity and can only be measured indirectly through measuring these two wood properties (Raymond et al., 2004). Current methods for measuring growth-strain in trees or logs, including the strain gauge method (Yoshida & Okuyama, 2002), the CIRAD-Forêt method and the Nicholson technique (Yang et al., 2005), are time-consuming and destructive. Alternatively, the 'splitting' test provides a fast assessment but is also destructive (Chauhan & Entwistle, 2010; Davies et al., 2017). However, a quick and non-destructive assessment of growth-strain is necessary for the segregation of logs with low growth-strain for solid wood processing.

NIR spectroscopy has been proven a powerful non-destructive tool to quickly predict chemical and physical properties of wood (Tsuchikawa, 2007; Tsuchikawa & Kobori, 2015). But only a few studies have attempted to predict growth-strain indirectly using NIR spectroscopy. Baillères et al. (2002) assumed growth-strain was related to the chemical composition of wood and a statistical model with moderate ($r^2 = 0.63$) prediction accuracy was built for longitudinal growth-strain in eucalypts based on NIR spectra obtained from wood powder (Baillères et al., 2002). Similarly growth-strain in green stems of the softwood

Cryptomerica japonica was moderately (r^2 = 0.61) correlated to NIR spectra in the range of 8300 to 12000 cm^{-1} (Watanabe et al., 2011). Both studies used partial least squares models, not taking advantage of the understanding of the effect of mechanical strain on band positions in NIR spectra.

NIR spectra can be collected in transmission or reflection mode. Transmission NIR can provide spectra of high quality but the thickness of wood sample is restricted to a few millimetres rendering it destructive (Schwanninger et al., 2011). Reflection mode NIR spectra can be captured by cameras (Thumm et al., 2010) or fibre optics from the surface of solid material removing restrictions in sample size and allowing non-destructive measurements. This is, however, at the compromise of signal intensity and consequently the analytical performance (Xiang et al., 2009).

NIR spectroscopy is sensitive to moisture (Osborne et al., 1993) and standing trees or freshly felled green logs contain highly variable amounts of water. For example the green moisture content in seven *Eucalyptus* species was reported to range from 62 to 102% (Oliveira et al., 2005). Although a strong linear correlation (r^2 = 0.98) has been reported between the applied mechanical strain and the NIR band position tentatively assigned to 2OH···6O in crystalline cellulose for dry eucalypt wood (Guo & Altaner, 2018), the effect of water on the detection of mechanical strain from NIR spectra in water saturated and green wood samples is unknown. Considering that crystalline cellulose is inaccessible to water, it might be possible that the band shifts are detectable in green wood. However, the strong and often overlapping signals from the variable amounts of water in the wood might interfere with signal interpretation. Additionally, growth-strain is known to vary over the surface of a stem (Valencia et al., 2011; Watanabe et al., 2011), but the length scale of these variations is also unknown.

This study 1) investigated the effect of moisture on the NIR band attributed to the 2OH···6O bond by monitoring the drying process of wet wood; 2) determined the correlation of applied tensile strain with the band shift of the 2OH···6O bond using transmission NIR for rewetted wood samples; 3) examined the effect of bending of green eucalyptus stems on reflection NIR spectra on the tension surface; and 4) checked the possibility of predicting growth-strain in green wood using 163 young *E. nitens* samples.

5.2 Materials and Methods

5.2.1 Drying of rewetted wood

A ~0.7 mm thick air-dried *E. regnans* wood strip was immersed in water for 5 days to reach full saturation. The water saturated sample immersed in water for 5 days to reach full saturation had a moisture content of 140.4% and was air-dried for 10 min, 30 min, 1 h and 1.5 h to reach moisture contents of 124.2%, 98.5%, 64.4%, 40.0%, respectively. To reach moisture contents below fibre saturation point (FSP), the sample was subsequently placed in containers over saturated K_2SO_4, NaCl, K_2CO_3, and LiCl solutions for at least 1 day each. The relative humidity in the four containers were 97.6%, 75.5%, 43.2%, 11.3%, allowing the sample to equilibrate to moisture contents of 26.5%, 17.5%, 10.0%, 3.5%, respectively. The sample was then oven-dried at 103 ℃ until it reached a constant weight. The drying process was monitored by acquiring transmission NIR spectroscopy at each drying stage using a Bruker Tensor 37 (Germany) spectrometer at a resolution of 8 cm^{-1} with 128 scans. Moisture contents were calculated based on the oven-dry weight and the weights of the sample after NIR collection.

5.2.2 Strain in air-dry, rewetted and green wood measured by transmission NIR

Six *E. regnans* wood strips, 16 mm in width (across the grain) and 85 mm in length (along the grain) were cut from an air-dried board and subsequently sanded to thicknesses of 0.5 to 1 mm. Three samples were rewetted as samples described above. A 2-year old *E. quadrangulata* tree was harvested from a nursery site in Woodville, New Zealand. Three thin (0.5 to 1 mm thick) wood strips with a dimension of 85×16 mm^2 were cut from the green stem. The samples were sealed in a plastic bag and put in a freezer up to four weeks to preserve their green state.

Strain gauges were glued onto the nine samples with an adhesive (Loctite 454, Australia). The samples were stretched to 8 strain levels (0 to 7) in a NIR spectrometer using a purposely manufactured device (Guo & Altaner, 2018). "Strain 0" represented no applied tensile force, while "Strain 7" was the greatest tensile force. Strain values were recorded using the strain gauges connected to a strain meter (TC-31K, Tokyo Sokki Kenkyujo, Japan). Transmission NIR spectra was collected using Tensor 37 spectrometer at a resolution of 8 cm^{-1} averaging 128 scans. Each sample was measured twice at each strain level resulting in 16 collected spectra.

The humidity in the lab was approx. 40%. The weights of the samples were recorded before and after collecting NIR spectra. The fully water saturated samples lost approx. 21% of their water-saturated masses during sample handling and spectra collection. Therefore, the spectral changes were caused by both drying and mechanical stress.

5.2.3 Strain in green wood detected by reflection NIR

Five thin (0.5 to 1 mm thick) wood strips (35×8 mm^2) from the green *E. quadrangulata* tree were prepared for the bending tests. Bending tests were conducted with a self-developed 4-point bending device (Figure 5-1) with a span of 120 mm. The green wood specimens were glued onto the surface of a 6 mm thick acrylic plastic beam. Eight strain levels (0 to 7) were applied by progressively driving a screw. The maximum strain ("Strain 7") was approx. 2300 µε. A strain gauge was attached to the wood sample to measure the tensile strain. Diffuse reflection NIR spectra were taken on the wood surface using a fibre optic probe (Model N-500, Bruker, Germany) connected to the Tensor 37 spectrometer at a resolution of 8 cm^{-1} averaging 128 scans. Each sample was measured twice at each strain level resulting in 16 collected spectra.
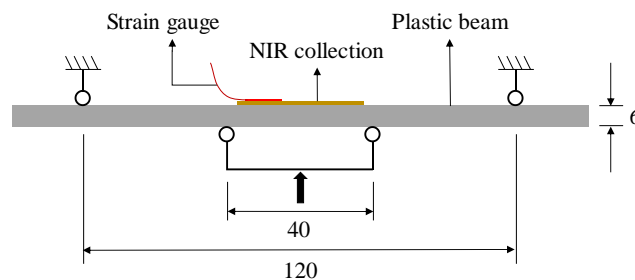
Figure 5-1 Four-point bending test device to bend small wood samples glued onto a plastic beam. Reflection NIR spectra can be collected from the wood sample while applying bending forces.

Dimensions shown are in millimetres.

5.2.4   Prediction of growth-strain measured by strain gauges using reflection NIR

Thirty-one ~3-year old *E. nitens* trees were harvested from a nursery site in Harewood, Christchurch, New Zealand. Each stem was cut into several samples with a length of more than 400 mm ranging between 31 and 120 mm in diameter. In total, 163 samples were obtained. The samples were debarked and the differentiating xylem on the surface was carefully removed before collecting NIR spectra. Two diffuse reflection NIR spectra were collected 180° apart on the circumference (Figure 5-2) under the same instrument settings as described above. Strain gauges were then glued onto the spectra collection positions before two holes (12 mm in diameter) were drilled 10 mm above and below the strain gauges to release growth-stresses.

NIR collection　　　Strain gauge

Drill hole
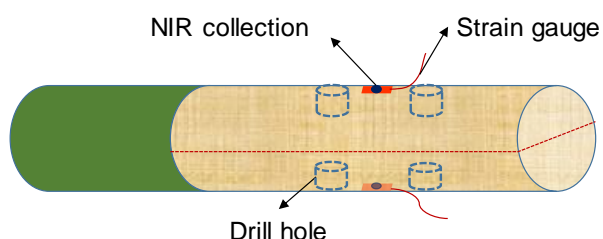
Figure 5-2 NIR collection and growth-strain measurement on *E. nitens* samples

5.2.5   Spectral analysis

The R software (R Core Team, 2017) was used for spectra processing and visualisation. Second derivative spectra were calculated using the Savitzky-Golay algorithm with a smoothing window length of 39 data points in the "pls" package (Mevik, Wehrens, & Liland, 2016). The band positions were calculated using a peak fitting method using a Gaussian function as described earlier (Guo & Altaner, 2018). For the rewetted and green samples, a linear baseline connecting two points at 6380 cm^{-1} and 6198 cm^{-1} was used to correct the baseline offset caused by moisture content (Supporting Figure 7 in Appendix F).

5.3 Results and Discussion

5.3.1   Drying of rewetted wood samples monitored by NIR spectroscopy

The drying process of a water saturated *E. regnans* sample was monitored by NIR. Above FSP, the absorbance increased upon drying (Figure 5-3). Therefore, the transparency of wood decreased in the drying process, similar to what was reported for paper (Forughi et al., 2016). Wood strongly scatters light due to the high refractive difference between the wood cell wall and the air in cell lumens. Free water filling the cell lumens reduced the refractive difference and consequently increased light transparency. As wood lost free water, more light was scattered and the absorbance increased.

However, below FSP, the absorbance decreased with the drying of the sample (Figure 5-3). As no free water remained in the cell lumens below FSP, the refractive difference of the sample was stable. However, bound water in the wood cell wall absorbs near infrared light. Losing water molecules resulted in less absorbance, especially in the bands assigned to

water including the OH stretching region (7200 to 6100 cm^{-1}) and the combination of the asymmetric stretching and bending of water molecules (around 5190 cm^{-1}) (Schwanninger et al., 2011; Workman & Weyer, 2008). Compared to wet wood, dry wood below FSP had a more defined band shape with visible shoulder peaks in the OH stretching region (7200 to 6100 cm^{-1}).
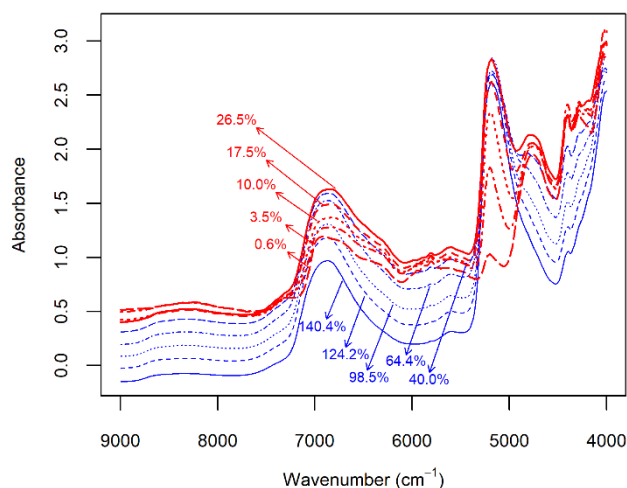
Figure 5-3 Transmission NIR spectra of a rewetted *E. regnans* wood sample at different moisture contents. Blue lines represent moisture content above FSP, red lines below FSP.

In the second derivative spectra, the bands at 6470 ± 10 cm^{-1} and 6286 ± 5 cm^{-1} were reported to be sensitive to mechanical stress (Guo & Altaner, 2018). The effect of moisture content on the band at around 6286 cm^{-1} in the second derivative spectra was examined in Figure 5-4A. The intensity of this band increased significantly as free water was removed. This suggested that the amount of information of cellulose in the NIR spectra increased with the loss of free water and the high moisture content concealed the structural information of crystalline cellulose.

A high moisture content also affected the minimum position of the band (Figure 5-4B), with the band positions shifting to higher wavenumbers as the wood sample dried. This effect, mainly caused by an overlapping water signal resulting in a skewed signal, could be removed with a linear baseline correction (Supporting Figure 7 in Appendix F) above 10.0% moisture content (Figure 5-4B). Below 10% moisture content, the band shifted by ~3.0 cm^{-1} to higher frequency as the moisture content decreased to 0.6%. Therefore, baseline correction can be used to remove the effect caused by changes in moisture content above FSP, the region of interest for this study.

Molecular deformations of the cellulose crystal caused by drying of cellulosic materials have been documented by X-ray diffraction (Abe & Yamamoto, 2006; Leppänen et al., 2011; Zabler et al., 2010). These occurred below 20% moisture content and were dominated by a lateral expansion (0.6%) of the cellulose crystal accompanied with 0.2% axial contraction (Zabler et al., 2010). In contrast, mechanical stretching only caused axial expansion of the cellulose unit cell without lateral changes. Changes in O···O distances affect the strength of hydrogen bonds, with longer distances weakening the hydrogen bonds and vice versa. Assuming a band shift rate of 10 cm^{-1}/% (Guo & Altaner, 2018), a 0.6% lateral expansion would result in a shift a hydrogen bonded O-H stretching band by 6 cm^{-1} to higher frequencies and 0.2% axial shrinkage will cause a shift to lower frequencies by 2 cm^{-1}. With the assumption that the O-H stretching vibrations in cellulose are highly coupled (Lee et al.,

2013), the observed band shift below 20% moisture of ~3.0 cm^{-1} to higher frequencies (Figure 5-4) indicated that lateral expansion was the dominant effect in the drying process.
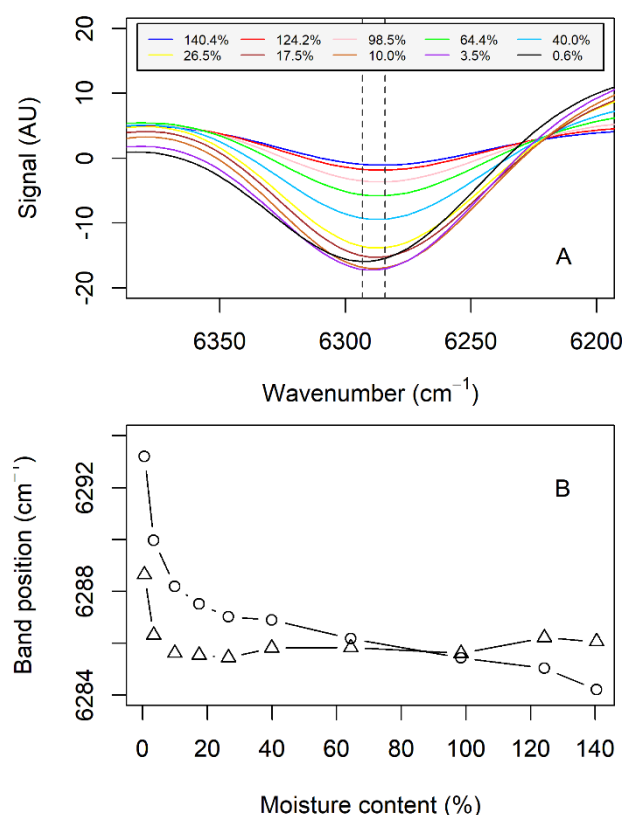
Figure 5-4 Second derivative spectra of a *E. regnans* wood sample at different moisture contents from 6380 cm^{-1} to 6200 cm^{-1} (A). Uncorrected (circles) and baseline corrected (triangles) band positions at corresponding moisture content (B). The minima in the second derivative spectra at 0.6% and 140.4% were labelled with dashed lines in Figure 3A.

5.3.2 Effect of stretching on transmission NIR spectra of air-dry, rewetted and green samples

5.3.2.1 Visualisation of band shifts in the second derivative spectra

Under tensile stress, covalent bonds like the glycosidic C–O–C bond in crystalline cellulose will elongate, weakening the bonds and consequently resulting in shifts of their stretching vibrations to lower frequencies (Eichhorn et al., 2001; Eichhorn & Young, 2001; Salmén & Bergström, 2009). In contrast, stretching vibrations of OH groups involved in hydrogen bonds will shift in opposite direction upon stretching because the weakening of the hydrogen bonds strengthens the OH groups. With the increase of tensile strain, the band at around

6286 cm^{-1} was reported to shift to higher frequencies for air-dry *E. regnans*, *Pinus radiata* and paper samples (Guo & Altaner, 2018). This was interpreted as the weakening of the intramolecular 2OH···6O hydrogen bonds in crystalline cellulose. Consistent with this, band shifts to higher wavenumbers were observed for rewetted *E. regnans* samples upon axial tensile loading (Figure 5-5).

The band position differed between the rewetted and the dry sample (Figure 5-5). The baseline offset caused by the overlapping water signal resulted in the band to appear at lower frequencies for the rewetted sample. The rewetted sample dried in the ambient environment during the NIR measurements. Therefore, the spectral changes of the rewetted sample resulted from the combined effects of drying and mechanical strain. Drying slightly skewed the band of interest (Figure 5-4) causing a shift to higher frequencies, the same direction as the effect of mechanical stretching. Consequently, without baseline correction, the band shift rate with regard to applied strain was greater in the rewetted (12.0 cm^{-1}/%) sample than the air-dry sample (9.4 cm^{-1}/%).
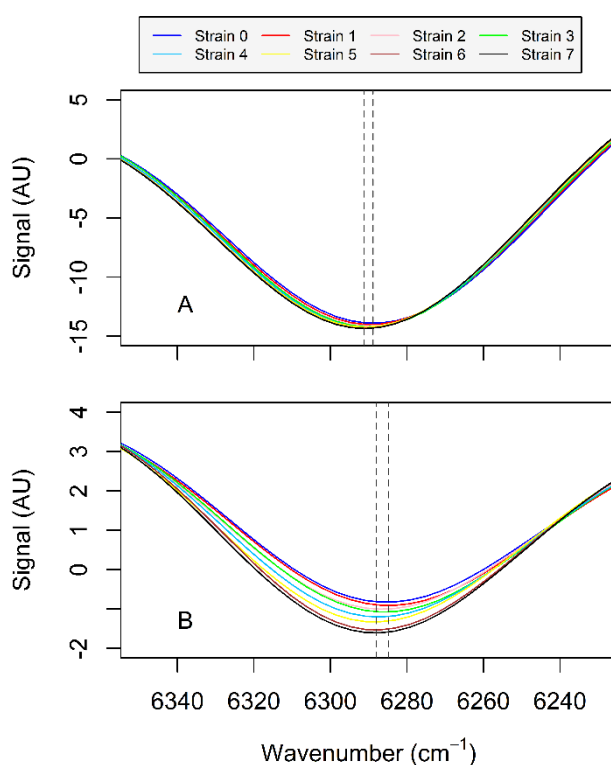
Figure 5-5 Band shifts in the second derivative spectra for an air-dry (A) and a rewetted (B) *E. regnans* sample under tensile stress. The minima positions at the lowest ("Strain 0") and highest ("Strain 7") strain levels were marked by dashed lines. The rewetted sample (B) dried during the spectra collection and lost 21% of its wet mass. NIR spectra were taken in transmission mode.

5.3.2.2 Quantification of mechanically induced band shifts

A strong linear relationship (r = 0.94) was found between band positions and mechanical strain for air-dry samples (Figure 5-6). The correlation coefficient was lower for the rewetted (r = 0.77) and green samples (r = 0.87) even after baseline correction to remove the skewing

effect of moisture. As seen in Figure 5-4A, the higher moisture content also weakened the 6286 cm⁻¹ band intensity, contributing to the lower correlation.
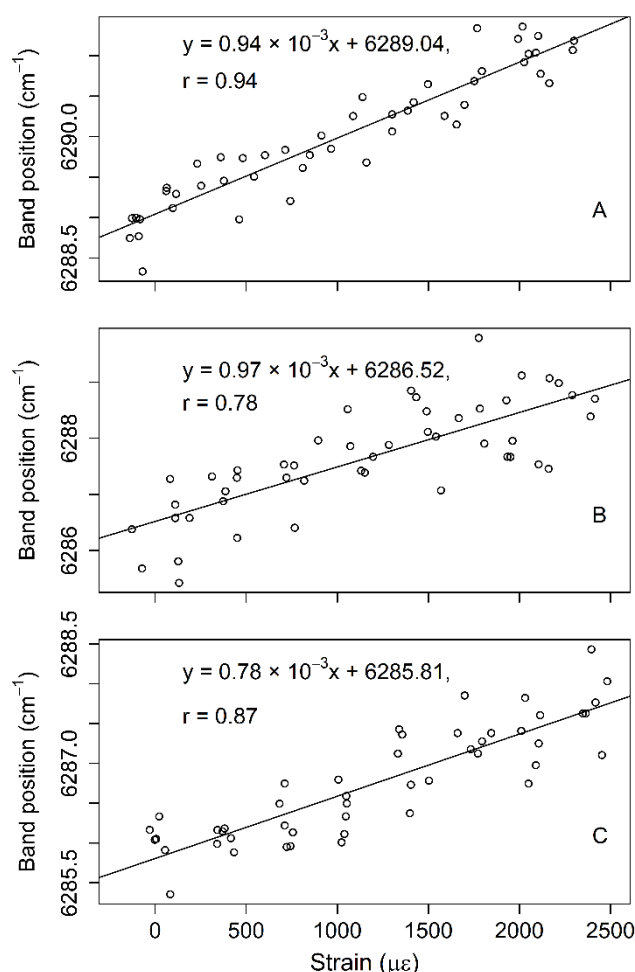
Figure 5-6 Quantification of the band shifts at around 6286 cm⁻¹ in the second derivative NIR transmission spectra of 3 air-dry (A), 3 rewetted (B) *E. regnans* and 3 green *E. quadrangulata* (C) samples under axial load. Band positions of rewetted and green samples were baseline corrected to remove the effect of water signal overlap.

The band shift rates with respect to mechanical strain showed similar values for air-dry (9.4 cm⁻¹/%) and rewetted wood (9.7 cm⁻¹/%) (Figure 5-6), consistent with the previously reported values of 10.0 ± 1.02 cm⁻¹/% for air-dry *E. regnans* wood samples (Guo & Altaner, 2018). This confirmed Salmén and Bergström (2009) findings of equal band shift rates in mid-range infrared spectra of spruce wood under tensile strain in humid and dry conditions. A lower band shift rate was measured for never-dried green wood (7.8 cm⁻¹/%) compared to previously dried samples (Figure 5-6). This indicated that less macroscopic strain was transferred into molecular strain of cellulose in green never-dried wood, what could be caused by slippage of microfibrils within the cell wall (Montero et al., 2012; Zabler et al., 2010). Further study is required to clarify whether the different behaviour of never-dried wood was a result of irreversible drying effects well described for lignocellulosic materials (Fernandes Diniz et al., 2004).

5.3.3 Band shifts caused by bending of green samples

NIR spectroscopy in reflection instead of transmission mode is needed to measure growth-stress rapidly and non-destructively, because only thin wood samples with a thickness up to a few millimetres are transparent to NIR radiation. Reflection NIR spectroscopy is not limited by sample size, but suffers from lower signal/noise ratios (Xiang et al., 2009). Bending tests on five green *E. quadrangulata* samples were used to investigate whether reflection NIR spectroscopy using a fibre optics probe on the tensile side can be used to measure molecular strain in green samples by monitoring the shift in band positions.

First, the second derivative of the refection NIR spectra of green wood samples were compared with that of the transmission NIR spectra of dry and green samples (Figure 5-7). Signals in the OH stretching region were most intense in transmission NIR spectra from dry samples. The additional water in green samples lowered the intensity of the bands. Further signal reduction was observed when acquiring NIR spectra in reflection NIR spectra as the fibre optic probe attenuated the incident light (Xiang et al., 2009).
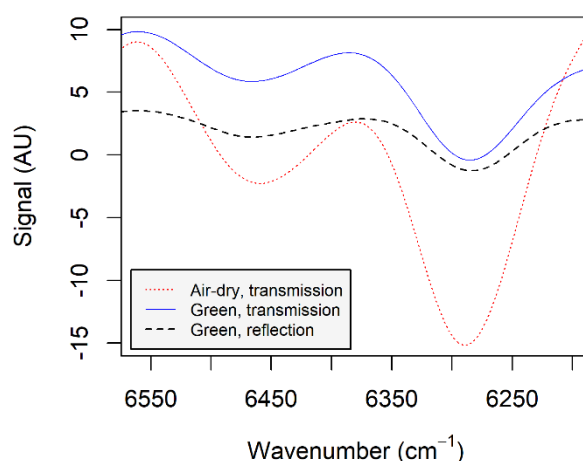
Figure 5-7 Second derivative NIR spectra of green *E. quadrangulata* wood samples ranging from 6550 to 6200 cm^{-1}, collected in transmission (solid) and reflection (dashed) as well as air-dry (dotted) *E. regnans* acquired in transmission mode.

However, still a significant linear relationship ($p < 0.001$) between the 2OH···6O (6286 ± 5 cm^{-1}) band position and the applied bending strain was detected in reflection NIR spectra (Figure 5-8). The correlation coefficient ($r = 0.60$) was lower than that for the green *E. quadrangulata* ($r = 0.87$) and rewetted *E. regnans* samples ($r = 0.77$) measured in transmission mode (Figure 5-6). The band shift rate of the green sample measured in the bending tests was with 0.78 cm^{-1}/% matched that of the tensile tests (Figure 5-6C). This supported the difference between never dried samples and dried samples discussed above. However, the initial band positions measured based in reflection spectra (6282.1 cm^{-1}) differed from those in transmission NIR spectra (6285.8 cm^{-1}). This was probably caused by spectra processing as the band position in the less intense reflection spectra were affected by the window size of the applied spectra smoothing algorithm.
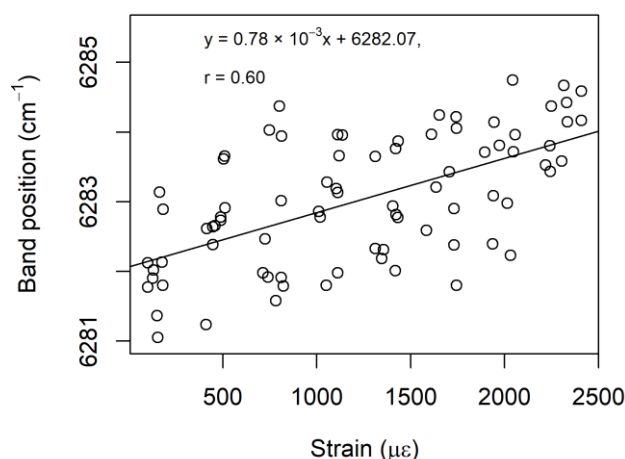
Figure 5-8 Relationship between band position in reflection NIR spectra and applied tensile strain in the bending tests of five green *E. quadrangulata* samples. Each sample was measured twice with 80 spectra obtained in total.

5.3.4 Determination of growth-strain and band position in reflection NIR spectra for green *E. nitens* stems

The final objective of this study was to predict growth-strain in green eucalyptus stems by reflection NIR spectroscopy. In the present study, the maximum growth-strain in the *E. nitens* stems was as high as 2400 µε (Figure 5-9A), a value of similar magnitude (1650 µε) as previously reported for this species at age 10-year-old (Chauhan & Walker, 2004). Assuming a band shift rate of 7.8 cm^{-1}/%, a band shift of 1.3 to 1.9 cm^{-1} was expected. Based on 163 samples, no correlation was found between the 6286 cm^{-1} band position and the growth-strain measured by strain gauges (Figure 5-9B). Partial least squares (PLS) modelling to predict growth-strain based on the NIR spectra also did not yield satisfactory results ($r^2 < 0.1$) (data not shown). Measuring growth-strain accurately is very challenging (Raymond et al., 2004) especially at low magnitude. The majority (76.5%) of the tested samples of this study had growth-strain values below 1000 µε (Figure 5-9A), negatively affecting the accuracy of data.
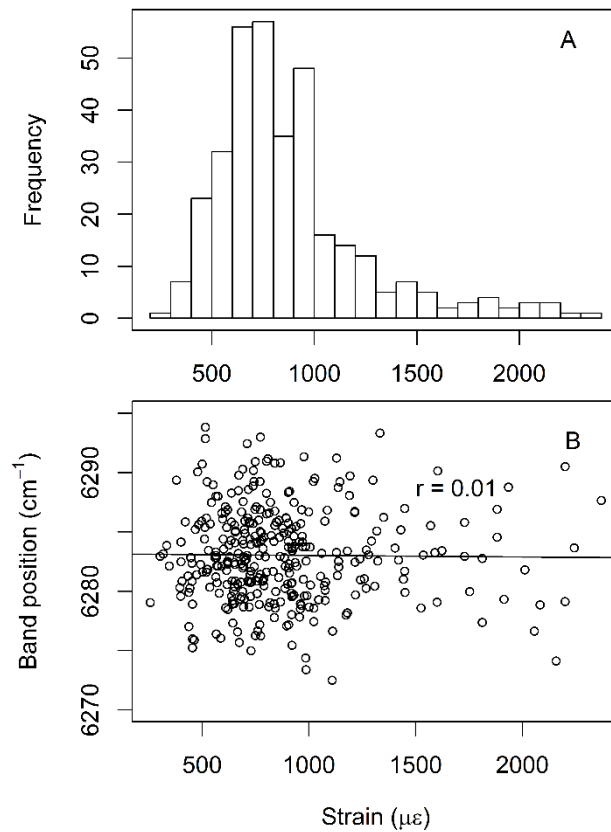
Figure 5-9 Distribution of growth-strain in 2-year old *E. nitens* (n = 163) (A); and correlation between growth-strain and baseline corrected NIR band position (B). The growth-strain was measured with strain gauges. Each data point represented one spectrum and the corresponding strain measurement. Two NIR reflection spectra were collected from each sample as shown in Figure 2.

The band positions for the 163 green samples ranged from 6293.8 to 6265.6 cm^{-1} (Figure 5-9B). However, growth-strain was only expected to induce a band shift of about 2 cm^{-1}, 10-times smaller than the observed variation. Therefore, the effects of signal overlap, poor signal to noise ratio of spectra and potentially surface properties dominated the variation in NIR band position, rather than molecular strain. Furthermore, the spatial variation in grain orientation (Watt et al., 2013), cell wall chemistry (Downes et al., 2014), growth-strain (Yoshida & Okuyama, 2002) and modulus of elasticity (Pereira et al., 2013) in wood at the millimetre length scale would lower the reported correlations as the correlated measurements were spatially separated. Such variation has been reported but is difficult to quantify quickly and non-destructively as needed for a practical application.

5.4 Conclusions

The moisture content of wood affects the absorbance of transmission NIR spectra. Moisture increased NIR absorbance below FSP due to increased water adsorption, while it decreased NIR absorbance above FSP by refractive index matching. Above FSP, the large quantity of free water reduced the relative signal intensity from crystalline cellulose and skewed the 2OH$\cdots$6O band at around 6285 cm^{-1}. The skewing effect could be removed by data

processing. Band shifts at around 6285 cm^{-1} caused by mechanical stretching were observed using transmission NIR spectroscopy in air-dry, rewetted and green wood samples. Never-dried green wood had a slightly lower band shift rate than previously dried wood. A moderate linear correlation was found between the 6286 ± 5 cm^{-1} band positions and the strain in the bending test for green *E. quadrangulata* samples monitored with non-destructive reflection NIR spectroscopy. However, no correlation was found between reflection NIR band positions and growth-strain for the green *E. nitens* stems in this study. Therefore the results suggested that the current NIR technology is not suitable to measure growth-strain in green wood non-destructively, mainly due to the low S/N ratio of the fibre optic probe method and the variable surface properties of green wood.

6 PREDICTING STRAIN IN REWETTED AND NEVER-DRIED EUCALYPT WOOD USING RAMAN SPECTROSCOPY

6.1 Introduction

Raman and mid-infrared (MIR) spectroscopy are complementary techniques measuring vibrational frequencies of chemical bonds (Larkin, 2011). The former is based on the Raman scattering phenomenon, while the latter detects the absorption of electromagnetic radiation. With technological advances, Raman spectroscopy is gaining popularity in various applications including material identification (Amer, 2009), forensic and pharmaceutical analysis (Vankeirsbilck et al., 2002) as well as chemical distribution imaging of plant cell walls (Gierlinger & Schwanninger, 2006; Richter et al., 2011). Portable Raman spectrometers are commercially available (Carron & Cox, 2010), opening up the possibility of measuring wood properties in the field rapidly and non-destructively. Compared to infrared spectroscopy, Raman spectroscopy is insensitive to water, which interferes with the structural information of plant material (Chapter 5) as it is typically water saturated when alive. Challenges of using Raman spectroscopy on lignocellulosic materials are the laser-excited florescence from lignin, which causes an intense background masking the Raman signal, and the high energy of the laser, which leads to thermal decomposition of the sample. Using 1064 nm near infrared (NIR) lasers dramatically reduces florescence from lignin (Agarwal, 2014) and water immersion sampling lessens thermal degradation (Agarwal, 1999).

Mechanical stress induces both macroscopic and molecular deformation of wood and cellulose. Axial elongation and lateral contraction of the cellulose crystal lattice in wood was observed upon tensile stress by X-ray diffraction (Peura et al., 2007; Zabler et al., 2010). Deformation of crystalline cellulose will cause changes in vibrational frequencies of chemical bonds, which were observed as band shifts in MIR (Altaner et al., 2014b), near infrared (NIR) (Guo & Altaner, 2018) and Raman spectra (Eichhorn & Young, 2001). IR spectroscopy detected the deformation of the COC glycosidic bonds at 1160 cm^{-1} and intramolecular O3H···O5 groups at 3348 cm^{-1} (Salmén & Bergström, 2009). NIR band shifts at 6286 ± 5 cm^{-1} and 6470 ± 10 cm^{-1} indicated intramolecular hydrogen bonds of crystalline cellulose elongated under tensile strain (Guo & Altaner, 2018).

Raman spectroscopy has been a powerful tool to study the molecular deformation of polymer fibres. Mitra et al. (1977) reported that the Raman frequencies assigned to the backbone structure of polydiacetylene decreased with the elongation of fibres. Following this work, Raman spectroscopy was used to study the molecular deformation of regenerated cellulose (Hamad & Eichhorn, 1997). The Raman band shift at around 1095 cm^{-1}, assigned to the stretching of the cellulose ring structure, has now also been reported for wood, natural flax and hemp fibres (Eichhorn et al., 2001; Gierlinger et al., 2006; Peetla et al., 2006). However, the effect of mechanical strain on Raman spectra in other region is not well understood.

Growth-stresses in trees, accumulated during cell wall maturation (Alméras & Clair, 2016), cause problems like end-splitting, heart checking and collapse and are the major cause restricting plantation-grown eucalypts from in solid wood processing (Yang & Waugh, 2001). Growth-strain, similar to mechanical strain, causes deformation of wood and cellulose on the

molecular level (Clair et al., 2011). A rapid and non-destructive evaluation of growth-stress by measuring growth-strain using Raman spectroscopy could potentially help to segregate logs with low growth-strain for high-value solid wood uses. Previous studies on the deformation mechanism of cellulosic materials focused on small areas of single fibres using a Raman microscope, requiring elaborate sample preparation. However, Raman spectrometers capable of direct surface sampling are available, enabling the collection of spectra without the limitation of sample size. This is also advantageous as mechanical properties of wood have been known to depend on sample size (Buchelt & Pfriem, 2011). Thin wood samples were shown to have different load-displacement curves compared to bulk wood (Navi et al., 1995) and the modulus of elasticity of wood microsections were lower than that of normal sized specimens (Yu et al., 2009).

In this study, thick wood strips were mechanically strained to confirm the effect on Raman spectra, previously only reported for microscopic samples. Multivariate statistical models were constructed to predict mechanical strain based on Raman spectra and the spectral changes attributed to strain were analysed in detail and the band shift rates were quantified. Further, the effect of pre-drying on the molecular strain was observed by Raman spectroscopy. Finally, the possibility of measuring growth-strain in green stems using Raman spectroscopy was evaluated.

6.2 Materials and methods

6.2.1   Tensile tests of rewetted and green wood monitored by Raman spectroscopy

An air-dry *Eucalyptus regnans* board with an oven-dry density of 0.51 g/cm^3 was sourced from Canterbury, New Zealand. Ten wood strips with a thickness of 0.5 to 1 mm (radial) were cut with a circular saw from the sapwood of the air-dry *E. regnans* board, which were sanded before being cut into the size as shown in Figure 6-1. The samples were re-saturated through immersion in water for at least 7 days and were referred to as "rewetted" wood in this study. A 2-year old *E. quadrangulata* tree with an oven-dry density of 0.68 g/cm^3 was harvested from a site in Woodville, New Zealand. The tree was kept in water during transport to the lab. Eight wood strips were prepared from the never-dried green tree in accordance to the procedure described above for the *E. regnans* samples. *E. quadrangulata* samples were put in a sealed plastic bag and stored in a freezer until tested.
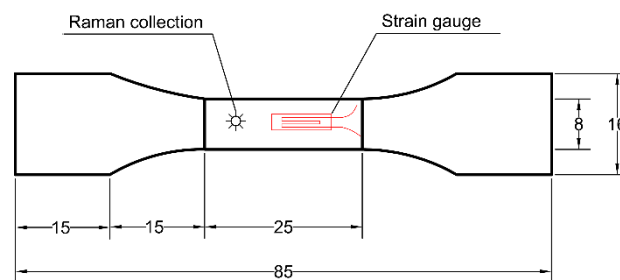
Figure 6-1 Schematic drawing of the wood samples used for tensile tests in combination with Raman spectroscopy. The length of the sample was in the longitudinal (grain) direction of wood. Dimensions are labelled in millimetres.

A purpose-built test rig, described previously (Guo & Altaner, 2018), was placed under a dispersive Raman spectrometer (Sierra 2.0, Metrohm Raman, USA) equipped with a 1064

nm NIR laser and an InGaAs array detector. The wood samples were mechanically stretched while simultaneously collecting Raman spectra at twelve strain levels, increasing progressively from "Strain 0" (approx. 0 µε) to "Strain 11" (maximum strain of approx. 4500 µε) with increments of approximately 410 µε. Applied macroscopic strain was measured by strain gauges (FLA-5-11, Tokyo Sokki Kenkyujo, Japan) glued onto the samples and connected to a TC-31K strain-meter (Tokyo Sokki Kenkyujo, Japan). The wood surface was kept wet during spectra collection to restrict thermal decomposition (Conti et al., 2016) and improve spectral quality (Agarwal, 1999). Two Raman spectra were taken at each strain level in the region from 2300 to 200 cm^{-1} with a laser power of 500 mW and an integration time of 30 s. Another two spectra were collected after returning to the relaxed state at the end of a stretching experiment. In total 36 spectra were acquired for each sample. The spectrometer featured orbital raster scan (ORS), a technique to reduce sample damage by moving the laser over a measuring area of 1 to 2 mm in diameter. The polarization direction of the incident light was parallel with the longitudinal direction of the wood samples.

6.2.2 Four-point bending tests of green wood combined with Raman spectroscopy

Another 10 green *E. quadrangulata* samples with sizes of 35 mm (longitudinal) × 8 mm (tangential) × 0.5 ~ 1 mm (radial) were prepared from the *E. quadrangulata* tree as described above. Green *E. quadrangulata* samples were glued onto an acrylic beam (160 × 10 × 6 mm^3) for the four-point bending tests. The self-developed device had a span of 120 mm as illustrated in Figure 4-1. Strain gauges were glued to the wood to measure the strain. Raman spectra were collected on the tension side of the samples at stepwise loading ("Strain 0"-minimum to "Strain 6"-maximum) and after unloading to relaxed state. Two Raman spectra were collected at each strain level using the same settings as described above, thus 16 spectra were acquired for each sample. The maximum strain ("Strain 6") was approx. 2200 µε.

6.2.3 Growth-strain and its prediction using Raman spectroscopy

Nine *E. bosistoana* trees were felled at Harewood, Christchurch (NZ). Two stem sections with length of more than 500 mm were sampled from each tree between 1 m to 2.2 m in height. The stems had under-bark large-end diameters ranging from 31 to 62 mm. After debarking and carefully scraping off the differentiating layer, Raman spectra were collected using the same settings as described above. Considering the variability of wood properties, 9 spectra were taken in an area of approx. 20 × 10 mm^2 on each side of a stem (Figure 6-2).

Following the spectra collection, strain gauges were attached to the stems in grain direction, centred at the spectra collection area (Figure 6-2). Two 12 mm diameter holes were drilled next to each strain gauge to release growth-stresses on both sides. One growth-strain measurement by a strain gauge corresponded to 9 Raman spectra. After the strain gauge measurements, the splitting method as described by Davies et al. (2017) was used to estimate the surface growth-strain (SGS) of the stem. For comparison, tension strain measured by strain gauges was converted to positive values. Each growth-strain value measured by the splitting method corresponded to two measurements with strain gauges.

70
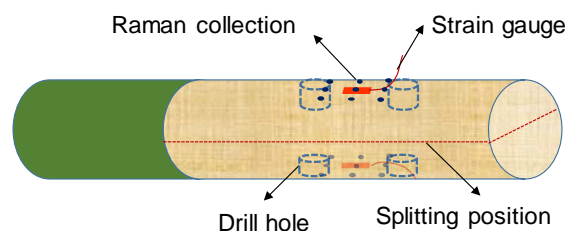
Figure 6-2 Schematic drawing of the experimental setup for Raman spectra collection and growth-strain measurements on green stems. The dashed red line indicates the cut for the splitting test.

6.2.4   Data analysis

1) Visualization of the Raman band shifts caused by mechanical strain

In order to visualize the band shift at around 1095 cm^{-1} upon tensile stress, Raman spectra were pre-processed and plotted in R (R Core Team, 2017). Raman spectra were smoothed using the Savitzky-Golay filter with a window length of 9 in the "signal" package (Signal developers, 2013) before being normalised using the standard normal variate (SNV) method (Stevens & Ramirez-Lopez, 2013) in the range of 1180 to 950 cm^{-1}.

2) Partial least square (PLS) modelling

PLS models were built to predict the applied mechanical strain based on Raman spectra in the region between 2300 and 200 cm^{-1}. The 258 spectra were split into a training group with 180 spectra from 7 samples and a validation group with 58 spectra from 3 samples. Five PLS models were developed using leave-one-out (LOO) cross-validation in the "pls" package (Mevik et al., 2016b) based on different spectra pre-processing, including baseline correction, SNV normalisation, second derivatives and spectra truncation (1180 ~ 950 cm^{-1}). Baseline correction was conducted with a modified polynomial algorithm in the "baseline" package (Liland & Mevik, 2015). Coefficients of determination (R^2) and root mean squared errors (RMSE) of the PLS models for the training and the validation group were extracted.

3) 'Slope' spectra and determination of band positions by peak fitting

Spectral changes caused by mechanical strain were analysed by the regression coefficients plot of the PLS model and 'slope' spectra. 'Slope' spectra were calculated to show the change rate of spectral intensity induced by mechanical strain as described previously (Altaner et al., 2014a; Guo & Altaner, 2018). It was calculated based on baseline corrected and normalised spectra. The average 'slope' spectrum was calculated as the average of 10 'slope' spectra of 10 rewetted *E. regnans* samples. To quantify the band shift at around 1095 cm^{-1}, a Cauchy-Lorentzian function was used to fit the spectra in the range from 1103 to 1084 cm^{-1} using the nonlinear least squares method in R. Band positions were extracted from the fitted model.

6.3   Results and discussions

6.3.1   Raman spectra of rewetted wood under tensile strain

6.3.1.1 Visualization of Raman band shifts

The signal intensity of Raman bands mainly depends on laser power and its frequency, polarizability and concentration of the chemical group, as well as the sample orientation (Smith & Dent, 2005). For biological materials, fluorescence and various physical effects such as surface roughness, particle size and sample inhomogeneity have noticeable influence on the Raman scattering intensity as well (Huang et al., 2010; Liland et al., 2016).

Due to these interfering factors, the intensities of the Raman spectra of the rewetted wood fluctuated and it was difficult to identify the small spectral changes caused by mechanical strain from the original spectra (Figure 6-3A). The fluctuations in the spectra could be removed by SNV normalisation in range from 1180 to 950 cm^{-1}, allowing to determine the effect of mechanical tensile strain on the position of the band centred at around 1095 cm^{-1} (Figure 6-3A inset). The 1095 cm^{-1} band was assigned to CC and CO stretching of the cellulose ring structure (Hamad & Eichhorn, 1997; Wiley & Atalla, 1987), indicating the elongation of cellulose chains and weakening of the covalent bonds in the cellulose backbone. This band shift had been reported for regenerated cellulose as well as single wood and other natural fibres using Raman microscopy (Eichhorn et al., 2001; Gierlinger et al., 2006; Hsieh et al., 2008). Our results showed that this tensile strain induced Raman band shift can also be observed in relatively thick (>0.5 mm) wood strips. A strong linear relationship (r = 0.997) was found between the peak position and the applied strain of the relatively thick *E. regnans* sample (Figure 6-3B). As strain increased from −53 µε to 4649 µε, the band position shifted from 1095.35 to 1093.57 cm^{-1}. The band shift rate for this sample was −3.79 cm^{-1}/%, which was greater compared to the values (−1.43 to −1.63 cm^{-1}/%) reported for single wood fibres (Gierlinger et al., 2006). The reasons will be discussed later in detail.
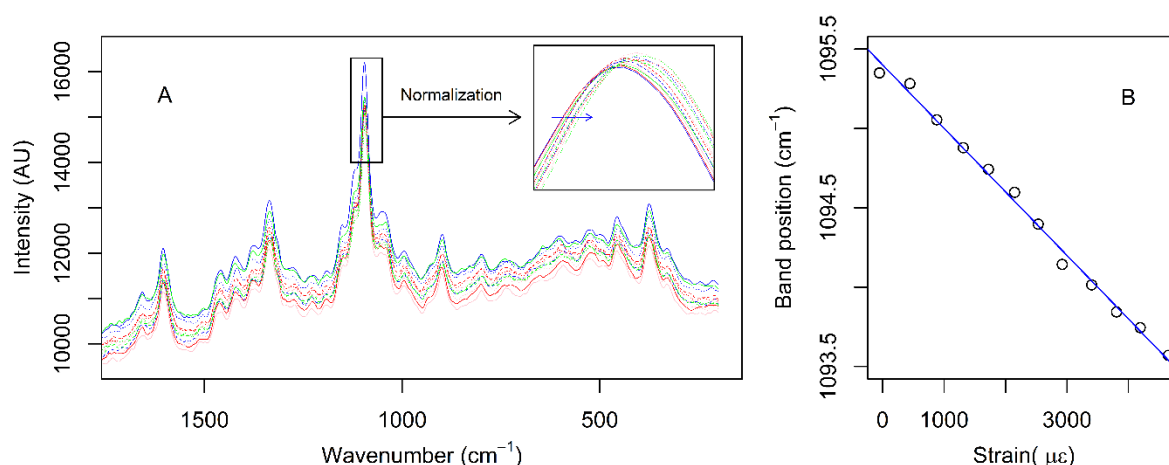
Figure 6-3 Unmodified Raman spectra at 12 tensile strain levels of one rewetted *E. regnans* wood sample (A) and the corresponding band shifts of the 1095 cm^{-1} band (B). Inset (A) shows the band at 1095 cm^{-1} after SNV normalisation in the region of 1180 to 950 cm^{-1}. "Strain 0" to "Strain 3" were represented with solid lines, "Strain 4" to "Strain 7" with dashed lines and "Strain 8" to "Strain 11" with dotted lines, each in the colour sequence blue, red, pink and green. The band at 1095 cm^{-1} shifted 1.78 cm^{-1} to lower frequencies with a strain increase of 4702 µε.

6.3.1.2 **Predicting strain based on Raman spectra using PLS modelling**

Table 1 shows the effects of spectral pre-processing on the PLS models to predict mechanical strain in wood. Baseline correction aimed to remove the effects of lignin fluorescence, while normalisation attempted to compensate multiplicative effects such as laser fluctuation and uncertainties in focusing (Liland et al., 2016). Second derivative is another way to reduce baseline effects and truncation to the region from 1180 to 950 cm^{-1} eliminated many variables unaffected by mechanical strain. The root mean square error of cross-validation (RMSECV) ranged from 384.8 to 515.3 µε, while the coefficient of determination of cross-validation varied between 0.88 and 0.94 (Table 6-1). Using the

models with the validation data resulted in comparable statistics. Baseline correction followed by normalisation resulted in the best performing PLS model (RMSEP = 427.5 με). The predicted and measured strain for the training group for this PLS model was shown in Figure 6-4A. The distribution of residuals suggested an unbiased model (Figure 6-4B). The models based on truncated spectra in the region of 1180 to 950 cm^{-1} and unmodified spectra achieved slightly reduced model statistics with RMSEPs of 452.4 and 459.7 με, respectively. However, more components were required for the unmodified spectra (Table 6-1). PLS modelling coupled with reflection NIR spectroscopy was successfully used to predict bending ($R^2 \geq 0.90$) and tensile load ($R^2 = 0.96$) on small air-dry wood samples (André et al., 2006; Sandak et al., 2013). As NIR is sensitive to moisture, this technique is of limited use for wood with high moisture content. Such non-destructively reflection NIR measurements of mechanical strain in green wood were found to be less accurate ($R^2 = 0.36$), due to the high moisture content interfering with structural information and a low signal to noise ratio (Chapter 5).

Table 6-1 Metrics of PLS models utilising unmodified and pre-processed Raman spectra to predict mechanical strain in rewetted *E. regnans* wood. The Raman spectral region was 2300 to 200 cm^{-1}, except for the truncated spectra, which ranged from 1180 to 950 cm^{-1}.

Pre-processing method	Training group		Number of components	Validation group	
	R^2 (CV)	RMSECV		R^2	RMSEP
Raw data	0.91	456.2	5	0.90	459.7
Baseline correction	0.93	409.5	4	0.90	477.8
Baseline correction + SNV	0.94	384.8	3	0.92	427.5
Second derivative	0.88	515.3	3	0.89	497.8
Truncation + SNV	0.93	396.3	3	0.91	452.4

SNV: standard normal variate (SNV) normalisation; CV: Leave-one-out cross-validation; RMSECV: root mean squared error of cross-validation; RMSEP: root mean squared error of prediction for the validation group; R^2: coefficient of determination.
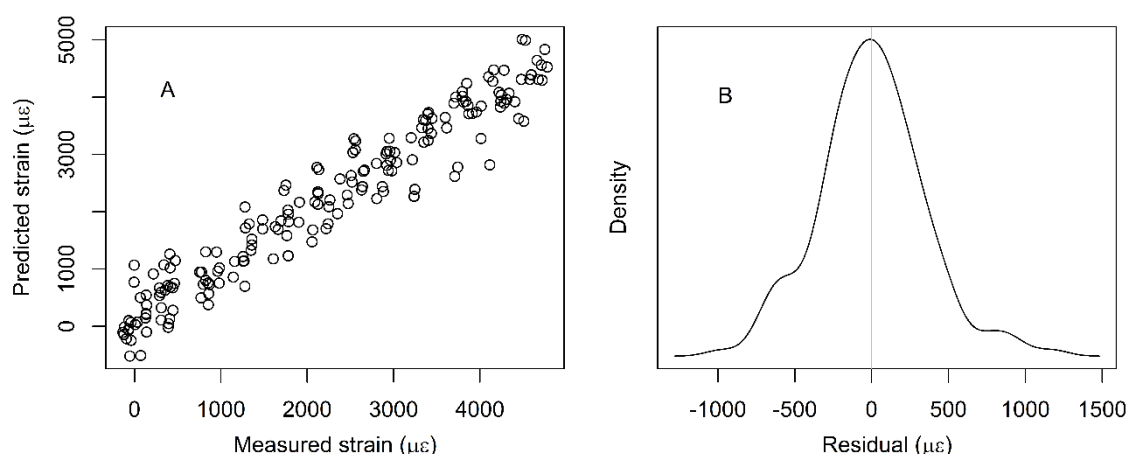
Figure 6-4 Measured and predicted tensile strain of rewetted *E. regnans* wood (A) and distribution of the residuals (B) for the PLS model based on baseline corrected and SNV normalised Raman spectra of the training group.

6.3.1.3 **Spectral changes analysed by regression coefficients and the average**

'slope' spectrum

Both, regression coefficients of the PLS model and 'slope' spectra reflect spectral changes caused by mechanical strain, but were calculated with different algorithms. The regression coefficients of the PLS model represent the change in the response variable (i.e. tensile strain) induced by one unit change in the predictor variables (i.e. the Raman intensities at each wavenumber). As shown in Figure 6-5, the PLS regression coefficients and the average 'slope' spectrum showed almost identical features, with spectral changes in the regions of 1500 to 850 cm^{-1} and 500 to 280 cm^{-1}. Split peaks at 1420, 1120, 1095, 895, 456 cm^{-1} with negative peaks immediately followed by positive peaks indicated band shifts to lower frequencies (Åkerholm et al., 2004; Altaner et al., 2014a).

The most dominant mechanical strain induced Raman band shift at around 1095 cm^{-1} (Figure 6-3 and Figure 6-5) was reported for various (lingo)cellulosic materials (Eichhorn et al., 2001; Gierlinger et al., 2006; Peetla et al., 2006). The band at 1127 cm^{-1} was previously reported to shift to lower wavenumbers for wood fibres under tensile strain (Gierlinger et al., 2006). Both bands were assigned to the stretching of cellulose CC and CO bonds, confirming the deformation of the cellulose skeleton (Gierlinger & Schwanninger, 2006). Additionally, in regenerated cellulose fibres the band at 895 cm^{-1} was also reported to shift upon stress, but with a lower sensitivity to strain than the band at 1095 cm^{-1} (Hamad & Eichhorn, 1997). The band at 895 cm^{-1} was tentatively assigned to the bending of HCO and HCC at C6 of cellulose (Agarwal, 1999; Wiley & Atalla, 1987), indicating that HCO and HCC at C6 was stretched upon tensile strain. This agrees with near infrared data that can be interpreted as the deformation of the intramolecular O2H⋯O6 upon stretching (Guo & Altaner, 2018). To the best of our knowledge, Raman band shifts at 1420 and 456 cm^{-1} due to mechanical strain have never been reported for (lingo)cellulosic material. The region from 1430 to 1350 cm^{-1} was assigned to the bending vibrations of COH groups (Wiley & Atalla, 1987). Therefore the Raman band shift at 1420 cm^{-1} suggested the molecular deformation of COH, which was consistent with MIR and NIR evidence of tensile strain induced deformation of OH groups involved in hydrogen bonds (Altaner et al., 2014b; Guo & Altaner, 2018; Hinterstoisser et al., 2003). The region between 250 and 550 cm^{-1} was mainly attributed to the skeletal bending motions of cellulose including CCC, COC, OCC and OCO bonds (Österberg et al., 2006; Wiley & Atalla, 1987).
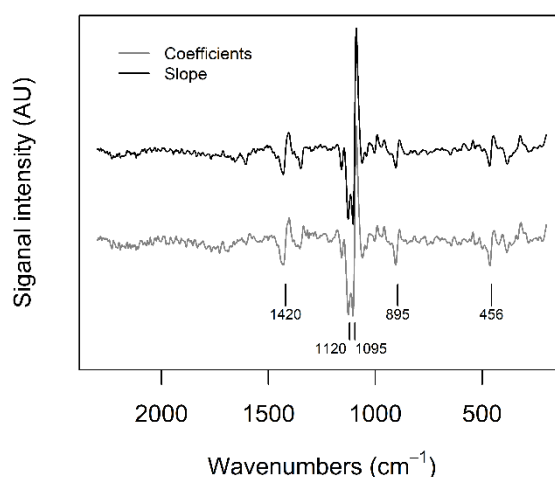
Figure 6-5 Regression coefficients (grey) of the PLS model based on baseline corrected and normalised spectra and the average 'slope' spectrum (black) for 10 strained rewetted *E. regnans* wood samples in the region from 2300 to 200 cm^{-1}.

6.3.2   Quantification of Raman band shifts caused by stretching

Apart from PLS modelling, another approach to predict strain is to use linear models based on the positions of the Raman band at around 1095 cm^{-1}. Raman band positions at around 1095 cm^{-1} were determined by fitting a Cauchy-Lorentzian function to the signal. The dependence of the Raman band position on tensile strain was quantified for rewetted *E. regnans* and green *E. quadrangulata* wood (Figure 6-6). As tensile strain increased from the relaxed state to the maximal applied strain level, the band at 1095 cm^{-1} shifted to lower wavenumbers for both, previously dried water-saturated and never-dried green wood, indicating elongation of the cellulose ring structure. With the release of the applied tensile stress, the Raman band returned to its original position. No significant differences were found between the band positions at "Strain 0" and the relaxed (RL) state (p = 0.31 and 0.27 for rewetted and green wood, respectively). Similar behaviour was reported for single wood fibres (Gierlinger et al., 2006). The results presented here showed that the Raman band at around 1095 cm^{-1} is sensitive to strain for wood samples with a thickness of 0.5 to 1 mm. Thin wood samples, only a few cells thick, behave differently from bulk wood during tensile tests due to unrestricted cellular and supramolecular deformations caused by removing the supporting structure of neighbouring tissue (Navi et al., 1995). With eucalyptus fibres having diameters of 10 to 20 μm (Wilkes, 1988), this effect was minimised here as the wood strips used in this study were comprised of more than 25 cells in thickness. For even larger wood samples MOE was shown to increase with sample thickness (Buchelt & Pfriem, 2011; Yu et al., 2009).
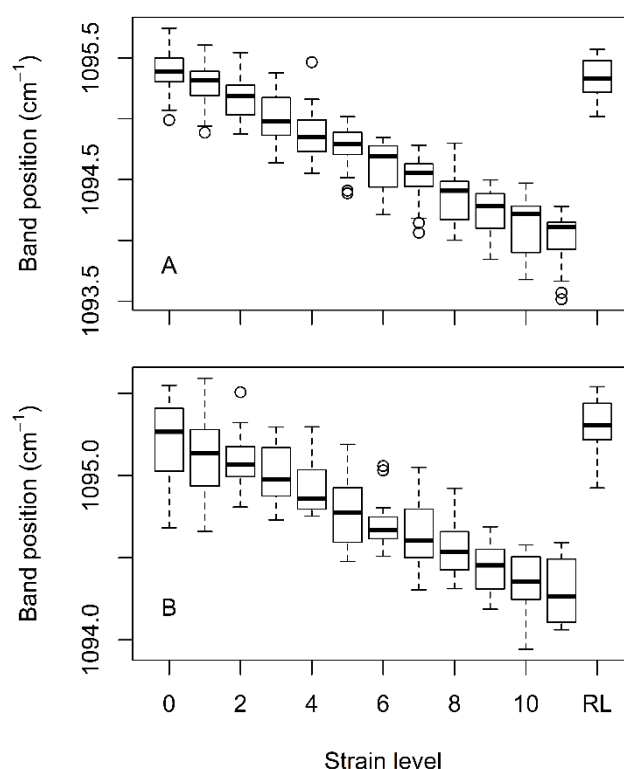
Figure 6-6 Dependence of the position of the Raman band at around 1095 cm^{-1} on tensile strain for rewetted *E. regnans* (A) wood (n = 10) and green *E. quadrangulata* (B) wood (n = 8). Raman spectra were collected as mechanical strain increased stepwise from "Strain 0" (approx. 0 με) to "Strain 11" (approx. 4500 με) and then returned to the relaxed (RL) state.

The mean Raman band position for rewetted *E. regnans* and green *E. quadrangulata* was 1095.41 (±0.15) and 1095.26 (±0.17) cm^{-1}, respectively (Table 2). The difference between *E. regnans* and *E. quadrangulata* was not statistically significant (p = 0.08). The observed variation could be caused by instrumentation like laser fluctuation or variation in wood anatomy and chemical composition (Agarwal, 2006). Additionally, the drying history was reported to affect the cellulose structure (Hill et al., 2010; Toba et al., 2012).

The band shift rate with respect to strain for rewetted *E. regnans* and green *E. quadrangulata* during the tensile tests was −3.06 and −2.15 cm^{-1}/% (Table 6-2). The significantly lower (p < 0.01) band shift rate for green wood resulted in a lower coefficient of determination (0.89) than for rewetted wood (0.95). NIR studies showed that green wood tended to have a lower band shift rate compared to rewetted wood at around 6286 cm^{-1} upon tensile strain (Chapter 5). This indicated that less macroscopic strain was transferred into molecular strain for never-dried green compared to previously-dried rewetted wood. Drying is known to cause irreversible conformational changes of cellulose in wood (Hill et al., 2010). A Raman study claimed that never-dried cellulose in wood is "less-than crystalline" with accessible internal chains (Agarwal et al., 2016). Further study is required to clarify the drying effects on mechanically induced Raman band shift rates of wood.

For the Raman band at around 1095 cm^{-1} band shift rates with respect to strain were reported to be −0.89 to −2.13 cm^{-1}/% for air-dried hemp fibres (Peetla et al., 2006), −1.43 to −1.63 cm^{-1}/% for air-dried single wood fibres (Gierlinger et al., 2006) and −2.4 cm^{-1}/% for tunicate cellulose whiskers (Šturcová et al., 2005). These band shift rates for air-dry materials were lower than the values detected in this study for wet and green wood (Table 6-2). This was despite dry fibres being expected to express higher band shift rates with respect to strain, because they are stiffer than wet wood fibres (Green et al., 2010). A likely explanation is the size effect on mechanical properties of wood. Thin thickness facilitates deformation which is restricted in larger samples by supporting tissue as discussed earlier (Buchelt & Pfriem, 2011; Navi et al., 1995; Yu et al., 2009).

Table 6-2 Average Raman band position at around 1095 cm^{-1} in the relaxed state and its average band shift rate with respect to mechanical strain for green and rewetted wood samples. 26 spectra were collected for each sample during tensile tests and 16 spectra for each sample during bending tests. The maximum tensile strain applied for the tensile and bending tests were approx. 4500 and 2200 με, respectively.

Species	Sample condition	Test	Sample size	Band position (cm^{-1})	band shift rate (cm^{-1}/%)	R^2
E. regnans	rewetted	tensile	10	1095.41 (0.15)	-3.06 (0.48)	0.95 (0.02)
E. quadrangulata	green	tensile	8	1095.26 (0.17)	-2.15 (0.19)	0.89 (0.05)
E. quadrangulata	green	bending	10	1095.10 (0.10)	-1.61 (0.54)	0.59 (0.14)

6.3.3   Raman band shifts in bending tests

Tensile strain was applied to green wood samples glued onto a plastic beam in a four-point bending test in analogy to Eichhorn and Young (2001), who reported Raman band shift at around 1095 cm^{-1} for microcrystalline cellulose composites on bent epoxy beams. Montero

et al. (2012) used a similar setup to measure the crystal deformation of cellulose in wood by X-ray diffraction. In agreement with the tensile tests, the Raman band at around 1095 cm^{-1} shifted to lower frequencies with increasing strain (Figure 6-7). The Raman band returned to its original position (p = 0.56), once the applied strain was released. Limited by the test device, fewer strain levels with lower maximum strain could be applied in the bending tests compared to the tensile tests (6.3.2). This contributed to a lower correlation between band positions and applied strain (Table 6-2).
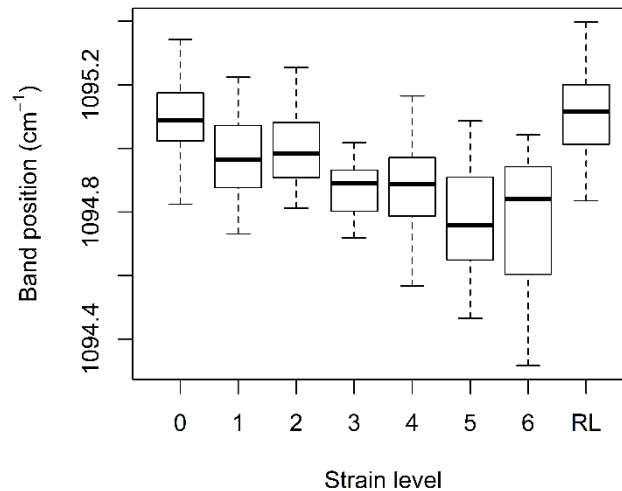
Figure 6-7 Dependence of the position of the Raman band at around 1095 cm^{-1} of green *E. quadrangulata* during a bending tests (n = 10). Raman spectra were collected on the tension side as strain increased stepwise from "Strain 0" to "Strain 6" and then returned to the relaxed (RL) state. The maximum strain was approx. 2200 µε.

The average band position of green *E. quadrangulata* in the relaxed state (1095.10 cm^{-1}) was slightly lower (p = 0.02) than that measured in the tensile tests (1095.26 cm^{-1}) (Table 6-2).This might be attributed to instrumental reasons, fluorescence and variations in wood structure. Consistent with the tensile test results, the average strain induced band shift rate of green *E. quadrangulata* in the bending tests was also lower than for the previously dried rewetted *E. regnans* wood (p < 0.001). Assuming wood species was not the dominating factor, the structural changes caused by drying of rewetted wood (Hill et al., 2010) were a likely explanation of this effect.

6.3.4 Growth-strain and its correlation with the 1095 cm^{-1} band position

Methods to measure growth-strain in trees, including the Nicholson technique (Nicholson, 1971), the CIRAD-Forêt method (Gerard et al., 1995) and the strain gauge method, had been reviewed by Yang et al. (2005). The splitting test proposed by Chauhan and Entwistle (2010) estimates SGS of the stem based on the opening at the ends after splitting the sample along the pith. It is a result of the overall growth-strain throughout the whole sample. In contrast, the other methods are a localized measurement of growth-strain. Although linear correlations were found between the methods (Chauhan & Entwistle, 2010; Yoshida & Okuyama, 2002), it is still challenging to build quantitative relationships between the different methods (Yang & Waugh, 2001).

As shown in Figure 6-8A, a strong linear relationship (r = 0.78) was found between the average SGS measured by strain gauges and the predicted SGS using the splitting method. But the growth-strain measured by strain gauges was significantly lower compared to the estimated SGS using the splitting method. Additionally, the growth-strain measured with the strain gauges at each side of the same stem differed by up to more than four times (data not shown), confirming asymmetric SGS around the stem (Nicholson, 1971).
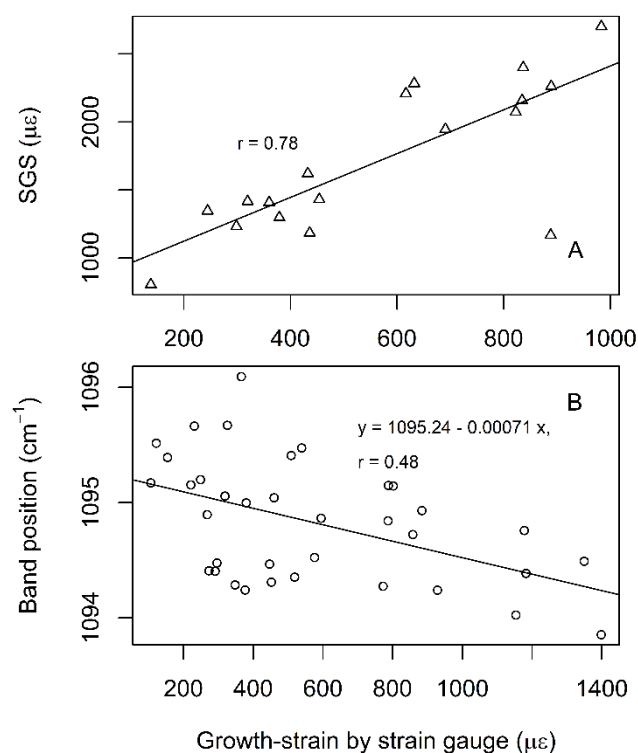
The positions of the Raman band at around 1095 cm^{-1} were moderately correlated (r = 0.48) with SGS measured using strain gauges (Figure 6-8B), but only a lower correlation (r = 0.27) was found between the Raman band positions and the SGS (data not shown). This agreed with the understanding that the Raman measurements reflected the localised molecular strain in the stem and that this strain is variable throughout the stem (Nicholson, 1971).

The band position in the relaxed state was with 1095.24 cm^{-1} consistent with values for green *E. quadrangulata* wood strips (Table 6-2). However, the slope of the linear fit was with −7.1 cm^{-1}/% more than twice the band shift rate of mechanically strained samples (Table 6-2). This suggested that the SGS values measured by strain gauges were underestimated, while the band shift rate based on SGS calculated from the splitting test was with −2.54 cm^{-1}/% similar to those obtained by mechanical strain. Similar discrepancies were reported between the CIRAD-Forêt method (Yoshida & Okuyama, 2002) and strain gauge measurements. Additionally, according to an X-ray diffraction study (Toba et al., 2013), molecular growth-stress remained in a wood block after being removed from the living stem. Therefore, in this experiment growth-strain was probably not completely released by drilling the holes.

PLS models based on NIR spectra of dried wood powders from hybrid progeny of *E. urophylla × E. grandis* predicted growth-strain with a R^2 of 0.63 (Baillères et al., 2002). This approach relied on an indirect correlation between cell wall chemistry and SGS as in wood powders stresses have been released. Such chemical differences are found between normal and reaction wood of tress (Gardiner et al., 2014; Timell, 1986), but not so pronounced between normal wood with varying growth-strain. Another study collected reflection NIR from the surface of green Sugi (*Cryptomeria japonica*) logs and reported a R^2 of 0.61 for the prediction growth-strain(Watanabe et al., 2011). But the sample size of this study was limited to 3 logs from one leaning tree which contained compression wood. This indirect approach is unlikely to succeed in growth-strain predictions for normal wood.

While this study has shown that the level of molecular strain causing surface growth strain in stems can be measured non-destructively with Raman spectroscopy, technological advances are needed for Raman spectroscopy to become commercially feasible for segregation of eucalyptus logs for solid wood processing. The relatively low correlation (r = 0.48) in the present study implied that estimations of growth-strain by Raman spectroscopy will result in falsely rejected good logs. This might be acceptable for a pulp chip business model, aiming to increase revenue by identifying top logs suitable for solid wood production, but is likely to be uneconomic for high value solid wood plantations, which will lose revenue by falsely rejecting quality logs. Technological challenges like measurement time and the focusing procedure of the dispersive system renders industrial applications inefficient. Furthermore, assuming a band shift rate of −3 to −7 cm^{-1}/%, 1000 µε only induces a band shift of 0.3 to 0.7 cm^{-1}, making it necessary to address factors like instrumental uncertainties, sample surface conditions, fluorescence, as well as variations in wood properties and growth-strain (Gerard et al., 1995; Nicholson, 1971; Yang et al., 2001).

Figure 6-8 Relationship between growth-strain measured by strain gauges and the estimated surface growth-strain (SGS) by the splitting method (A) and the dependence of the Raman band at around 1095 cm^{-1} on growth-strain measured by strain gauges (B). Each band position was calculated as the average of 9 Raman spectra collected on the wood surface at the location of the strain gauge.

6.4 Conclusion

A partial least squares model based on pre-processed spectra was able to predict mechanical strain with a root mean square error of 427.5 µε and R^2 of 0.92. The major spectral changes caused by mechanical strain were in the regions of 1500 to 850 cm^{-1} and 500 to 280 cm^{-1}. Apart from the predominant band shift at 1095 cm^{-1}, detailed analysis suggested that mechanical strain also caused Raman band shifts at 1420, 1120, 895, 456 cm^{-1}. The spectral changes could be interpreted as the molecular deformation of the cellulose skeleton, HCO and HCC groups at C6 as well as COH structures. Further, studies with green wood indicated that the Raman band shift rate with respect to strain was lower in never-dried green wood than previously dried rewetted wood. Therefore, proportion of macroscopic strain transferred into molecular strain of cellulose was different for green and rewetted wood, which was probably related to irreversible drying effects. A moderate correlation was found between the band positions at around 1095 cm^{-1} and the growth-strain measured by strain gauges, indicating that the technology can potentially be used to segregate logs for solid wood production, but improvements in Raman instrumentation are needed.

7 SYNOPSIS

Growth-stress is a major obstacle for the high-value solid wood uses of eucalypts. The overreaching objective of this study was to measure stress in wood rapidly and non-destructively, especially growth-stress in green wood. Stress in wood, whether it is applied mechanical stress or growth-stress generated by the plant itself, causes deformation both at the macroscopic and the molecular scale. The structural changes in cellulose, and consequently wood, caused by stress can be measured using spectroscopic techniques. Near infrared and Raman spectroscopy share the advantages of easy sampling, portability and accessing rich chemical information, making them potential candidates to measure stress or strain in wood rapidly and non-destructively. Non-destructive measurements require spectroscopy in the reflectance mode.

1) Growth-strain in logs and its effects on eucalypt wood utilization

As presented in chapter 2, the first objective was to demonstrate the effects of growth-strain in *E. globoidea* logs on the production and properties of peeled veneer and LVL. The veneer recovery varied between logs ranging from 23.6% to 74.5% and was correlated to growth-strain. Growth-strain in logs was also found to be related to the splitting in veneers. High-quality veneers could be obtained from *E. globoidea* logs with low growth-strain levels at yields of up to 74.5%. But the variation between logs was large in the existing resource without genetic selection. A few logs with relatively high growth-strain levels produced veneers which were unusable for LVL production due to severe splitting. The dynamic MOE of the veneers ranged from 9.59 to 20.26 GPa.

The large variation in both growth-strain and stiffness suggested the potential for genetic improvement through a breeding program, as both traits were shown to be heritable (Davies et al., 2017; Murphy et al., 2005). No correlation was found between splitting length in the veneers and log stiffness, indicating the possibility of finding trees with high stiffness and low growth-strain levels suitable for veneer and LVL production. For the existing resource, a feasible approach would be to segregate logs with low growth-strain levels for high value uses and use the logs with high growth-strain levels for products like bioenergy or pulp. However, as all current methods to measure growth-strain are intrusive and time-consuming, a fast and non-destructive approach to segregate logs based on growth-strain is needed.

2) Molecular deformation of air-dry wood and paper studied by NIR

Compared to other forms of IR spectroscopy, NIR spectra can easily be obtained and commercially used for monitoring industrial processes. Therefore NIR was chosen to investigate the potential to non-destructively measure growth-strain in wood. While other techniques were extensively used to study mechanical strain in cellulose and wood (Eichhorn et al., 2001; Montero et al., 2012; Salmén & Burgert, 2009), NIR was largely ignored by the scientific community for this purpose. In order to measure strain in wood, the mechanical strain induced changes in NIR spectra of air-dry wood and cellulose were examined in detail. The major spectral changes caused by mechanical strain were found in the region between 6600 and 6000 cm^{-1}, attributed to the first overtone of OH stretching. With the increase of applied tensile strain, bands at 6470 ± 10 cm^{-1} and 6286 ± 5 cm^{-1} were found to shift to higher wavenumbers in the second derivative spectra. These were tentatively assigned to the intramolecular hydrogen bonded OH groups 3OH···5O and 2OH···6O, respectively. The band shifts were interpreted as the contraction and strengthening of OH groups, as a result of the stretching of the intramolecular hydrogen bonds. The band shift rate with respect to strain at around 6286 cm^{-1} was half of that at around 6470 cm^{-1}. This suggested that the glycosidic bonds in cellulose deformed upon tensile stress. For wood samples in a bending tests, the NIR band at around 6286 cm^{-1}

81

shifted to higher wavenumbers at the tension side, and as expected to lower wavenumbers at the compression side. The strong correlation between band positions at around 6286 cm^{-1} and applied strain levels indicated that, it might be possible to measure strain in wood rapidly and non-destructively based on the NIR band shift.

3) Effects of desorption and isotope exchange on wood under mechanical stress studied by NIR

In order to better understand the load transfer process in wood on the molecular level, deuteration combined with NIR spectroscopy was used to provide structural information of wood under mechanical stress. Polarized NIR spectra of deuterated wood indicated that hydroxyl groups in inaccessible cellulose were more oriented in the axial direction compared to accessible cellulose. As a hygroscopic material, wood is sensitive to the environmental fluctuations, and moisture changes affect spectral changes caused by mechanical stress. Spectral changes caused by desorption were differentiated from those induced by mechanical stress by averaging the loading and unloading cycles. The bands at 6420, 6240 and 4670 cm^{-1} showed similar features for protonated and deuterated wood, indicating that the inaccessible cellulose was the main load-bearing component in wood. However, a signal at around 4700 cm^{-1}, tentatively assigned to OD groups, showed a response to mechanical strain in deuterated wood. This suggested that inaccessible cellulose might also contributed to the load transfer of wood. Additionally, the NIR data confirmed evidence that apart from changes in humidity or temperature, tensile stress increased the water adsorption of wood (Simposon, 1971; Treloar, 1953).

4) Predicting strain in rewetted and green wood using NIR spectroscopy

As rewetted wood dried, its NIR absorbance changed with moisture content. Above fibre saturation point (FSP) absorbance increased due to increased scattering by replacing free water in the cell lumens with air, which has a different refractive index. In contrast, NIR absorbance decreased below FSP due to fewer bound water molecules in the cell wall absorbing NIR light without changing the refractive index difference between air-filled cell lumens and cell walls. Above FSP, free water reduced the signal intensity from crystalline cellulose and skewed the band of interest at around 6286 cm^{-1}, which was successfully removed by baseline correction.

Mechanically induced band shifts at around 6286 cm^{-1} were detected for air-dry, rewetted and green wood samples using NIR in transmission mode. But the correlation coefficients were lower for rewetted and green wood than air-dry wood, reflecting their reduced signal intensities at high moisture content. Further, the band shift rates differed between never-dried green wood and previously dried rewetted wood, implying differences in the transfer of macroscopic into molecular strain.

Reflection NIR spectroscopy was used to non-destructively predict mechanical strain in green wood. Reflection NIR with a fibre optic probe lowered the spectra quality further. A moderate correlation was found between the position of the band centred at around 6286 cm^{-1} and the mechanical strain in green wood upon bending. However, the surface growth strain in green *E. nitens* logs did not correlate with the position of this band. The main challenges included the low signal to noise ratio of reflection NIR spectroscopy combined with the interference of the water signal as well as uncertainty in the growth-strain measurements.

5) Predicting strain in rewetted and green wood using Raman spectroscopy

Raman spectroscopy is insensitive to water, which is an advantage over NIR spectroscopy when measuring strain in water saturated wood. In order to predict strain in rewetted wood, partial least squares (PLS) models developed based on Raman spectra were able to successfully predict mechanical strain in thick wood samples with a root mean square error of 427.5 µε. The spectral changes caused by strain were mainly in two regions, 1500 to 850 cm^{-1} and 500 to 280 cm^{-1}. The widely reported band shift (Gierlinger et al., 2006; Hamad & Eichhorn, 1997; Peetla et al., 2006) at 1095 cm^{-1} upon mechanical strain of cellulose was also observed, indicating the elongation of cellulose ring structure. Band shifts were also identified at 1420, 1120, 895, 456 cm^{-1}, which were interpreted as the molecular deformation of CC and CO bonds of cellulose skeleton, HCO and HCC at C6 as well as COH structures upon tensile stress.

The band shift rate with regard to strain at around 1095 cm^{-1} was lower for green wood than rewetted wood, which was consistent with the NIR data (Chapter 5). This suggested that the transfer from macroscopic to molecular strain was less for never-dried green wood than previously dried rewetted wood. This might have been related to the irreversible changes in cellulose structure during drying which were deduced from X-ray diffraction studies (Hill et al., 2010; Leppänen et al., 2011). The band shift rates for the solid wood samples were greater than the reported values for single wood (Gierlinger et al., 2006) and hemp fibres (Eichhorn et al., 2001) as well as regenerated cellulose films (Hsieh et al., 2008). Thick wood samples are known be stiffer, due to neighbouring cell walls restricting some forms of deformation (Navi et al., 1995; Yu et al., 2009). This size effect is consistent with the observed greater band shift rates reported in this study.

The position of the Raman band at around 1095 cm^{-1} was moderately related to released growth-strain measured with strain gauges. The relatively low R^2 suggested that predictions of growth-strain with Raman spectroscopy would result in a significant amount of wrongly rejected logs. This might be economically viable for upgrading an already profitable chip wood resource by identifying logs suitable for higher value solid wood products rather than trying to reject unsuitable logs from a sawmilling operation. Further advances in Raman instrumentation are needed to make the measurements fast and robust enough for industrial application.

Overall, the studies showed that growth-strain in wood is very challenging to measure because of relatively small magnitude compared to applied mechanical strain, its large variation and the presence of water. A strain of 1000 µε induces a NIR band shift of roughly 0.8 cm^{-1} at around 6286 cm^{-1} and a Raman band shift of −0.2 to −0.7 cm^{-1} at around 1095 cm^{-1} for green eucalypt wood. Considering the technical limitations and signal intensities, it was difficult to measure such small changes precisely using non-destructive NIR spectroscopy and Raman spectroscopy.

LIMITATIONS AND FUTURE RESEARCH

1) The bonding quality of the *E. globoidea* veneers was unsatisfactory in the study. Technical solutions including alternative adhesive formulations and pressing parameters should solve this problem, as experience with other dense eucalypts in countries such as Australia has shown.

2) The molecular deformation of pure cellulose sheets of cellulose Iβ, cellulose Iα and regenerated cellulose could be studied using NIR spectroscopy. Comparative studies using these materials and wood could potentially provide new information on the contribution of lignin and hemicellulose in the load transfer of wood. These experiments might also clarify whether the signal at around 7344 cm^{-1} in the 'slope' spectra was related to the CH···O

hydrogen bonds between cellulose sheets. A supporting study would be to monitor the effects of temperature on the thermal expansion of cellulose on the molecular level using NIR spectroscopy.

3) The accuracy of non-destructive NIR prediction of strain was limited by the signal intensity of reflection NIR using a fibre optic probe. Reflection NIR rather than transmission NIR enables easy sampling and non-destructive measurement. But the signal to noise ratio of reflection NIR was low compared to transmission NIR spectroscopy. Advances in reflection NIR technology might result in a successful application for growth-strain measurements.

4) In chapter 4, the wood samples were partially deuterated and re-protonated during sample handling. Exposing completely deuterated cellulose sheets in the air will have the accessible cellulose protonated and the inaccessible cellulose deuterated. Tensile tests on this kind of cellulose sheets studied by NIR spectroscopy might provide insights into the structure of cellulose on both molecular and supramolecular levels. Coupling effects might be removed by doping protonated or deuterated samples with 5−10% of the other isotope, a technique previously used for MIR investigations of hydrogen bonds in sugar monomer crystals (Rozenberg et al., 2000).

5) Factors like fluorescence, laser fluctuations and uncertainties in focusing affected the Raman spectra, reducing the accuracy in the strain prediction. To measure the relatively small growth-strain, a reliable Raman system with high sensitivity is needed. FT-Raman spectrometer or dispersive systems such as the Sequentially Shifted Excitation (SSE) technique might be able to mitigate fluorescence while retaining good sensitivity (Conti et al., 2016).

6) Spatial variation of wood properties, in particular growth-strain is not well understood. The NIR and Raman band positions in the relaxed state varied between samples, which might not only be caused by spatial variation in wood anatomical or its chemical composition but also unreleased, residual stress/strain in the wood. Additionally, growth-strain was reported to vary along the circumference within trees (Nicholson, 1971), but the scale of the variations in terms of spatial distance remains unclear. Microscopic spectroscopy including IR and Raman would be useful tools to investigate the extent of these variations in wood.

7) The differences in band shift rates with respect to strain observed for previously-dried rewetted wood and never-dried green wood, indicating a lower strain transfer from the macroscopic to the molecular level for green wood, which is worth studying in more detail to better understand the wood cell wall. The irreversible effect of drying on cellulose structure was probably responsible for this difference. Further studies combining NIR and Raman spectroscopy and X-ray diffraction could potentially shed light on the structure of cellulose in never-dried wood.

REFERENCES

Abe, K., & H. Yamamoto. (2006). Change in mechanical interaction between cellulose microfibril and matrix substance in wood cell wall induced by hygrothermal treatment. *Journal of Wood Science, 52*(2), 107-110.

Acevedo, A., C. Bustos, J. P. Lasserre, & W. Gacitua. (2012a). Nose bar pressure effect in the lathe check morphology to *Eucalyptus nitens* veneers. *Maderas. Ciencia y tecnologia, 14*(3), 289-301. doi: 10.4067/S0718-221X2012005000004

Acevedo, A., C. Bustos, J. P. Lasserre, & W. Gacitua. (2012b). Nose bar pressure effect in the lathe check morphology to Eucalyptus nitens veneers. *Maderas. Ciencia y tecnologia, 14*(3).

Agarwal, U. P. (1999). An overview of Raman spectroscopy as applied to lignocellulosic materials. *Advances in lignocellulosics characterization*, 201-225.

Agarwal, U. P. (2006). Raman imaging to investigate ultrastructure and composition of plant cell walls: distribution of lignin and cellulose in black spruce wood (Picea mariana). *Planta, 224*(5), 1141. doi: 10.1007/s00425-006-0295-z

Agarwal, U. P., S. A. Ralph, R. S. Reiner, & C. Baez. (2016). Probing crystallinity of never-dried wood cellulose with Raman spectroscopy. *Cellulose, 23*(1), 125-144. doi: 10.1007/s10570-015-0788-7

Åkerholm, M., B. Hinterstoisser, & L. Salmén. (2004). Characterization of the crystalline structure of cellulose using static and dynamic FT-IR spectroscopy. *Carbohydrate research, 339*(3), 569-578.

Åkerholm, M., & L. Salmén. (2001). Interactions between wood polymers studied by dynamic FT-IR spectroscopy. *Polymer, 42*(3), 963-969.

Ali, M., A. M. Emsley, H. Herman, & R. J. Heywood. (2001). Spectroscopic studies of the ageing of cellulosic paper. *Polymer, 42*(7), 2893-2900. doi: http://dx.doi.org/10.1016/S0032-3861(00)00691-1

Alméras, T., & B. Clair. (2016). Critical review on the mechanisms of maturation stress generation in trees. *Journal of the Royal Society Interface, 13*(122), 20160550.

Altaner, C. M., D. C. Apperley, & M. C. Jarvis. (2006). Spatial relationships between polymers in Sitka spruce: Proton spin-diffusion studies *Holzforschung* (Vol. 60, pp. 665).

Altaner, C. M., Y. Horikawa, J. Sugiyama, & M. C. Jarvis. (2014a). Cellulose Iβ investigated by IR-spectroscopy at low temperatures. *Cellulose, 21*(5), 3171-3179.

Altaner, C. M., & M. C. Jarvis. (2008). Modelling polymer interactions of the 'molecular Velcro' type in wood under mechanical stress. *Journal of Theoretical Biology, 253*(3), 434-445. doi: http://dx.doi.org/10.1016/j.jtbi.2008.03.010

Altaner, C. M., L. H. Thomas, A. N. Fernandes, & M. C. Jarvis. (2014b). How cellulose stretches: synergism between covalent and hydrogen bonding. *Biomacromolecules, 15*(3), 791-798.

Andersson, S., H. Wikberg, E. Pesonen, S. L. Maunu, & R. Serimaa. (2004). Studies of crystallinity of Scots pine and Norway spruce cellulose. *Trees, 18*(3), 346-353. doi: 10.1007/s00468-003-0312-9

André, N., N. Labbé, T. G. Rials, & S. S. Kelley. (2006). Assessment of wood load condition

by Near Infrared (NIR) spectroscopy. *Journal of Materials Science, 41*(7), 1879-1886.

Archer, R. R. (1987). *Growth stresses and strains in trees*. Berlin: Springer-Verlag Gmbh.

AS/NZS. (2012a). Methods of test for veneer and plywood *Method 2: Bond quality of plywood (chisel test)*. Wellington: Standards Australia/ Standards New Zealand.

AS/NZS. (2012b). Plywood-Structural *Part 0: Specifications*. Wellington: Standards Australia/ Standards New Zealand.

AS/NZS. (2016). Adhesives for timber and timber products *Part 1: Adhesives for manufacture of plywood and laminated veneer lumber (LVL)*. Wellington: Standards Australia/ Standards New Zealand.

Atalla, R. H., & D. L. Vanderhart. (1984). Native cellulose: a composite of two distinct crystalline forms. *Science, 223*(4633), 283-285.

Baillères, H., F. Davrieux, & F. Ham-Pichavant. (2002). Near infrared analysis as a tool for rapid screening of some major wood characteristics in a eucalyptus breeding program. *Annals of Forest Science, 59*(5-6), 479-490.

Bal, B. C., & I. Bektaş. (2012). The effects of some factors on the impact bending strength of laminated veneer lumber. *BioResources, 7*(4), 5855-5863.

Bao, C. F., H. Z. Jiang, M. X. Jiang, X. X. Lu, Q. X. Luo, & Y. S. Zhang. (2001). Differences in wood properties between juvenile wood and mature wood in 10 species grown in China. *Wood Science and Technology, 35*(4), 363-375. doi: 10.1007/s002260100099

Barnett, J., & V. A. Bonham. (2004). Cellulose microfibril angle in the cell wall of wood fibres. *Biological reviews, 79*(2), 461-472.

Barr, N. (1996). *Growing eucalypt trees for milling on New Zealand farms*. Wellington, New Zealand: New Zealand Farm Forestry Association.

Bonnet, M., D. Courtier-Murias, P. Faure, S. Rodts, & S. Care. (2017). NMR determination of sorption isotherms in earlywood and latewood of Douglas fir. Identification of bound water components related to their local environment. *Holzforschung, 71*(6), 481. doi: 10.1515/hf-2016-0152

Bootle, K. R. (2005). *Wood in Australia. Types, properties and uses* (2nd ed.). Sydney: McGraw-Hill Book Company.

Borrega, M., P. Ahvenainen, R. Serimaa, & L. Gibson. (2015). Composition and structure of balsa (Ochroma pyramidale) wood. *Wood Science and Technology, 49*(2), 403-420.

Boyd, J. (1982). An anatomical explanation for visco-elastic and mechano-sorptive creep in wood, and effects of loading rate on strength. In P. Baas (Ed.), *New perspectives in wood anatomy* (pp. 171-222): Martinus Nijhoff/ Dr W.Junk Publishers.

Brett, C. T. (2000). Cellulose microfibrils in plants: biosynthesis, deposition, and integration into the cell wall. *International review of cytology, 199*, 161-199.

Buchelt, B., & A. Pfriem. (2011). Influence of wood specimen thickness on its mechanical properties by tensile testing: solid wood versus veneer. *Holzforschung, 65*(2), 249-252.

Bucur, V. (2011). *Delamination in Wood, Wood Products and Wood-Based Composites* (1st ed.). Dordrecht: Springer.

Burgert, I. (2006). Exploring the Micromechanical Design of Plant Cell Walls. *American Journal of Botany, 93*(10), 1391-1401.

Carrick, J., & K. Mathieu. (2005). *Durability of Laminated Veneer Lumber made from Blackbutt.* Paper presented at the Proceedings of the 10DBMC International Conference on Durability of Building Materials and Components, France.

Carron, K., & R. Cox. (2010). Qualitative Analysis and the Answer Box: A Perspective on Portable Raman Spectroscopy. *Analytical Chemistry, 82*(9), 3419-3425. doi: 10.1021/ac901951b

Chauhan, S., & K. Entwistle. (2010). Measurement of surface growth stress in Eucalyptus nitens Maiden by splitting a log along its axis. *Holzforschung, 64*(2), 267-272.

Chauhan, S. S., & J. Walker. (2004). Relationships between longitudinal growth strain and some wood properties in *Eucalyptus nitens*. *Australian Forestry, 67*(4), 254-260.

Chauhan, S. S., & J. C. F. Walker. (2006). Variations in acoustic velocity and density with age, and their interrelationships in radiata pine. *Forest Ecology and Management, 229*(1), 388-394. doi: https://doi.org/10.1016/j.foreco.2006.04.019

Clair, B., T. Alméras, G. Pilate, D. Jullien, J. Sugiyama, & C. Riekel. (2011). Maturation stress generation in poplar tension wood studied by synchrotron radiation microdiffraction. *Plant physiology, 155*(1), 562-570.

Clair, B., T. Alméras, H. Yamamoto, T. Okuyama, & J. Sugiyama. (2006). Mechanical behavior of cellulose microfibrils in tension wood, in relation with maturation stress generation. *Biophysical Journal, 91*(3), 1128-1135.

Conti, C., A. Botteon, M. Bertasa, C. Colombo, M. Realini, & D. Sali. (2016). Portable Sequentially Shifted Excitation Raman spectroscopy as an innovative tool for in situ chemical interrogation of painted surfaces. *Analyst, 141*(15), 4599-4607.

Davies, N. T., L. A. Apiolaza, & M. Sharma. (2017). Heritability of growth strain in *Eucalyptus bosistoana*: a Bayesian approach with left-censored data. *New Zealand Journal of Forestry Science, 47*, 5. doi: 10.1186/s40490-017-0086-2

de Carvalho, A. M., F. A. R. Lahr, & G. Bortoletto Jr. (2004). Use of Brazilian eucalyptus to produce LVL panels. *Forest products journal, 54*(11), 61.

De Rosa, I. M., C. Santulli, & F. Sarasini. (2010). Mechanical and thermal characterization of epoxy composites reinforced with random and quasi-unidirectional untreated Phormium tenax leaf fibers. *Materials & Design, 31*(5), 2397-2405.

Djahedi, C., M. Bergenstråhle-Wohlert, L. A. Berglund, & J. Wohlert. (2016). Role of hydrogen bonding in cellulose deformation: the leverage effect analyzed by molecular modeling. *Cellulose, 23*(4), 2315-2323.

Donaldson, L. (2008). Microfibril angle: measurement, variation and relationships–a review. *IAWA Journal, 29*(4), 345-386.

Downes, G. M., J. G. Nyakuengama, R. Evans, R. Northway, P. Blakemore, R. L. Dickson, *et al.* (2002). Relationship between wood density, microfibril angle and stiffness in thinned and fertilized Pinus radiata. *Iawa Journal, 23*(3), 253-265.

Downes, G. M., M. Touza, C. Harwood, & M. Wentzel-Vietheer. (2014). NIR detection of non-recoverable collapse in sawn boards of Eucalyptus globulus. *European Journal of Wood and Wood Products, 72*(5), 563-570.

Driemeier, C., F. M. Mendes, & L. Y. Ling. (2015). Hydrated fractions of cellulosics probed by infrared spectroscopy coupled with dynamics of deuterium exchange. *Carbohydrate Polymers, 127*, 152-159.

Dumitriu, S. (2004). *Polysaccharides: structural diversity and functional versatility*: CRC press.

Eichhorn, S. J., A. Dufresne, M. Aranguren, N. E. Marcovich, J. R. Capadona, S. J. Rowan*, et al.* (2010). Review: current international research into cellulose nanofibres and nanocomposites. *Journal of Materials Science, 45*(1), 1-33.

Eichhorn, S. J., J. Sirichaisit, & R. J. Young. (2001). Deformation mechanisms in cellulose fibres, paper and wood. *Journal of Materials Science, 36*(13), 3129-3135.

Eichhorn, S. J., & R. J. Young. (2001). The Young's modulus of a microcrystalline cellulose. *Cellulose, 8*(3), 197-207. doi: 10.1023/a:1013181804540

Eichhorn, S. J., R. J. Young, & G. R. Davies. (2005). Modeling Crystal and Molecular Deformation in Regenerated Cellulose Fibers. *Biomacromolecules, 6*(1), 507-513. doi: 10.1021/bm049409x

Fackler, K., & M. Schwanninger. (2010). Polysaccharide degradation and lignin modification during brown rot of spruce wood: a polarised Fourier transform near infrared study. *Journal of Near Infrared Spectroscopy, 18*(6), 403.

Faix, O., & J. Böttcher. (1992). The influence of particle size and concentration in transmission and diffuse reflectance spectroscopy of wood. *Holz als Roh-und Werkstoff, 50*(6), 221-226.

Fang, C.-H., D. Guibal, B. Clair, J. Gril, Y.-M. Liu, & S.-Q. Liu. (2008). Relationships between growth stress and wood properties in poplar I-69 (*Populus deltoides Bartr.* cv. "Lux" ex I-69/55). *Annals of Forest Science, 65*(3), 307.

Fang, L., & J. M. Catchmark. (2014). Structure characterization of native cellulose during dehydration and rehydration. *Cellulose, 21*(6), 3951-3963. doi: 10.1007/s10570-014-0435-8

Farrell, R., S. Blum, D. Williams, & D. Blackburn. (2011). The potential to recover higher value veneer products from fibre managed plantation eucalypts and broaden market opportunities for this resource: Part A *Project No: PNB139-0809*. Melbourne: Forest & Wood Products Australia.

Fengel, D., & G. Wegener. (1984). Wood: Chemistry, ultrastructure, reactions. *Walter de Gruyter, 613*, 1960-1982.

Fernandes, A. N., L. H. Thomas, C. M. Altaner, P. Callow, V. T. Forsyth, D. C. Apperley*, et al.* (2011). Nanostructure of cellulose microfibrils in spruce wood. *Proceedings of the National Academy of Sciences, 108*(47), E1195-E1203.

Fernandes Diniz, J. M. B., M. H. Gil, & J. A. A. M. Castro. (2004). Hornification—its origin and interpretation in wood pulps. *Wood Science and Technology, 37*(6), 489-494. doi: 10.1007/s00226-003-0216-2

Forughi, A., S. Green, & B. Stoeber. (2016). Optical transparency of paper as a function of moisture content with applications to moisture measurement. *Review of Scientific Instruments, 87*(2), 023706.

Fournier, M., B. Chanson, B. Thibaut, & D. Guitard. (1994). Measurements of residual growth strains at the stem surface. Observations on different species. *Annales des Sciences Forestières, 51*(3), 249-266.

French, A. D., M. Concha, M. K. Dowd, & E. D. Stevens. (2014). Electron (charge) density studies of cellulose models. *Cellulose, 21*(2), 1051-1063. doi: 10.1007/s10570-013-

0042-0

FSC. (2012). Strategic review on the future of forest plantations. Helsinki, Finland: Forest Stewardship Council.

Gardiner, B., J. Barnett, P. Saranpää, & J. Gril. (2014). *The biology of reaction wood*: Springer.

Gaunt, D., B. Penellum, & H. M. McKenzie. (2003). *Eucalyptus nitens* laminated veneer lumber structural properties. *New Zealand Journal of Forestry Science, 33*(1), 114-125.

Gerard, J., H. Bailleres, M. Fournier, & B. Thibaut. (1995). Wood quality in plantation Eucalyptus - a study of variation in three reference properties. *Bois et Forêts des Tropiques, 245*, 101-110.

Gierlinger, N., & M. Schwanninger. (2006). Chemical imaging of poplar wood cell walls by confocal Raman microscopy. *Plant Physiology, 140*(4), 1246-1254.

Gierlinger, N., M. Schwanninger, A. Reinecke, & I. Burgert. (2006). Molecular changes during tensile deformation of single wood fibers followed by Raman microscopy. *Biomacromolecules, 7*(7), 2077-2081. doi: 10.1021/bm060236g

Glass, S. V., & S. L. Zelinka. (2010). Moisture relations and physical properties of wood. In R. J. Ross (Ed.), *Wood handbook : wood as an engineering material*. Madison, Wisconsin: Department of Agriculture, Forest Service, Forest Products Laboratory.

Green, D. W., J. E. Winandy, & D. E. Kretschmann. (2010). Mechanical properties of wood. In R. J. Ross (Ed.), *Wood handbook: wood as an engineering material*. Madison, Wisconsin: Department of Agriculture, Forest Service, Forest Products Laboratory.

Guo, F., & C. M. Altaner. (2018). Molecular deformation of wood and cellulose studied by near infrared spectroscopy. *Carbohydrate Polymers, 197*, 1-8. doi: https://doi.org/10.1016/j.carbpol.2018.05.064

Hague, J. R. B. (2013). Utilisation of plantation eucalypts in engineered wood products (F. W. P. Australia, Trans.). Melbourne, Australia.

Hamad, W. Y., & S. Eichhorn. (1997). Deformation Micromechanics of Regenerated Cellulose Fibers Using Raman Spectroscopy. *Journal of Engineering Materials and Technology, 119*(3), 309-313. doi: 10.1115/1.2812262

Harrington, J. J. (2002). Hierarchical modelling of softwood hygro-elastic properties.

Haslett, A. N. (1990). Properties and utilisation of exotic speciality timbers grown in New Zealand. Part VI: Eastern blue gums and stringy barks. Eucalyptus botryoides Sm. Eucalyptus saligna Sm. Eucalyptus globoidea Blakey. Eucalyptus muellerana Howitt. Eucalyptus pilularis Sm *FRI Bulletin 119* (Vol. 119). Rotorua: New Zealand Forest Research Institute.

Hayakawa, D., Y. Nishiyama, K. Mazeau, & K. Ueda. (2017). Evaluation of hydrogen bond networks in cellulose Iβ and II crystals using density functional theory and Car–Parrinello molecular dynamics. *Carbohydrate research, 449*, 103-113.

Hill, S. J., N. M. Kirby, S. T. Mudie, A. M. Hawley, B. Ingham, R. A. Franich*, et al.* (2010). Effect of drying and rewetting of wood on cellulose molecular packing. *Holzforschung, 64*(4), 421-427. doi: 10.1515/hf.2010.065

Hineno, M., & H. Yoshinaga. (1972). Far-infrared spectra of glucose, sorbose, saccharose and cellobiose at liquid He temperature. *Spectrochimica Acta Part A: Molecular Spectroscopy, 28*(11), 2263-2268.

Hinterstoisser, B., M. Åkerholm, & L. Salmén. (2001). Effect of fiber orientation in dynamic FTIR study on native cellulose. *Carbohydrate Research, 334*(1), 27-37. doi: http://dx.doi.org/10.1016/S0008-6215(01)00167-7

Hinterstoisser, B., M. Åkerholm, & L. Salmén. (2003). Load Distribution in Native Cellulose. *Biomacromolecules, 4*(5), 1232-1237. doi: 10.1021/bm030017k

Hofstetter, K., B. Hinterstoisser, & L. Salmén. (2006). Moisture uptake in native cellulose–the roles of different hydrogen bonds: a dynamic FT-IR study using Deuterium exchange. *Cellulose, 13*(2), 131-145.

Hsieh, Y.-C., H. Yano, M. Nogi, & S. J. Eichhorn. (2008). An estimation of the Young's modulus of bacterial cellulose filaments. *Cellulose, 15*(4), 507-513.

Huang, J., S. Romero-Torres, & M. Moshgbar. (2010). Practical considerations in data pre-treatment for NIR and Raman spectroscopy. *American Pharmaceutical Review, 13*(6), 116.

Iglesias, T., & D. Wilstermann. (2009). *Global Eucalyptus Map (v 1.2). GIT forestry consulting's eucalyptologics: information resources on Eucalyptus cultivation worldwide* Retrieved from http://git-forestry-blog.blogspot.com/2009/10/global-eucalyptus-map-2009-in-buenos.html

Inagaki, T., H. Yonenobu, & S. Tsuchikawa. (2008). Near-Infrared Spectroscopic Monitoring of the Water Adsorption/Desorption Process in Modern and Archaeological Wood. *Applied Spectroscopy, 62*(8), 860-865.

Jacobs, M. R. (1945). *The growth stresses of woody stems*. Canberra: Commonwealth Forestry Bureau.

Jarvis, M. (2003). Chemistry: cellulose stacks up. *Nature, 426*(6967), 611-612.

Jarvis, M. C. (2018). Structure of native cellulose microfibrils, the starting point for nanocellulose manufacture. *Philosophical Transactions of the Royal Society A: Mathematical, Physical and Engineering Sciences, 376*(2112), 20170045. doi: 10.1098/rsta.2017.0045

Jarvis, M. C., & M. C. McCann. (2000). Macromolecular biophysics of the plant cell wall: Concepts and methodology. *Plant Physiology and Biochemistry, 38*(1), 1-13. doi: https://doi.org/10.1016/S0981-9428(00)00172-8

Jin, K., Z. Qin, & M. J. Buehler. (2015). Molecular deformation mechanisms of the wood cell wall material. *Journal of the Mechanical Behavior of Biomedical Materials, 42*, 198-206. doi: http://dx.doi.org/10.1016/j.jmbbm.2014.11.010

Jones, T. G., R. M. McConnochie, T. Shelbourne, & C. B. Low. (2010). Sawing and grade recovery of 25-year-old *Eucalyptus fastigata*, *E. globoidea*, *E. muelleriana* and *E. pilularis*. *New Zealand Journal of Forestry Science, 40*, 19-31.

Keckes, J., I. Burgert, K. Fruhmann, M. Muller, K. Kolln, M. Hamilton, *et al.* (2003). Cell-wall recovery after irreversible deformation of wood. *Nature Materials, 2*(12), 810-813. doi: http://www.nature.com/nmat/journal/v2/n12/suppinfo/nmat1019_S1.html

Kennedy, S., H. Dungey, A. Yanchuk, & C. Low. (2011). *Eucalyptus fastigata*: Its current status in New Zealand and breeding objectives for the future. *Silvae Genetica, 60*(6), 259-266.

Khoshhesab, Z. M. (2012). Reflectance IR spectroscopy. In T. Theophile (Ed.), *Infrared Spectroscopy - Materials Science, Engineering and Technology*: InTech.

Kljun, A. (2011). Comparative Analysis of Crystallinity Changes in Cellulose I Polymers Using ATR-FTIR, X-ray Diffraction, and Carbohydrate-Binding Module Probes. *Biomacromolecules, 12*(11), 4121-4126. doi: 10.1021/bm201176m

Koch, M., S. Hunsche, P. Schumacher, M. C. Nuss, J. Feldmann, & J. Fromm. (1998). THz-imaging: a new method for density mapping of wood. *Wood Science and Technology, 32*(6), 421-427. doi: 10.1007/bf00702799

Kröling, H., S. Mehlhase, J. Fleckenstein, N. Nubbo, A. Endres, S. Schabel*, et al.* (2013). *Engineering and Modeling of Tensile Strength of Paper-Thermoset Composites.* Paper presented at the 19th International Conference on Composite Materials.

Kubler, H. (1987). Growth stresses in trees and related wood properties. *Forestry Abstracts, 48*(3), 131-189.

Lachenbruch, B., J. R. Moore, & R. Evans. (2011). Radial variation in wood structure and function in woody plants, and hypotheses for its occurrence *Size-and age-related changes in tree structure and function* (pp. 121-164): Springer.

Larkin, P. (2011). *Infrared and raman spectroscopy: principles and spectral interpretation*. Amsterdam;Boston;: Elsevier.

Lausberg, M., K. Gilchrist, & J. Skipwith. (1995). Wood properties of *Eucalyptus nitens* grown in New Zealand. *New Zealand Journal of Forestry Science, 25*(2), 147-163.

Leblon, B., O. Adedipe, G. Hans, A. Haddadi, S. Tsuchikawa, J. Burger*, et al.* (2013). A review of near-infrared spectroscopy for monitoring moisture content and density of solid wood. *Forestry Chronicle, 89*(05), 595-606. doi: 10.5558/tfc2013-111

Lee, C. M., J. D. Kubicki, B. Fan, L. Zhong, M. C. Jarvis, & S. H. Kim. (2015). Hydrogen-Bonding Network and OH Stretch Vibration of Cellulose: Comparison of Computational Modeling with Polarized IR and SFG Spectra. *The Journal of Physical Chemistry B, 119*(49), 15138-15149. doi: 10.1021/acs.jpcb.5b08015

Lee, C. M., J. D. Kubicki, B. Fan, L. Zhong, M. C. Jarvis, & S. H. Kim. (2015). Hydrogen-Bonding Network and OH Stretch Vibration of Cellulose: Comparison of Computational Modeling with Polarized IR and SFG Spectra. *The Journal of Physical Chemistry B*, 15138-15149.

Lee, C. M., N. M. A. Mohamed, H. D. Watts, J. D. Kubicki, & S. H. Kim. (2013). Sum-Frequency-Generation Vibration Spectroscopy and Density Functional Theory Calculations with Dispersion Corrections (DFT-D2) for Cellulose Iα and Iβ. *The Journal of Physical Chemistry B, 117*(22), 6681-6692. doi: 10.1021/jp402998s

Lee, Y. S. (2009). *Principles of terahertz science and technology* (Vol. 170): Springer Science & Business Media.

Leppänen, K., I. Bjurhager, M. Peura, A. Kallonen, J.-P. Suuronen, P. Penttilä*, et al.* (2011). X-ray scattering and microtomography study on the structural changes of never-dried silver birch, European aspen and hybrid aspen during drying. *Holzforschung, 65*(6), 865. doi: 10.1515/HF.2011.108

Li, Y., & C. M. Altaner. (2018). Predicting extractives content of Eucalyptus bosistoana F. Muell. Heartwood from stem cores by near infrared spectroscopy. *Spectrochimica Acta Part A: Molecular and Biomolecular Spectroscopy*, 78-87. doi: https://doi.org/10.1016/j.saa.2018.02.068

Liland, K. H., A. Kohler, & N. K. Afseth. (2016). Model□based pre□processing in Raman

spectroscopy of biological samples. *Journal of Raman Spectroscopy, 47*(6), 643-650.

Liland, K. H., & B.-H. Mevik. (2015). baseline: Baseline Correction of Spectra. https://CRAN.R-project.org/package=baseline

Lin, S. Y., & C. W. Dence. (1992). *Methods in lignin chemistry* (1 ed.): Springer-Verlag Berlin Heidelberg.

Malan, F. S. (1995). Eucalyptus improvement for lumber production. *Seminario Internacional de Utilização da Madeira de Eucalipto, 15*, 1-19.

Mantsch, H. H., & D. Naumann. (2010). Terahertz spectroscopy: The renaissance of far infrared spectroscopy. *Journal of Molecular Structure, 964*(1), 1-4.

Maréchal, Y., & H. Chanzy. (2000). The hydrogen bond network in Iβ cellulose as observed by infrared spectrometry. *Journal of Molecular Structure, 523*(1), 183-196. doi: http://dx.doi.org/10.1016/S0022-2860(99)00389-0

Margadant, R. (1981). Why not peel locally grown Eucalyptus. *Wood Southern Africa, 6*(10), 8-22.

McGavin, R. L. (2016). *Analysis of small-log processing to achieve structural veneer from juvenile hardwood plantations.* PhD, The University of Melbourne, Melbourne.

McKenzie, H. (1993). Growing durable hardwoods - a research strategy. *New Zealand Journal of Forestry, 38*(3), 25-27.

McKenzie, H., J. Turner, & C. Shelbourne. (2003). Processing young plantation-grown *Eucalyptus nitens* for solid-wood products. 1: Individual-tree variation in quality and recovery of appearance-grade lumber and veneer. *New Zealand Journal of Forestry Science, 33*(1), 62-78.

McKinley, R., C. Shelbourne, C. Low, B. Penellum, & M. Kimberley. (2002). Wood properties of young *Eucalyptus nitens*, *E. globulus*, and *E. maidenii* in Northland, New Zealand. *New Zealand Journal of Forestry Science, 32*(3), 334-356.

McWhannell, F. B. (1960). *Eucalypts for New Zealand farms, parks and gardens.* Hamilton, N.Z: Paul's Book Arcade.

Meglen, R. R., & S. S. Kelley. (2003). US Patent No. 6,525,319 B2.

Mevik, B.-H., R. Wehrens, & K. H. Liland. (2016a). pls: partial least squares and principal component regression *R package version 2.6-0.*

Mevik, B.-H., R. Wehrens, & K. H. Liland. (2016b). Pls: Partial least squares and principal component regression. https://CRAN.R-project.org/package=pls

Millen, P. (2009). *NZ Dryland Forests Initiative: a market focused durable eucalypt R&D project.* Paper presented at the Revisiting eucalypts 2009 : workshop proceedings, Christchurch.

Millen, P., S. van Ballekom, C. Altaner, L. Apiolaza, E. Mason, R. McConnochie*, et al.* (2018). Durable eucalypt forests–a multi-regional opportunity for investment in New Zealand drylands. *New Zealand Journal of Forestry, 63*(1), 11-23.

Miller, J. T., P. Cannon, & C. E. Ecroyd. (1992). Introduced forest trees in New Zealand: recognition, role, and seed source. 11. *Eucalyptus nitens* (Deane et Maiden) Maiden *FRI Bulletin 124* (Vol. 124). Rotorua: New Zeland Forest Research Institute.

Miller, J. T., A. E. Hay, & C. E. Ecroyd. (2000). Introduced forest trees in New Zealand:

recognition, role, and seed source. 18. ash eucalypts *FRI Bulletin 124* (Vol. 124). Rotorua: New Zealand Forest Research Institute.

Millner, J. (2006). *The performance of Eucalyptus species in Hill country.* PhD, Massey University, Palmerston North, New Zealand.

Mitsui, K., T. Inagaki, & S. Tsuchikawa. (2008). Monitoring of hydroxyl groups in wood during heat treatment using NIR spectroscopy. *Biomacromolecules, 9*(1), 286-288.

Montero, C., B. Clair, T. Alméras, A. v. d. Lee, & J. Gril. (2012). Relationship between wood elastic strain under bending and cellulose crystal strain. *Composites Science and Technology, 72*(2), 175-181. doi: https://doi.org/10.1016/j.compscitech.2011.10.014

MPI. (2016). National exotic forest description (NEFD) (33rd ed.). Wellington: Ministry for Primary Industries.

Mukhamadeeva, R. M., R. G. Zhbankov, V. I. Kovalenko, V. F. Sopin, & G. N. Marchenko. (1990). Low-frequency IR spectra of various structural modifications of cellulose. *Journal of Applied Spectroscopy, 52*(4), 403-407. doi: 10.1007/bf00660537

Murphy, T. N., M. Henson, & J. K. Vanclay. (2005). Growth stress in Eucalyptus dunnii. *Australian Forestry, 68*(2), 144-149. doi: 10.1080/00049158.2005.10674958

Navi, P., P. K. Rastogi, V. Gresse, & A. Tolou. (1995). Micromechanics of wood subjected to axial tension. *Wood Science and Technology, 29*(6), 411-429. doi: 10.1007/BF00194199

Newman, R. H., S. J. Hill, & P. J. Harris. (2013). Wide-angle x-ray scattering and solid-state nuclear magnetic resonance data combined to test models for cellulose microfibrils in mung bean cell walls. *Plant physiology, 163*(4), 1558-1567.

Nicholson, J. E. (1971). A rapid method for estimating longitudinal growth stresses in logs. *Wood Science and Technology, 5*(1), 40-48. doi: 10.1007/bf00363119

Nishiyama, Y., A. Isogai, T. Okano, M. Müller, & H. Chanzy. (1999). Intracrystalline Deuteration of Native Cellulose. *Macromolecules, 32*(6), 2078-2081. doi: 10.1021/ma981563m

Nishiyama, Y., G. P. Johnson, A. D. French, V. T. Forsyth, & P. Langan. (2008). Neutron crystallography, molecular dynamics, and quantum mechanics studies of the nature of hydrogen bonding in cellulose Iβ. *Biomacromolecules, 9*(11), 3133-3140.

Nishiyama, Y., P. Langan, & H. Chanzy. (2002). Crystal structure and hydrogen-bonding system in cellulose Iβ from synchrotron X-ray and neutron fiber diffraction. *Journal of the American Chemical Society, 124*(31), 9074-9082.

Nishiyama, Y., J. Sugiyama, H. Chanzy, & P. Langan. (2003). Crystal Structure and Hydrogen Bonding System In cellulose Iα from Synchrotron X-ray and Neutron Fiber Diffraction. *Journal of the American Chemical Society, 125*(47), 14300-14306.

Okuyama, T., H. Yamamoto, M. Yoshida, Y. Hattori, & R. Archer. (1994). Growth stresses in tension wood: role of microfibrils and lignification. *Annales des Sciences Forestieres, 51*(3), 291-300.

Oliveira, J. T. d. S., J. C. Hellmeister, & M. Tomazello Filho. (2005). Variation of the moisture content and specific gravity in the wood of seven eucalypt species. *Revista Árvore, 29*(1), 115-127.

Ona, T., T. Sonoda, K. Ito, M. Shibata, T. Kato, & Y. Ootake. (1997). Non-destructive determination of wood constituents by Fourier transform Raman spectroscopy. *Journal*

of Wood chemistry and Technology, 17(4), 399-417.

Osborne, B. G., T. Fearn, & P. H. Hindle. (1993). *Practical NIR spectroscopy with applications in food and beverage analysis* (2 ed.): Longman scientific and technical.

Österberg, M., U. Schmidt, & A.-S. Jääskeläinen. (2006). Combining confocal Raman spectroscopy and atomic force microscopy to study wood extractives on cellulose surfaces. *Colloids and Surfaces A: Physicochemical and Engineering Aspects, 291*(1), 197-201. doi: https://doi.org/10.1016/j.colsurfa.2006.06.039

Ozarska, B. (1999). A review of the utilisation of hardwoods for LVL. *Wood Science and Technology, 33*(4), 341-351. doi: 10.1007/s002260050120

Page, D., & T. Singh. (2014). Durability of New Zealand grown timbers. *New Zealand Journal of Forestry, 58*(4), 26-30.

Peetla, P., K. C. Schenzel, & W. Diepenbrock. (2006). Determination of mechanical strength properties of hemp fibers using near-infrared Fourier transform Raman microspectroscopy. *Applied Spectroscopy, 60*(6), 682-691.

Pereira, J., J. Xavier, J. Morais, & J. Lousada. (2013). Assessing wood quality by spatial variation of elastic properties within the stem: Case study of Pinus pinaster in the transverse plane. *Canadian Journal of Forest Research, 44*(2), 107-117. doi: 10.1139/cjfr-2013-0207

Pérez, S., & D. Samain. (2010). Structure and engineering of celluloses. *Advances in carbohydrate chemistry and biochemistry, 64*, 25-116.

Peura, M., K. Kölln, I. Grotkopp, P. Saranpää, M. Müller, & R. Serimaa. (2007). The effect of axial strain on crystalline cellulose in Norway spruce. *Wood Science and Technology, 41*(7), 565-583.

Pönni, R., E. Kontturi, & T. Vuorinen. (2013). Accessibility of cellulose: Structural changes and their reversibility in aqueous media. *Carbohydrate Polymers, 93*(2), 424-429. doi: https://doi.org/10.1016/j.carbpol.2012.12.025

Pönni, R., L. Rautkari, C. A. S. Hill, & T. Vuorinen. (2014). Accessibility of hydroxyl groups in birch kraft pulps quantified by deuterium exchange in D2O vapor. *Cellulose, 21*(3), 1217-1226. doi: 10.1007/s10570-014-0166-x

Popescu, C.-M., & M.-C. Popescu. (2013). A near infrared spectroscopic study of the structural modifications of lime (Tilia cordata Mill.) wood during hydro-thermal treatment. *Spectrochimica Acta Part A: Molecular and Biomolecular Spectroscopy, 115*, 227-233. doi: https://doi.org/10.1016/j.saa.2013.06.002

Popescu, C.-M., G. Singurel, M.-C. Popescu, C. Vasile, D. S. Argyropoulos, & S. Willför. (2009). Vibrational spectroscopy and X-ray diffraction methods to establish the differences between hardwood and softwood. *Carbohydrate Polymers, 77*(4), 851-857. doi: https://doi.org/10.1016/j.carbpol.2009.03.011

Poynton, R. J. (1979). *Eucalyptus globoidea* Blakely. In R. J. Poynton (Ed.), *Tree Planting in Southern Africa: The eucalypts* (pp. 316-324). South Africa: Department of Forestry.

R Core Team. (2017). A language and environment for statistical computing *R foundation for statistical computing*. Vienna, Austria.

Raymond, C. A., P. D. Kube, L. Pinkard, L. Savage, & A. D. Bradley. (2004). Evaluation of non-destructive methods of measuring growth stress in Eucalyptus globulus: relationships between strain, wood properties and stress. *Forest Ecology and*

Management, 190(2–3), 187-200. doi: http://dx.doi.org/10.1016/j.foreco.2003.10.011

Reid, M., & R. Fedosejevs. (2006). Terahertz birefringence and attenuation properties of wood and paper. *Applied Optics, 45*(12), 2766-2772.

Richter, S., J. Müssig, & N. Gierlinger. (2011). Functional plant cell wall design revealed by the Raman imaging approach. *Planta, 233*(4), 763-772.

Rozenberg, M., A. Loewenschuss, & Y. Marcus. (2000). Infrared spectra and hydrogen bonding of pentitols and pyranosides at 20 to 300 K. *Carbohydrate Research, 328*(3), 307-319. doi: http://dx.doi.org/10.1016/S0008-6215(00)00117-8

Salmén, L. (2015). Wood morphology and properties from molecular perspectives. *Annals of Forest Science, 72*(6), 679-684.

Salmén, L., & E. Bergström. (2009). Cellulose structural arrangement in relation to spectral changes in tensile loading FTIR. *Cellulose, 16*(6), 975-982.

Salmén, L., & I. Burgert. (2009). Cell wall features with regard to mechanical performance. A review COST Action E35 2004–2008: Wood machining–micromechanics and fracture. *Holzforschung, 63*(2), 121-129.

Salmén, L., J. S. Stevanic, & A.-M. Olsson. (2016). Contribution of lignin to the strength properties in wood fibres studied by dynamic FTIR spectroscopy and dynamic mechanical analysis (DMA). *Holzforschung, 70*(12), 1155. doi: 10.1515/hf-2016-0050

Sandak, J., A. Sandak, D. Pauliny, V. Krasnoshlyk, & O. Hagman. (2013). Near infrared spectroscopy as a tool for estimation of mechanical stresses in wood. *Advanced Materials Research, 778*, 448-453.

Schmidt, M., N. Gierlinger, U. Schade, T. Rogge, & M. Grunze. (2006). Polarized infrared microspectroscopy of single spruce fibers: Hydrogen bonding in wood polymers. *Biopolymers, 83*(5), 546-555. doi: 10.1002/bip.20585

Schwanninger, M., J. C. Rodrigues, & K. Fackler. (2011). A review of band assignments in near infrared spectra of wood and wood components. *Journal of Near Infrared Spectroscopy, 19*(5), 287.

Shelbourne, C., B. Bulloch, C. Low, & R. McConnochie. (2002). Performance to age 22 years of 49 eucalypts in the Wairarapa district, New Zealand, reviewed with results from other trials. *New Zealand Journal of Forestry Science, 32*(2), 256-278.

Shinzawa, H., K. Awa, & Y. Ozaki. (2011). Compression-induced morphological and molecular structural changes of cellulose tablets probed with near infrared imaging. *Journal of Near Infrared Spectroscopy, 19*(1), 15-22.

Signal developers. (2013). Signal: Signal processing. http://r-forge.r-project.org/projects/signal/

Simmonds, J. H. (1927). *Trees from other lands for shelter and timber in New Zealand: eucalypts*. Auckland: Brett Printing and Publishing Company.

Simposon, W. T. (1971). Moisture changes induced in red oak by transverse stress. *Wood and Fiber Science, 3*(1), 13-21.

Smith, E., & G. Dent. (2005). *Modern Raman spectroscopy: a practical approach*: John Wiley & Sons, Ltd.

Stevens, A., & L. Ramirez-Lopez. (2013). An introduction to the prospectr package *R package version 0.1.3*.

Stokke, D. D., Q. Wu, & G. Han. (2013). *Introduction to wood and natural fiber composites*: John Wiley & Sons.

Šturcová, A., G. R. Davies, & S. J. Eichhorn. (2005). Elastic modulus and stress-transfer properties of tunicate cellulose whiskers. *Biomacromolecules, 6*(2), 1055-1061. doi: 10.1021/bm049291k

Šturcová, A., I. His, D. C. Apperley, J. Sugiyama, & M. C. Jarvis. (2004). Structural Details of Crystalline Cellulose from Higher Plants. *Biomacromolecules, 5*(4), 1333-1339. doi: 10.1021/bm034517p

Suontama, M., C. B. Low, G. T. Stovold, M. A. Miller, K. R. Fleet, Y. Li*, et al.* (2015). Genetic parameters and genetic gains across three breeding cycles for growth and form traits of *Eucalyptus regnans* in New Zealand. *Tree Genetics & Genomes, 11*(6), 133. doi: 10.1007/s11295-015-0957-8

Tarmian, A., I. Burgert, & E. E. Thybring. (2017). Hydroxyl accessibility in wood by deuterium exchange and ATR-FTIR spectroscopy: methodological uncertainties. *Wood Science and Technology, 51*(4), 845-853. doi: 10.1007/s00226-017-0922-9

Telfer, E. J., G. T. Stovold, Y. J. Li, O. B. Silva, D. G. Grattapaglia, & H. S. Dungey. (2015). Parentage Reconstruction in *Eucalyptus nitens* Using SNPs and Microsatellite Markers: A Comparative Analysis of Marker Data Power and Robustness. *PLoS ONE, 10*(7), e0130601. doi: 10.1371/journal.pone.0130601

Thomas, L. H., V. T. Forsyth, A. Šturcová, C. J. Kennedy, R. P. May, C. M. Altaner*, et al.* (2013). Structure of cellulose microfibrils in primary cell walls from collenchyma. *Plant Physiology, 161*(1), 465-476.

Thumm, A., M. Riddell, B. Nanayakkara, J. Harrington, & R. Meder. (2010). Near Infrared Hyperspectral Imaging Applied to Mapping Chemical Composition in Wood Samples. *Journal of Near Infrared Spectroscopy, 18*(6), 507-515.

Timell, T. E. (1986). *Compression Wood in Gymnosperms* (Vol. 1): Springer-Verlag Berlin Heidelberg.

Toba, K., H. Yamamoto, & M. Yoshida. (2012). Mechanical interaction between cellulose microfibrils and matrix substances in wood cell walls induced by repeated wet-and-dry treatment. *Cellulose, 19*(4), 1405-1412. doi: 10.1007/s10570-012-9700-x

Toba, K., H. Yamamoto, & M. Yoshida. (2013). Micromechanical detection of growth stress in wood cell wall by wide-angle X-ray diffraction (WAX). *Holzforschung, 67*(3), 315-323.

Treloar, L. R. G. (1953). The absorption of water by cellulose, and its dependence on applied stress. *Transactions of the Faraday Society, 49*(0), 816-823. doi: 10.1039/TF9534900816

Tsoumis, G. T. (1991). *Science and technology of wood: structure, properties, utilization*. New York: Van Nostrand Reinhold.

Tsuchikawa, S. (2007). A review of recent near infrared research for wood and paper. *Applied Spectroscopy Reviews, 42*(1), 43-71.

Tsuchikawa, S., & H. Kobori. (2015). A review of recent application of near infrared spectroscopy to wood science and technology. *Journal of Wood Science, 61*(3), 213-220. doi: 10.1007/s10086-015-1467-x

Tsuchikawa, S., & H. Siesler. (2003a). Near-infrared spectroscopic monitoring of the diffusion

process of deuterium-labeled molecules in wood. Part I: Softwood. *Applied Spectroscopy, 57*(6), 667-674.

Tsuchikawa, S., & H. Siesler. (2003b). Near-infrared spectroscopic monitoring of the diffusion process of deuterium-labeled molecules in wood. Part II: Hardwood. *Applied Spectroscopy, 57*(6), 675-681.

Turnbull, J. (2007). Development of sustainable forestry plantations in China: a review *Impact Assessment Series Report No. 45*. Canberra: Australian Centre for International Agricultural Research.

Twede, D., S. E. Selke, D.-P. Kamdem, & D. Shires. (2014). *Cartons, crates and corrugated board: handbook of paper and wood packaging technology* (Second ed.): DEStech Publications, Inc.

Valencia, J., C. Harwood, R. Washusen, A. Morrow, M. Wood, & P. Volker. (2011). Longitudinal growth strain as a log and wood quality predictor for plantation-grown *Eucalyptus nitens* sawlogs. *Wood Science and Technology, 45*(1), 15-34. doi: 10.1007/s00226-010-0302-1

van Ballekom, S., & P. Millen. (2017). *NZDFI: achievements, constraints and opportunities.* Paper presented at the Durable eucalypts on drylands: protecting and enhancing value, Blenheim, New Zealand.

van de Kuilen, J. W. G., A. Ceccotti, Z. Xia, & M. He. (2011). Very Tall Wooden Buildings with Cross Laminated Timber. *Procedia Engineering, 14*, 1621-1628. doi: http://dx.doi.org/10.1016/j.proeng.2011.07.204

VanderHart, D. L., & R. Atalla. (1984). Studies of microstructure in native celluloses using solid-state carbon-13 NMR. *Macromolecules, 17*(8), 1465-1472.

Wada, M. (2002). Lateral thermal expansion of cellulose Iβ and IIIᵢ polymorphs. *Journal of Polymer Science Part B: Polymer Physics, 40*(11), 1095-1102.

Wada, M., R. Hori, U.-J. Kim, & S. Sasaki. (2010). X-ray diffraction study on the thermal expansion behavior of cellulose Iβ and its high-temperature phase. *Polymer Degradation and Stability, 95*(8), 1330-1334. doi: http://dx.doi.org/10.1016/j.polymdegradstab.2010.01.034

Wang, Y., J. Lian, J. Wan, Y. Ma, & Y. Zhang. (2015). A supramolecular structure insight for conversion property of cellulose in hot compressed water: Polymorphs and hydrogen bonds changes. *Carbohydrate Polymers, 133*, 94-103. doi: http://dx.doi.org/10.1016/j.carbpol.2015.06.110

Watanabe, A., S. Morita, & Y. Ozaki. (2006a). Study on Temperature-Dependent Changes in Hydrogen Bonds in Cellulose Iβ by Infrared Spectroscopy with Perturbation-Correlation Moving-Window Two-Dimensional Correlation Spectroscopy. *Biomacromolecules, 7*(11), 3164-3170. doi: 10.1021/bm0603591

Watanabe, A., S. Morita, & Y. Ozaki. (2006b). A study on water adsorption onto microcrystalline cellulose by near-infrared spectroscopy with two-dimensional correlation spectroscopy and principal component analysis. *Applied spectroscopy, 60*(9), 1054-1061.

Watanabe, A., S. Morita, & Y. Ozaki. (2006c). Temperature-dependent structural changes in hydrogen bonds in microcrystalline cellulose studied by infrared and near-infrared spectroscopy with perturbation-correlation moving-window two-dimensional

correlation analysis. *Applied spectroscopy, 60*(6), 611-618.

Watanabe, K., I. Kobayashi, S. Saito, N. Kuroda, & S. Noshiro. (2013). Nondestructive evaluation of drying stress level on wood surface using near-infrared spectroscopy. *Wood Science and Technology, 47*(2), 299-315. doi: 10.1007/s00226-012-0492-9

Watanabe, K., K. Yamashita, & S. Noshiro. (2011). Non-destructive evaluation of surface longitudinal growth strain on Sugi (Cryptomeria japonica) green logs using near-infrared spectroscopy. *Journal of Wood Science, 58*(3), 267-272. doi: 10.1007/s10086-011-1238-2

Watt, M. S., M. O. Kimberley, J. J. Harrington, M. J. Riddell, D. J. Cown, & J. R. Moore. (2013). Differences in intra-tree variation in spiral grain angle for radiata pine. *New Zealand Journal of Forestry Science, 43*(1), 12. doi: 10.1186/1179-5395-43-12

Wertz, J.-L., J. P. Mercier, & O. Bédué. (2010). *Cellulose science and technology*: CRC Press.

Wickholm, K., P. T. Larsson, & T. Iversen. (1998). Assignment of non-crystalline forms in cellulose I by CP/MAS 13C NMR spectroscopy. *Carbohydrate Research, 312*(3), 123-129. doi: https://doi.org/10.1016/S0008-6215(98)00236-5

Wiley, J. H., & R. H. Atalla. (1987). Band assignments in the raman spectra of celluloses. *Carbohydrate Research, 160*(Supplement C), 113-129. doi: https://doi.org/10.1016/0008-6215(87)80306-3

Wilkes, J. (1988). Variations in wood anatomy within species of Eucalyptus. *IAWA Journal, 9*(1), 13-23. doi: doi:https://doi.org/10.1163/22941932-90000461

Workman, J., & L. Weyer. (2008). *Practical guide to interpretive near-infrared spectroscopy*. Boca Raton, FL: Taylor & Francis.

Xiang, D., R. LoBrutto, J. Cheney, B. W. Wabuyele, J. Berry, R. Lyon*, et al.* (2009). Evaluation of Transmission and Reflection Modalities for Measuring Content Uniformity of Pharmaceutical Tablets with Near-Infrared Spectroscopy. *Applied Spectroscopy, 63*(1), 33-47. doi: 10.1366/000370209787169696

Yamamoto, H. (1998). Generation mechanism of growth stresses in wood cell walls: roles of lignin deposition and cellulose microfibril during cell wall maturation. *Wood Science and Technology, 32*(3), 171-182. doi: 10.1007/bf00704840

Yan, C., B. Yang, & Z. Yu. (2013). Terahertz time domain spectroscopy for the identification of two cellulosic fibers with similar chemical composition. *Analytical Letters, 46*(6), 946-958.

Yang, J. L., H. Baillères, R. Evans, & G. Downes. (2006). Evaluating growth strain of *Eucalyptus globulus* Labill. from SilviScan measurements. *Holzforschung, 60*(5), 574-579.

Yang, J. L., H. Baillères, T. Okuyama, A. Muneri, & G. Downes. (2005). Measurement methods for longitudinal surface strain in trees: a review. *Australian Forestry, 68*(1), 34-43. doi: 10.1080/00049158.2005.10676224

Yang, J. L., D. Fife, & A. C. Matheson. (2001). Growth strain in three provenances of plantation-grown *Eucalyptus globulus* Labill. *Australian Forestry, 64*(4), 248-256.

Yang, J. L., & S. Pongracic. (2004). The impact of growth stress on sawn distortion and log end splitting of 32-year old plantation blue gum *Project no: PN03.1312*. Vicroria: Forest and Wood Products Research & Development Corporation.

Yang, J. L., & G. Waugh. (2001). Growth stress, its measurement and effects. *Australian Forestry, 64*(2), 127-135.

Yoshida, M., & T. Okuyama. (2002). Techniques for Measuring Growth Stress on the Xylem Surface Using Strain and Dial Gauges *Holzforschung* (Vol. 56, pp. 461).

Yu, Y., Z.-h. Jiang, & G.-l. Tian. (2009). Size effect on longitudinal MOE of microtomed wood sections and relevant theoretical explanation. *Forestry Studies in China, 11*(4), 243-248.

Yu, Y., D. Ren, Y. Zhou, & W. Yu. (2006). Preliminary study on gluability of *E. urophylla* veneer. *China Forest Products Industry, 33*(4), 20-23.

Zabler, S., O. Paris, I. Burgert, & P. Fratzl. (2010). Moisture changes in the plant cell wall force cellulose crystallites to deform. *Journal of Structural Biology, 171*(2), 133-141. doi: http://dx.doi.org/10.1016/j.jsb.2010.04.013

Zhang, N., S. Li, L. Xiong, Y. Hong, & Y. Chen. (2015). Cellulose-hemicellulose interaction in wood secondary cell-wall. *Modelling and Simulation in Materials Science and Engineering, 23*(8), 085010.

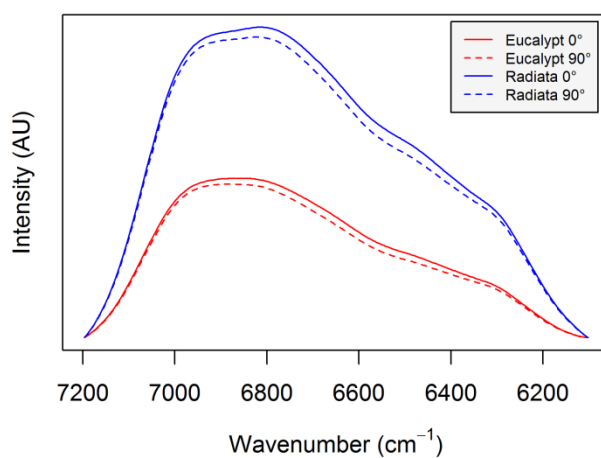# APPENDIX A: STRESS RELAXATION OF WOOD AND PAPER
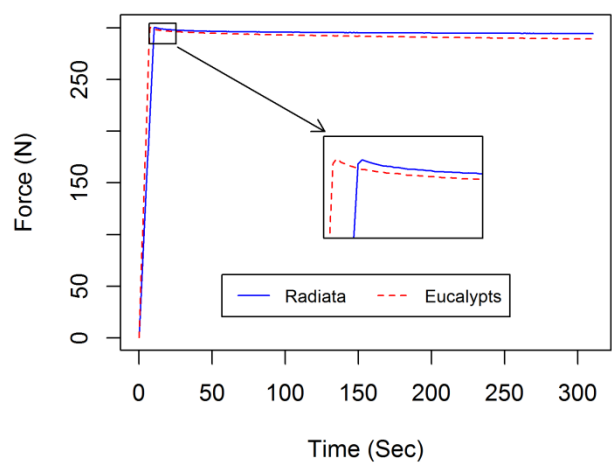
Supporting Figure 1. Stress relaxation of radiata pine (solid line) and eucalypt (dashed line) wood
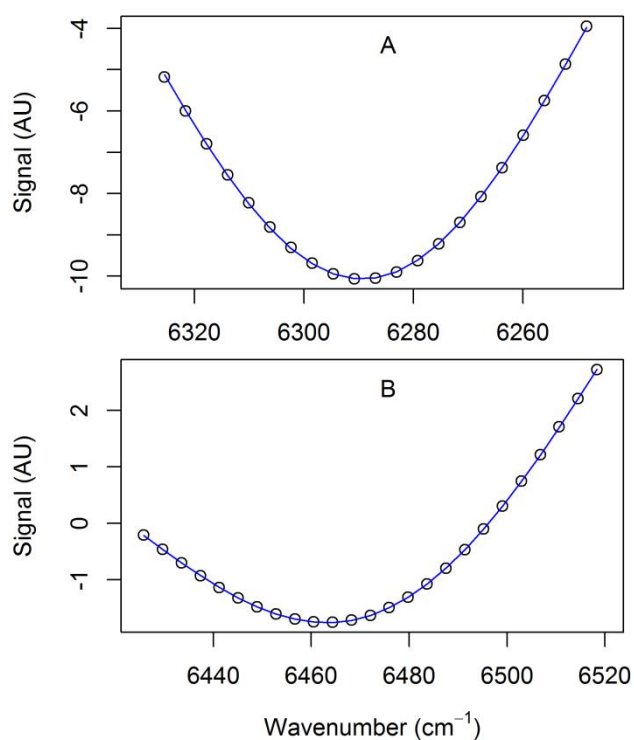
samples
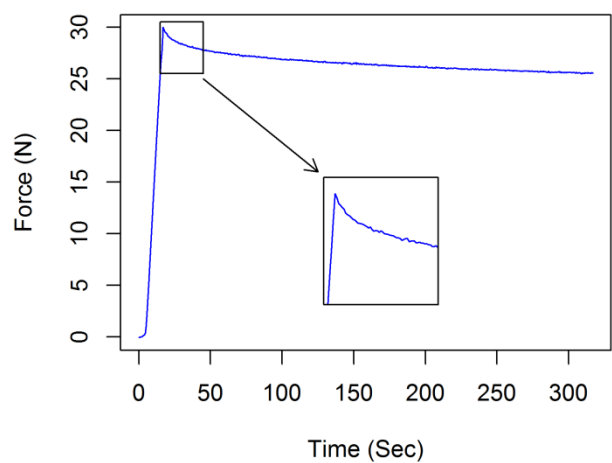
Supporting Figure 2. Stress relaxation of a paper sample

# APPENDIX B: PARALLEL AND PERPENDICULAR POLARISED NIR SPECTRA

Supporting Figure 3. Baseline corrected NIR spectra of eucalypt (red) and radiata pine (blue) wood in the region of 6100 to 7200 cm^{-1} using parallel polarised (0°) light and perpendicular polarised (90°) light.

APPENDIX C: PEAK FITTING IN R

Supporting Figure 4. Fitted NIR bands in the 2nd derivative spectra at ~6286 cm^{-1} with a Gaussian function (A) and at ~6469 cm^{-1} with a skewed Lorentzian function (B). Blue solid line: fitted function; open circles: measured data.
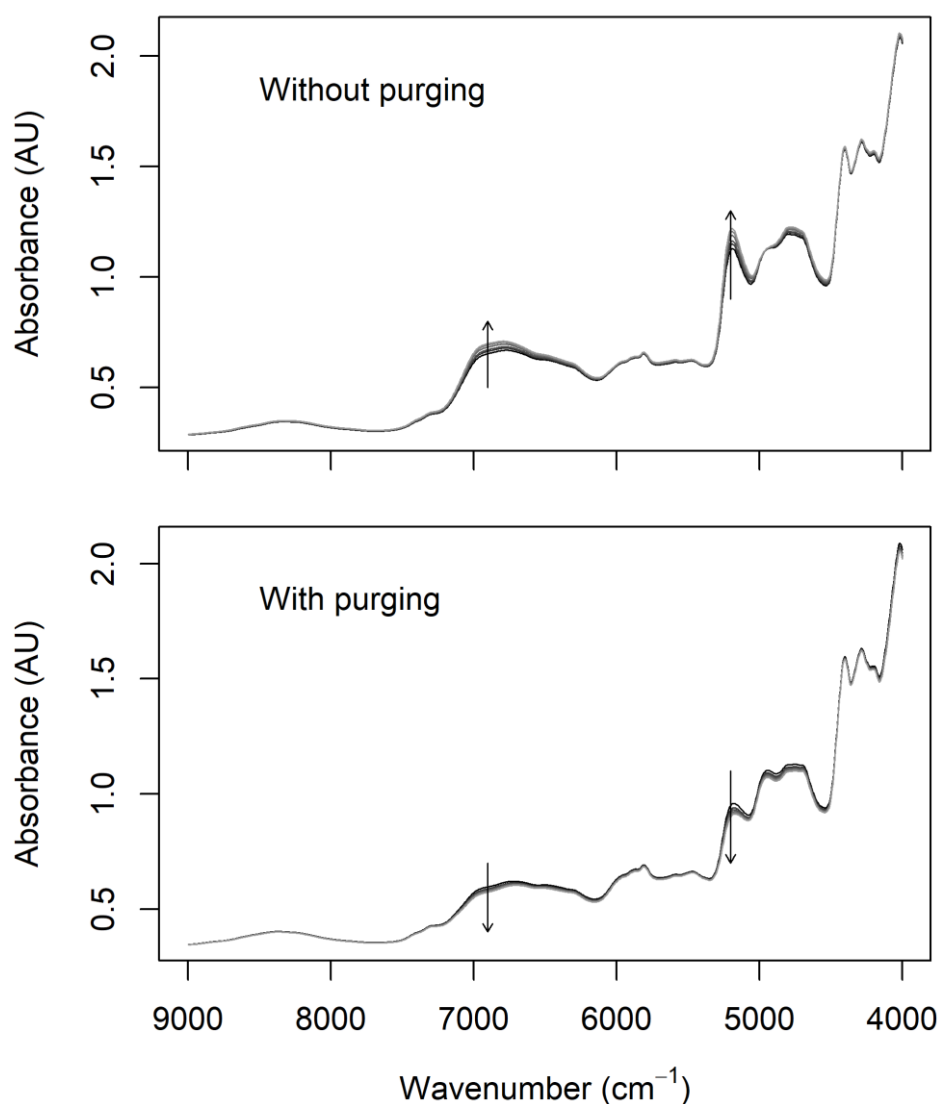
APPENDIX D: NIR SPECTRA OF LIGNIN, OVEN-DRY WOOD AND PAPER
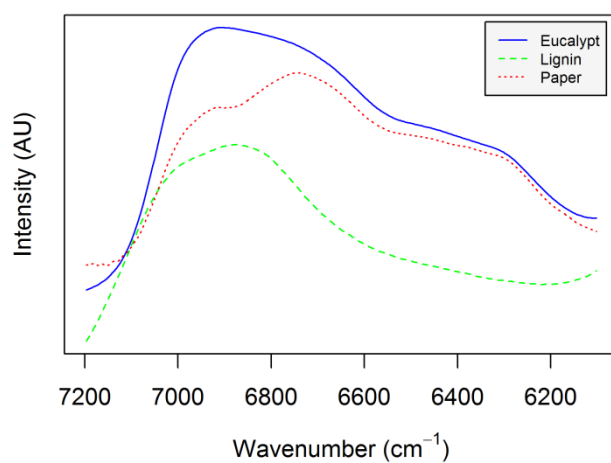
Supporting Figure 5. NIR spectra of alkali lignin, oven-dry eucalypt wood and oven-dry paper in the region of 6100 to 7200 cm^{-1}. Spectra of lignin was measured using fibre probe in reflection mode.

APPENDIX E: NIR SPECTRA OF DEUTERATED WOOD AFFECTED BY RE-PROTONATION

Supporting Figure 6 Original NIR spectra of deuterated sample measured over time with or without D_2O vapour purging. Without purging, the signals at around 6900 and 5200 cm^{-1} increased over time due to re-protonation. Since samples were re-protonated during sample handling and transportation, OH groups in these samples were re-exchanged to OD groups with D_2O purging.

APPENDIX F: BASELINE CORRECTION REMOVING THE EFFECT OF MOISTURE CONTENT
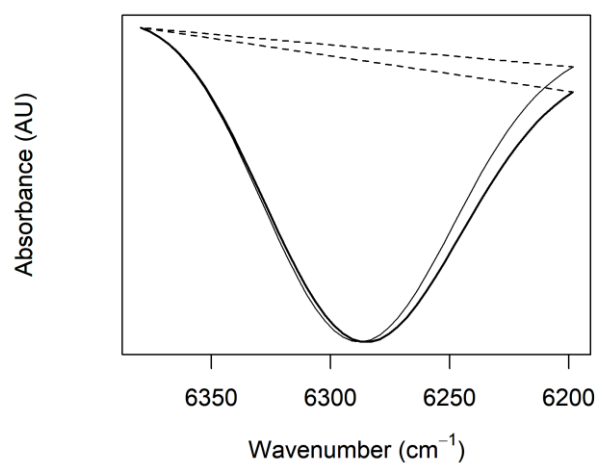
Supporting Figure 7 Baseline correction was used to remove the drying effect during NIR measurements. Baselines (dashed) connecting two points at 6198 and 6380 cm^{-1} were subtracted in the second derivative spectra. The thick line represents the spectrum of a rewetted sample at "Strain 0", the thin line at "Strain 8". The rewetted sample was losing water during spectra collection.